2002

Fatigue Life of Pultruded and Hand Lay-Up GFRP Exposed to Different Environmental Conditions.

Mohammed Asif Iqbal

FATIGUE LIFE OF PULTRUDED AND HAND LAY-UP GFRP EXPOSED TO DIFFERENT ENVIRONMENTAL CONDITIONS

By

Mohammed Asif Iqbal

B.S. Winona State University, Minnesota, 1997

A THESIS

Submitted in Partial Fulfillment of the

Requirements for the Degree of

Master of Science

(in Civil Engineering)

The Graduate School

The University Of Maine

May, 2001

Advisory Committee:

Habib J. Dagher, Professor of Civil Engineering, Advisor

Roberto Lopez-Anido, Assistant Professor of Civil Engineering

Beckry Abdel-Magid, Professor of Composite Materials Engineering,

Winona State University, Minnesota

FATIGUE LIFE OF PULTRUDED AND HAND LAY-UP GFRP EXPOSED TO DIFFERENT ENVIRONMENTAL CONDITIONS

By Mohammed Asif Iqbal

Thesis Advisor: Dr. Habib Dagher

An Abstract of the Thesis Presented
in Partial Fulfillment of the Requirements for the
Degree of Master of Science
(in Civil Engineering)
May, 2001

The use of unidirectional Glass Fiber Reinforced Polymer (GFRP) composites to reinforce glulam beams in tension has been proven by researchers at University of Maine and others to improve both allowable strength and ductility. The addition of 3% E-glass FRP has been shown to increase the allowable flexural strength by as much as 100%. These promising findings can be used in practice only if the GFRP will maintain a major proportion of its strength/stiffness mechanical properties over the life of the structure.

This study focuses on the fatigue life of two types of E-glass/phenolic GFRP (hand lay-up and pultruded) with special emphasis on the effect of environmental degradation on the fatigue life of pultruded GFRP. Fatigue life of

pultruded GFRP was evaluated after treatment in salt water, hot water, freeze-thaw, and UV weathering.

Static tests indicate that hot water (45°C) causes the higher reduction in tensile strength. The Young's modulus did not change significantly for any of the exposed specimens. Fatigue tests were conducted at constant amplitude at a frequency of 20Hz, and S-N curves were developed for each exposure group. The results show that except for UV weathering, the fatigue life of all the exposed specimens exhibited slight statistically significant improvement for low stress fatigue tests. Residual strength tests conducted at 10% of ultimate strength exhibited no statistically significant (α=0.05) reduction in tensile strength or modulus at 3 million cycles of fatigue.

The fatigue data was plotted using S-N diagrams and modeled using Log-linear equations. From the models, allowable strength for design purposes was recommended using statistical analysis. One-sided lower 95% tolerance limit for 95% of the population (5% LTL) were developed for pultruded control and hand lay-up specimens.

ACKNOWLEDGEMENTS

The author would like to thank those who have strived to make this research a success both in it's content and purpose. The author's advisor, Dr. Habib Dagher is acknowledged for his continuous support and encouragements throughout the research. The National Science Foundation is acknowledged for funding a good portion of this research. The author would also like to thank the rest of his committee members: Dr. Roberto Lopez-Anido who has helped with a number of technical issues concerning FRP materials, and special thanks to Dr. Beckry Abdel-Magid of Winona State University who has always extended help professionally and personally. The author would like to thank Don Strong, Tom Tripp, William Manion and Dr. Michael Peterson for their advice and help with many of the equipment needed for this research. Doreen Parent and Marcy Smith are acknowledged for their enduring task at assisting Habib in keeping track with the author's research.

The author acknowledges the company of his colleagues who have been a constant support morally and professionally: Cihat Tascioglu, Eoin Battles, Shane O'Neil and Mustafa Palancioglu. The author's good friend and colleague Keith Wood is acknowledged for his effort in editing a number of chapters of this thesis. Most importantly, the author would like to thank his parents, Mohammed Nurul Huq and Hasna Ara Begum for their continued loving support and encouragements throughout this experience. He would also like to thank his wife Zobaida for her blessed company and for giving them their first child, Numan.

TABLE OF CONTENTS

LIST OF TABLES

LIST OF FIGURES

1 INTRODUCTION

Two types of E-glass/phenolic FRP (Fiber Reinforced Plastic) materials were developed at the Advanced Engineered Wood Composites Center, University of Maine, for use as tension reinforcement in glulam beams. The FRPs were designed to be compatible with hygrothermal properties of glulam beams and conventional wood (PRF) adhesives. The first type of FRP is a pultruded product. The second is a hand lay-up type produced by impregnating stitched glass fabric with phenolic resin and curing under standard room temperature. FRPs can be used to reinforce glulam beams just as steel is used to reinforce concrete beams. The reasons for reinforcing glulam beams include higher flexural strength and stiffness, better use of lower grade lumber, reduced beam size use of lumber.

FRP materials are a promising reinforcement for wood members because they can be designed to match the hygrothermal properties of wood, their high strength to weight ratio and high corrosion and creep resistance compared to conventional constructional materials. Over the past twenty years fiber reinforced plastics, have been used successfully in civil infrastructure applications such as bridges, piers, walkways, pipelines, and building panels etc. (Gentry et al, 1998; Liao et al, 1998). The common types of reinforcements are glass, carbon and Aramid whereas vinylester, polyester and epoxy are used as common resin matrix materials.

As with any new material, engineers need to have a good understanding of the properties and performance of this material before they can design its use

in any application. When the FRP is used in bridge applications, it is subjected to cyclic loads from vehicular traffic. This cyclic or fatigue loading can reduce the strength and stiffness of most conventional construction materials such as steel and aluminum. This weakening of a material is called fatigue and is mostly due to the propagation of cracks within the material. Cyclic loading can reduce both tensile strength and stiffness of a material. Fatigue damage is an important concern because materials can thus fail at stresses or loads much below their ultimate strengths. Although numerous research has been done on the fatigue of FRP materials by the defense industry, and NASA in particular, the very fact that composite materials behave differently depending on the composition, orientation of reinforcement, and manufacturing method makes it difficult to apply the results of one test to another. For design purposes it is always required that the exact properties for the particular FRP used are well documented and understood. Thus, this study was designed to evaluate the fatigue performance of the two types of E-glass/phenolic FRP wood reinforcements developed at University of Maine, under normal and environmentally aged conditions. It is intended that this study will allow engineers to design wood structural members with the FRP reinforcements with safe allowable limits.

The objectives of this study are:

1. To evaluate the fatigue performance of the two E-glass/phenolic FRP wood reinforcements developed at the University of Maine under control conditions.

2. To evaluate the fatigue life of the pultruded E-glass/phenolic FRP after it has been subjected to accelerated environmental degradation.
3. To evaluate the feasibility of using the two FRP for bridge applications.
4. To recommend safe fatigue life design values.

The objectives were accomplished in four stages. The first stage included literature review and organization of methodologies recommended by code officials such as AASHTO, ICBO, BOCA, Caltrans, NIST and ASTM E 632 concerning the use of FRP materials for civil infrastructure applications and measuring service life of building components. The use of FRP reinforced glulam beams for bridge application is a new technology that is yet to be addressed by AASHTO. However, there are other evaluation criteria and specifications pertaining to the use of FRP in general. California Department of Transportation (Caltrans) was among the first to specify tests for evaluating performance of FRP materials used as concrete column wrapping/casing for seismic retrofitting. International Conference of Building Officials (ICBO) also specifies tests for evaluating FRP materials for masonry reinforcement [ICBO AC 125]. These specifications along with other general recommendations from ASTM and NIST, and recent research in this field were used to design a suitable test program for evaluating the fatigue and long-term durability of the two E-glass/phenolic FRPs. Thus this stage included identifying degradation factors and mechanisms. Once all the information was studied, an experimental plan was developed with proper regard to statistical significance and required sample size.

The second stage involved conditioning the pultruded FRP material in different environmental exposures, staggering the tests such that post-conditioning tests could be conducted without much delay. The norm of environmental exposure tests is to simulate accelerated environments that the FRP is likely to be exposed to or come in contact with. Since the FRP was designed for exterior applications, this includes freeze-thaw cycling, simulated salt water, Ultra Violet (UV) radiation from sunlight, moisture, and hot water. Thus, the degradation mechanisms considered are hygrothermal changes, chemical attack such as hydrolysis, photo-oxidation, and moisture corrosion. The third stage involved determination of physical and mechanical properties of the FRPs after pre-determined exposure periods. This was done to evaluate the severity of the exposure factors. Physical properties tested were density, volume fraction of fiber, resin and voids, and glass transition temperature (Tg). Mechanical properties included static tensile strength and stiffness, and interlaminar shear strength.

The fourth stage, which was the longest in this study, involved evaluation of the fatigue strength, and statistical analysis for design recommendations. Fatigue testing involved testing coupons in tension-tension set-up under constant amplitude, stress ratio (R), and frequency. Specimens tested at low stresses required considerable amount of time. A specimen tested at 20% UTS required 42 hours to undergo 3 million cycles of continuous fatigue. Residual strength tests were also conducted at 10% UTS to study reduction in tensile strength and stiffness due to fatigue loading. This was followed by recommendations using

statistical methods to evaluate safe design life based on tolerance limits of the fatigue S-N curves.

This study consists of six chapters along with appendices. The first chapter introduces the reader to the objectives and rationale of this study along with a summary of the methodology. Chapter 2, Literature Review, summarizes recent work on fatigue evaluation of FRP materials, environmental durability, and long-term performance. Chapter 3, Materials and Methodology, gives description of the materials studied including the manufacturing process. The methodology followed for conditioning and testing the specimens is described and justified. Chapter 4, Results of Physical and Mechanical Tests, describes the results of the tests conducted to evaluate static physical and mechanical properties. These properties were later used to develop fatigue parameters and baseline properties to compare with that of conditioned specimens. Chapter 5 gives the results of fatigue tests, including the S-N curves and residual strength findings. The statistical bounds on the S-N curves are also included. Chapter 6, Conclusions and Recommendations, summarizes all the findings and proposes design allowable limits for fatigue. Recommendations for future work are also given.

Several appendices are included to provide further documentation for the work. An appendix on SI unit conversion is also given.

2 LITERATURE REVIEW

2.1 Introduction to Fatigue

The concept of fatigue failure was discovered back in the 1800s when European investigators observed that a number of railroad (axle) and bridge components made of steel were cracking when subjected to repeated loading. It was in the mid 1800s when A. Wohler proposed a method to mitigate or in some cases eliminate fatigue failure. This method gave rise to the development of the 'Stress-Life response diagram' approach to fatigue design. But it was not until the early part of the 1900s that the physical basis of fatigue began to be understood (Taylor, 1989).

Fatigue in general is the reduction or decay of mechanical properties of a material subjected to cyclic loading. "*Fatigue*" is defined by ASTM E 1150 as: "the process of progressive localized permanent structural change occurring in a material subjected to fluctuating stresses and strains at some point or points and that may culminate in cracks or complete fracture after a significant number of fluctuations" (ASTM 1999). It is well known that when materials are subjected to fluctuating loads above their fatigue limit, they may fail at stresses well below their ultimate tensile strengths. This implies that cyclic loading can reduce the strength of a material. In fact, it has been reported that 50-90% of the failure of engineering components and structures are attributed to fatigue (Gao et al, 1994; Beynon et al, 1995). This premature failure or damage is often catastrophic and caused many injuries and financial losses in the past. To utilize structures

effectively and efficiently, the fatigue strength of the materials used must be well understood.

Fatigue strength is a measure of the materials resistance to the formation of cracks. It is a relative term and corresponds to a given number of cycles. For example in Figure 2.0 we observe that the fatigue strength at one million cycles is about 30%UTS. If cracks did not occur in materials, then fatigue would not be an issue. Thus fatigue falls within the study of fracture mechanics. Cracks may initiate from weak regions and points of high stress concentration. Cracks can also arise from surface imperfections and defects such as voids which are inherent in the material as a product of the manufacturing process (Beynon et al 1995).

Crack growth (damage mechanism) is much more complex in FRP materials compared to metallic materials because of its non-homogeneous content and anisotropic characteristics of its strength and stiffness (Whitworth et al, 1998). Fatigue damage initiates as micro crack in the matrix material and interfacial cracking between the matrix and fiber (Agarwal, 1990). As for steel, K.J. Miller (Baynon et al (Eds), 1999) states that it is the development of a specific dislocation structure, which leads to the formation of a crack.

Material failure occurs when the size of these cracks grows or propagates to a critical size. The crack growth process has two distinct phases namely (1) initiation and, (2) propagation. The initiation phase is said to be the time required to form a crack. The propagation phase is marked by growth of these cracks.

With the advent of specialized techniques such as Ultrasonic C-Scanning (best for observing delamination), Photomicrography, X-ray radiography (best for observing in plane damage such as transverse crack), Scanning Electron Microscopy (SEM), fluorescence and Non-destructive evaluation (NDE) methods, it has become easier to study the quality, quantity and behavior of cracks. Many theories of crack growth have been postulated to relate crack to the stress field. It was A.A. Griffith who first proposed an energy balance equation for fracture back in 1920 and to whom the origin of modern fracture mechanics for engineering practice is attributed (ASM Hand Book, 1998).

Fatigue is an important issue for engineers because most engineering materials such as steel, aluminum and Fiber Reinforced Plastics (FRP) are prone to fatigue damage when subjected to cyclic loading while in service. Fatigue is of particular interest to bridge engineers because bridges are continuously subjected to cyclic loading. Since bridges have been made of steel for a long time, a wealth of information, arising from the numerous fatigue researches exists today for steel connections and details. Fatigue design of steel members are described in the American Association of State Highway and Transportation Officials (AASHTO) specifications. Fatigue data pertaining to FRP in bridge applications is quite limited because it is still an emerging new technology. Data on the combination of fatigue with environmental degradation of FRP is very limited in open literature.

The growing use of composite materials in the transportation industry and the demand for better long-term performance makes fatigue analysis an important consideration.

2.2 AASHTO Fatigue Design Code for Steel

Fatigue design of steel members depends on the type of member being considered. Reduction factors are based on the geometry of the member. Fatigue strength of connections and joints are given special attention in AASHTO specifications because this is where most failures occur. The fatigue limit states are defined in terms of the accumulated cycles i.e. the maximum number of cycles that can be endured by a given member geometry before fatigue fracture occurs. Specification of load alone is not adequate and thus stress-range and frequency (traffic) of the loading are considered. Since truckloads are the heaviest, frequency is defined in terms of the truck loading in a given period. Research has shown that the average daily traffic (ADT) per lane under normal conditions, which includes all vehicles, is physically limited to 20,000 (AASHTO Section C3.6.1.4.2). Some 15-20% of this traffic is due to trucks depending on where the bridge is located. The fatigue limits for steel structures are calculated as described below (AASHTO, 1994):

Average daily truck traffic on a single lane. $(ADTT)_{SL} = p \times ADTT$

where p depends on the number of lanes available to trucks. p=1 (one lane)

In urban areas $ADTT_{SL} = 0.15 \times ADT$ (AASHTO Table 3.6.1.4.2.1)

In rural areas $ADTT_{SL} = 0.20 \times ADT$

Basic design:

$$\mathbf{y\,\Delta f \leq (\Delta F)_n} \qquad \text{Eqn 2-1}$$

where,

y = load factor (0.75 for fatigue)

Δf = live load stress range due to the passage of the fatigue load

ΔF = nominal fatigue resistance

n = 1 for fatigue

Equation 2-1 simply states that the applied fatigue load multiplied with the load factor shall be less than the nominal fatigue resistance. Nominal fatigue resistance is given by:

$$\mathbf{(\Delta F)_n = (A/N)^{1/3} \geq \tfrac{1}{2}\,(\Delta F)_{TH}} \qquad \text{Eqn 2-2}$$

where,

$(\Delta F)_n$ is the nominal fatigue resistance (ksi).

$N = (365)\,(75)\,n\,(ADTT)_{SL}$, where n is the number of stress range cycles per truck taken from AASHTO Table 6.6.1.2.5-2.

A = detail category constant taken from AASHTO Table 6.6.1.2.5-1.

$(\Delta F)_{TH}$ = constant amplitude fatigue threshold (ksi) taken from AASHTO Table 6.6.1.2.5-3.

Equation 2-2 above states that the fatigue resistance must be equal to or greater than half the constant amplitude fatigue threshold of the particular geometry considered. If the fatigue stress range (load) is below the threshold, the

member is said to have infinite life. The design life is considered 75 years and can be changed depending on the use of the bridge. The constant N approximates the number of load cycles the bridge is expected to endure during its service. Consider a single span steel girder bridge longer than 40 ft (n=1) designed to last 75 years. Assuming we are designing a plain (detail category A) section, the constant A is given as $250x10^8$ (AASHTO Table 6.6.1.2.5-1). The constant amplitude fatigue threshold for this member is given as 24 ksi. The fatigue resistance $(\Delta F)_n$ of this member would thus be 6.11 ksi. Since this number is less than half the fatigue threshold, the design stress range of 12 ksi will be used.

2.3 Fatigue of FRP (Polymer Composites) Materials

2.3.1 General Overview

Curtis et al (1989) reported that the increasing use of FRP in primary structures is mainly because of their high strength and stiffness combined with low density compared to steel. However, like steel, FRP materials also undergo fatigue degradation when subjected to cyclic loading. Unidirectional FRP materials have been shown to posses excellent fatigue resistance in the fiber direction. This is because the load in the longitudinal direction is primarily carried by the fiber, which exhibits excellent resistance to fatigue compared to the matrix material (Agarwal, 1990).

Exposure to fatigue leads to the formation of cracks first in the matrix and then into the fiber. FRP materials can be made in a variety of laminate combinations (laminates with different orientations) and shapes, and this makes fatigue analysis rather difficult.

Fatigue failure is first seen in the most brittle component (lowest failure strain). As a result, the matrix (resin) material is damaged first by the formation of cracks. Fatigue failure in a FRP laminate may occur in many forms such as fiber fracture, failure in fiber-matrix interface, delamination, matrix cracking and void growth (Stinchcomb et al, 1995). Cracking results in the lowering of both stiffness and strength of FRP materials. As a result the residual strength and stiffness decrease with increasing crack density. Crack accumulation and density varies depending on the orientation of the laminates.

In multidirectional laminates, cracking occurs in succession from the weakest layer (off axis-90°) to the strongest layer (0°) (ASM Hand Book, 1998). When the crack growth reaches a certain limit, stresses cannot be transferred from the matrix to the fibers. At this stage only the fibers carry load and final failure occurs due to fiber fracture.

In unidirectional FRP material, since fibers virtually carry the entire load, the matrix shows extensive longitudinal splitting parallel to the fibers caused by interfacial damage. This can result in brush-like failure characteristic of most unidirectional materials (Curtis, 1989). Fabric based or woven FRP materials offer greater versatility in producing complex shapes but are known to exhibit lower static stiffness and strengths due to the distortion of fibers in the weave.

Curtis (1989) also reports that another reason for this is that high fiber volume fraction (60-65) is usually not achievable in woven FRP. Fatigue strengths of woven unidirectional FRP are also low compared to non-woven unidirectional FRP mainly due to the effect of stress-concentrations near fiber tow crossover points in the fabric, which induce premature damage in the fiber/matrix interface.

The degradation process in the matrix in an FRP is primarily controlled by the bulk strain in the matrix. Polymer composites or FRP made with carbon fibers (typically with stiffness of 220-700 GPa and failure strains of 0.6-1.8%) exhibit lower strains in the matrix (see section 2.3.2) and as a result have better fatigue strengths (shallow S-N curve). Using glass-fiber reinforced plastics (GFRP), which have lower stiffness (typically with stiffness of 70-80 GPa and strains of 2.5-3.5%) compared to carbon fibers leads to greater matrix strains and thus comparatively lower fatigue strengths (steeper S-N curve) (Curtis, 1989, 1991). Aramid fiber has stiffness between that of carbon and glass fibers (typically 120 GPa) and as a result is expected to show intermediate fatigue behavior. Aramid fibers are sensitive to fatigue (may defibrillate) but carbon and glass fibers do not show this effect.

A good composite must have strong and durable fiber-matrix interface to reduce both crack initiation and propagation. During fatigue, the rise in temperature caused due to viscoelastic energy dissipation may also contribute to the weakening of the material and shortening of its fatigue life (Agarwal, 1990).

Unidirectional composites are not the optimum design for fatigue. This is because of the splitting in the fiber direction resulting from low transverse strength and imperfect gripping condition (Agarwal, 1990). This problem may be mitigated by providing a few plies in the 90° directions. The 90° plies help in terminating crack growth as seen in Figure 2.1.

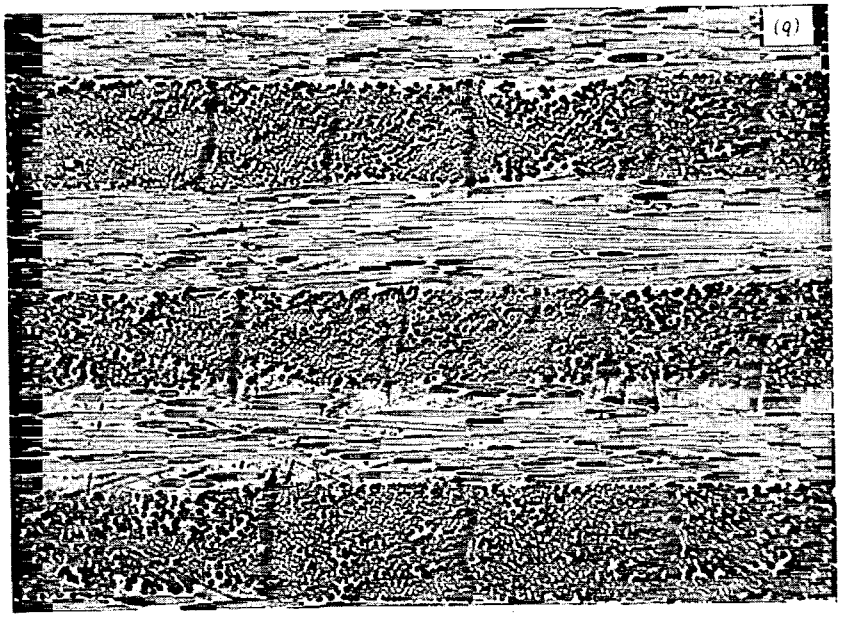

Figure 2.1 Delamination-Crack Terminations on a Cross -ply Laminate (Agarwal, 1990)

2.3.2 Representation of Fatigue Life: S-N Curves

The most common method of presenting fatigue data is to plot the applied stress (S) against the number of cycles (N) to failure. These plots are called S-N curves. The ordinate is usually the maximum stress or stress range ($\Delta S = S_{max}-S_{min}$), strain or the stress or strain amplitude that is usually plotted on a linear scale.

The abscissa of the plot is usually the number of cycles to failure for a fixed stress or strain cycle and is usually plotted on a logarithmic scale. The stress ratio (R), defined as the ratio of minimum to maximum stress and the test frequency (Hz) are kept constant for all the specimens for which an S-N curve is developed. All materials including metals and composites exhibit a negative slope. This shows that for all materials, the number of cycles to failure increases as the applied cyclic load decreases. As for the exact shape of the curve, it depends on the material and testing variables. The S-N curve of composite materials generally depend on factors such as:

Material variables:

1. Fiber material and volume fraction (V_f)
2. Matrix material (resin)
3. Ply orientation
4. Interface properties

Test variables:

1. Type of loading (tension-tension, tension-compression)
2. Mean stress
3. Frequency
4. Environment

The S-N curves of FRP materials are generally linear (Figure 2.2) for lives less than one million cycles.

The S-N curve of a typical FRP material may be expressed using a linear equation:

$$\sigma_{app}/\ \sigma_{stat} = A + B \log N \qquad \text{Eqn 2-3}$$

where A and B are material constants. Another model for S-N curve of unidirectional FRP material is given by S. Subramanian, and K.L. Reifsnider (Sridharan et al, 1998):

$$\sigma_{app}/\ \sigma_{stat} = A_n - B_n [\log (N)]^{Pn} \qquad \text{Eqn 2-4}$$

where,

σ_{app} - applied stress

σ_{stat} - static strength

A_n, B_n, Pn are material constants.

At a very low stress, the S-N curve of most ferrous and non-ferrous materials flattens indicating infinite life. Infinite life is said to exist when the applied stress is below the fatigue threshold. Since fatigue involves cycling over a range of stresses (between maximum and minimum stresses), it is more appropriate to use the *stress range* term rather than stress alone. Although steel and its alloys are known to exhibit distinct endurance limit it is generally not true for non-ferrous materials. In FRP materials, the term endurance limit is better explained by fatigue threshold, which is that stress or load below which a crack does not form or grow.

Fatigue threshold of FRP materials have been studied by a few authors including Taylor (1989) and is reported to be dependent on many factors such as type of reinforcements, matrix, curing method and fiber orientations.

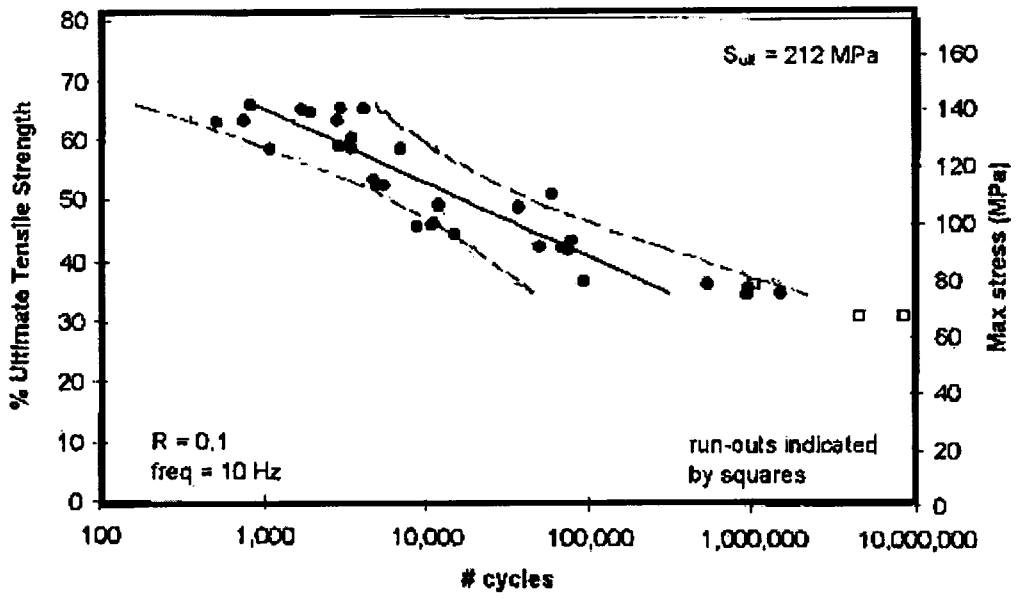

Figure 2.2 Typical S-N Curve with 95% Confidence Bands (Hayes et al, 1998)

Among the resins, Agarwal (1990) reports that epoxy exhibits the best fatigue property because of their inherent toughness, durability, low shrinkage during cure, and high mechanical strength. FRP made with high modulus fibers such as graphite or carbon, aramid, and boron fibers show excellent fatigue resistance when properties are fiber controlled in the testing direction. This is due to the fact that these fibers are more environmentally stable compared to glass fibers, and has low strain to failure, which induce low strains in the matrix material.

As a result the S-N curves of FRP made with these fibers have smaller slopes. Some examples of fatigue strength of different composites are given in Table 2.1.

Table 2.1 Typical Fatigue Strength of Unidirectional FRP Materials

Material systems	Fatigue Strength (ksi)				R	Reference
	10^6 cycles		10^7 cycles			
	ksi	MPa	Ksi	MPa		
E-glass / Phenolic	30	207			0	Branco et al, 1994
E-Glass / Epoxy	30	207			0.1	Agarwal, 1990
Graphite / Epoxy	140	965	30	207	0.1	Agarwal, 1990
Kevlar 49 / Epoxy	150	1034	140	965	0.1	Agarwal, 1990
E-Glass / vinyl ester	9	62			0.1	Hayes et al, 1998
S2 Glass / Epoxy	50	345			0.1	Hayes et al, 1998
Boron / Epoxy	150	1034	140	965	0.1	Agarwal, 1990
2024-T351 Aluminum	21 (threshold)	145			0.1	Chatterjee et al, 1997
Steel	24 (threshold)	166			0.1	AASHTO, 1994

2.3.3 Standard Method for Fatigue Testing of FRP

Parameters for the fatigue testing are usually specified to closely approximate real-life situation. Thus, specimens may be tested in tension-tension, tension-compression or compression-compression fatigue. Testing can be done on both life-size specimens and on coupon level.

Although there are no guidelines for testing life-size specimens in the laboratory, researchers have followed AASHTO load specifications when testing a bridge member (Lopez-Anido et al, 1999).

Coupon testing of FRP materials can be carried out according to ASTM D3479 "Tension-Tension Fatigue of Polymer Matrix Composite Materials", which is described in the methodology section (section 3.5.3.1). The coupons are usually machined to a rectangular or dog-bone shape. The aforementioned ASTM method suggests rectangular specimens. Gripping is a continuous and irksome problem in fatigue testing because specimens are prone to failure at the grips. However rectangular specimens have been used successfully when well-machined and proper grips are used. It is also much easier to fabricate defect-free rectangular specimens compared to dog-bone specimens, which require specialized machinery such as CNC and water jet cutting systems.

Servo hydraulic machines such as those manufactured by INSTRON and MTS are commonly used to apply fatigue loading. The loading pattern can be sinusoidal, triangular or square and the amplitude may be constant or variable. Constant amplitude sinusoidal loading is a common method used to test composite materials (Branco et al, 1996). Frequencies ranging from 5 to 20 Hz have been used to study fatigue behavior of FRP materials (Branco et al, 1992). A point on the S-N curve represents a specimen tested at a particular stress range and the corresponding number of cycles at which it failed; stress ratio (R) and frequency being the same for all specimens. If a specimen is tested for high cycle life, a simple S-N curve may require many months to develop.

2.3.4 Residual Strength Modeling of FRP Materials

Residual strength is the remaining static strength of the FRP after it has been subjected to a given number of cycles (Figure 2.3). To obtain the residual strength, a specimen is fatigued for a given number of cycles at a particular stress range and then tested statically to failure. Hayes et al. (1998) suggested an equation for modeling residual (remaining) strength of FRP material:

$$S_{res}/S_{uts} = 1 - (1 - S_a/S_{uts})\,(n/N)^{\alpha} \qquad \text{Eqn 2-5}$$

where S_{res} is the residual strength,

S_{ult} is the ultimate strength

S_a is the applied stress

N is the life of the specimen

n is the number of loading cycles applied on the specimen.

α accounts for the non-linearity in the strength reduction curve.

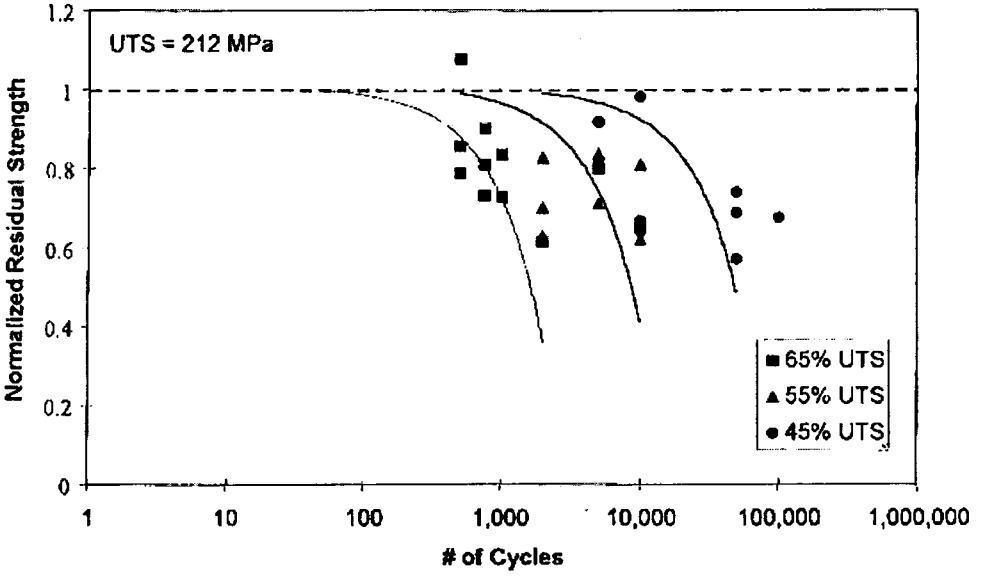

Figure 2.3. Typical Residual Strength Curve of an FRP Material (Hayes et al, 1998).

Residual strength tests indicate the extent of damage in a material and allow one to predict properties of a material after it has been subjected to cyclic loading. This tool is very useful for estimating remaining service life of materials used in structures such as bridges.

2.3.5 Fatigue of Phenolic Composites

Although today vinyl ester and polyester composites dominate the construction industry for structural applications, the reasons for using phenolic resins are many. In the construction industry fire hazards are a growing concern. Phenolic resins are known to perform better at high temperatures compared to other resins. Traditionally, phenolic materials were used in a variety of household goods such as handles in cooking utensils, radio buttons, and counter-tops. This is due to their excellent thermal and dimensional stability at elevated temperatures, and due to superior chemical and corrosion resistance compared to other thermosetting polymeric materials.

Phenolic compounds are also known to possess low toxicity and low smoke emission at temperatures up to 200°C (Branco, 1996). These properties have been advantageously used today in the making of Phenolic fiber-reinforced polymers for structural applications. Among the fibers, glass fiber seems to be the most attractive reinforcement for phenolic resins due to their high tensile strength, corrosion resistance and low cost.

Phenolic composites reinforced with glass fibers have been well received by the auto and aerospace industries, which uses them for interior molding and body panels such as cockpit panels and seats in aircraft, pulleys, intake manifolds, water pumps, and valve covers etc (Branco et al, 1994). They have also been successfully used as body frames in railway carriages and buses not only because of high strength/weight ratio and better creep resistance at high temperature but also because of faster manufacturing processes available today. Although phenolic composites are not yet widely used by the construction industry, phenolic adhesive such as phenol resorcinol formaldehyde (PRF) is widely used by the plywood industry for exterior application. This is due to its ability to form excellent adhesive bond with wood. The chemical structure of Phenolic compounds is also similar to that of Lignin present in wood species (Bodig, 1992).

Phenolic composites are thus an excellent choice for reinforcing wood and wood composites. However as this concept is quite new, the data available in the open scientific literature pertaining to phenolic GFRP is quite limited. Most available data consists of thermal and tensile properties in the form of product literature published by manufacturers. Most durability data of composites is currently available from the use of FRP by the aerospace industries. This data is mostly restricted to epoxy resins and carbon fibers. Very few articles in the open literature pertain to durability of E-glass reinforced phenolic composites.

Branco and Ferreira (1994, 1996) tested tension-tension fatigue properties of pultruded and hand lay-up phenolic GFRP at varying temperatures, frequencies, stress ratios and fiber lay-up. It was observed that the fatigue strength of phenolic composites, like other composites, increases with the fiber volume fraction. The Young's modulus and rupture stress were shown to decrease as the temperature was increased from 20° C to 200°C. The authors tested dog-bone coupons measuring 220mm in length, 22mm in width and 2mm thick. The narrow part of the coupon (gauge length) was only 40mm long. A silane-coupling agent was used to enhance bonding during manufacturing.

They have observed that the fatigue strength at room temperature of pultruded unidirectional E-glass phenolic composites (700MPa UTS) was 40%UTS at 10^4 cycles and 30%UTS at 10^6 cycles for R=0 and frequency of 10 Hz. Fatigue strength decreased by 10% when the frequency was reduced from 10Hz to 1.5Hz. All the different types of hand lay-up composites have shown higher fatigue lives when the stress ratio was increased from R=0 to R=0.4-0.5. The pultruded specimens were tested at room temperature only, and their fatigue strengths were shown to be lower (10%) than unidirectional hand lay-up specimens at 2 million cycles. Woven pultruded composites gave the lowest fatigue strength data of all the composites tested. From SEM scans, the authors have concluded that the main failure mechanism was shear delamination between the resin and the fiber.

The S-N curves were modeled using log-log linear regression analysis as shown below.

$$\text{Log}(\Delta\sigma) = a\ \text{Log}(N) + b \qquad \text{Eqn 2-5}$$

where $\Delta\sigma$ is the applied stress range and N is the number of cycles to failure. The constants *a* and *b* are material specific parameters. Hand lay-up unidirectional composites were also tested for their fatigue strength at 1.5, 10 and 25Hz. Branco et al (1996) reported that at room temperature, the fatigue life of a unidirectional pultruded GFRP (700 MPa UTS) was approximately 1 million cycles at 21%UTS. They also reported that a woven pultruded E-glass phenolic FRP with 305 MPa UTS had a fatigue life of 1 million cycles at 28% UTS.

It was concluded that fatigue strength increased when the testing frequency was increased from 1.5Hz to 10Hz. Further increase to 25Hz had negligible effect on fatigue life. It was observed that virtually no loss in stiffness occurred up to 75% of the fatigue life. The modulus starts to reduce after 75% of the fatigue life and the maximum reduction occurs when there is only about 15% of the life remaining. The authors stated that the fatigue strength of phenolic composites were lower than those of epoxy and polyester matrices.

2.3.6 Design Methodology for Fatigue of Composite Materials

To account for fatigue, composites are designed to carry stresses well below their ultimate tensile strength. Typically these stresses are selected from the S-N curves where the curve tends to flatten. The design is also very much dependent on the application.

Composites are most sensitive to fatigue when they are subjected to high frequency and stresses such as in high-speed cutting tools and machinery. As a result, the life of such composites will be estimated differently from say a structural member in a building subjected to wind loads.

The basic fatigue design method for any material is to ensure that the particular member has infinite life when subjected to fluctuating loads. The condition of infinite life is met when the maximum stress range induced is less than the fatigue threshold stress range. The fatigue threshold stress range is that stress range just sufficient to initiate and grow a short fatigue crack [58]. Since below this threshold no cracks are expected to occur, a material is said to exhibit infinite life. Fatigue limit and Endurance limit can be and often is used as synonyms of fatigue threshold although fatigue threshold is specifically derived from fracture mechanics concepts and the others are not.

Tolerance limits are also used to estimate safe design life of composites. The tolerance limit method has been used for fatigue design of steel, wood and polymer composites (Wirsching, 1983; Bond et al, 1998; Roland et al, 1996). The most common method is to use the lower 95% tolerance (one-sided) for 95% of the population. This tolerance is also called the 5% Lower Tolerance Limit (LTL). This tolerance limit describes a lower limit to the data, above which one can say that at least 95% of future observations (or sampled normal population) will have a 95% survival probability.

The 5% LTL was used here because it provides a precise statistical lower boundary which is not too stringent for widely scattered fatigue data (Bond et al, 1998). This method has been in use for a long time and has been used to study fatigue of steel connections (Little (Ed), 1979).

2.4 Environmental Degradation of Composite Materials

The sources of degradation from the environment are many. Moisture is the most common source and is known to affect both the fibers and the matrix. Ultraviolet light from the sun, concrete pore water and salt water from de-icing salts cause damage to both fiber and matrix. The synergistic effects of temperature and fatigue have been studied by Branco et al. (1994) and Liao et al (1998). Strong acids and bases are also known to cause significant damage to FRP material.

Fatigue testing of environmentally conditioned Phenolic composites is yet to be found in literature. Since Vinyl Ester composites are widely used in the construction industry, it is worthwhile mentioning some of the findings pertaining to fatigue strength of these composites. Hayes et al (1998) studied the effects of moisture on the fatigue strength of glass/vinyl ester composites. They have stated that moisture acts as a plasticizer in the matrix and thus lowers the glass transition temperature (Tg). The lowering of glass transition temperature causes reduction in modulus, tensile strength, and fracture toughness. When the composite is dried, the effect of plasticization is reduced, although permanent damage such as matrix cracking, hydrolysis and fiber-matrix debonding can occur due to the swelling stresses.

The combined effects of moisture, temperature and stress are difficult to model and predict. In this study Hayes et al (1998) have used off-the-shelf unidirectional pultruded composite plates with random-fiber continuous strand mat layers. They fail to report the exact quantity of unidirectional and random mat layers. The total fiber volume fraction was 50-55%. The coupons were 6" long, 1" wide and 1/8" thick. Samples were tested in tension-tension fatigue at 10Hz and stress ratio R=0.1. The authors have concluded that the results are dependent on fiber and matrix lay-up, laminate lay-up, pre-conditioning methods, solution contents and the environmental conditions during fatigue. The damage due to moisture is fiber-dominated and is irreversible. The static tensile strength was reduced by as much as 26% at a moisture concentration of 0.95% by weight. This reduction in static strength causes a vertical shift in the S-N curve. Thus moisture does not affect fatigue mechanism.

2.5 Summary

Fatigue has been a design consideration ever since engineers realized that metals such as steel and aluminum might fail at stresses well below the UTS when subjected to fluctuating loads. With the advent of high strength fibers such as Carbon, Kevlar, Boron and Glass, metals are being replaced in some application in favor of FRP materials mainly due to their high strength to weight ratio. Glass fiber reinforced plastics (GFRP) composites are widely used because of comparatively low unit cost. Like steel, FRP materials are also prone to fatigue degradation due to crack initiation and propagation.

Fatigue behavior is commonly represented by an S-N curve, which plots the number of load cycles it takes to fail a specimen when subjected to a particular stress range. Unidirectional (0°) FRP material in general performs better in fatigue than multidirectional laminate FRP. Fatigue failure in unidirectional FRP material initiates with matrix cracking or splitting parallel to fiber direction. This results in fiber-matrix debonding and ineffective load distribution, which leads to fracture of weaker fibers and consequently total failure.

In multidirectional laminates failure occurs in succession from the 90° to the 0° plies. For a given type of laminate and testing parameters FRP materials with higher fiber volume fraction show higher fatigue performance. Carbon and Epoxy show the best fatigue properties among fibers and matrix materials respectively.

Moisture can cause significant damage to FRP materials by degrading the fiber-matrix interface. Among the fibers mentioned above, carbon fibers are least affected by moisture (Curtis, 1989). A strong interface ensures protection to the fiber. Fatigue data of E-glass phenolic composites are scarce in literature and some authors have stated that the fatigue strength of phenolic composites in general is lower than those of epoxy and polyester matrices. The basic fatigue design method for any composite is to limit the maximum stress range such that it is lower than the constant amplitude fatigue threshold.

3 MATERIALS AND METHODOLOGY

3.1 Introduction

This chapter describes the materials used in the study; pultruded and hand lay-up GFRP, the methods used to condition the specimens prior to testing, and the testing methods followed to determine physical, mechanical and fatigue properties. The pultruded GFRP was exposed to five different types of environments, which include control (at RT air), freeze-thaw, hot water, UV weathering, and simulated seawater. The exposed specimens were then tested for the change in mechanical and fatigue properties at the end of the exposure period. The hand lay-up GFRP was not exposed to any of the environments but tested for static and fatigue control properties.

3.2 Rationale

The mechanical properties of GFRP are known to degrade when exposed to a variety of environments including high temperature and humidity. Strong acids and bases are also known to cause significant reduction in the mechanical properties of GFRP. Thus, it becomes imperative to study the extent of damage for design purposes. Other factors such as salt from deicing materials and concrete pore water are studied because GFRP used in Glulam beams for bridge application may be exposed to these chemicals. Since it is not always practical to study long-term durability on in-service structures, accelerated tests are performed in the laboratory on small-scale specimens such as coupons to

simulate real life conditions. In this study GFRP plates were conditioned in different solutions and environmental exposures. After the conditioning period, ASTM specified coupons were cut and promptly tested for physical and mechanical properties. To maintain consistency in the testing methods, American Standards for Testing and Materials (ASTM) specified methods were followed in all cases. International Conference of Building Officials (ICBO), Acceptance Criteria (AC) 125 in particular specifies evaluation tests for FRP materials for reinforced and unreinforced masonry. This specification recommends tests to evaluate FRP materials for exterior purposes. These methods were followed for conditioning the specimens to the different exposure environments. ASTM E 632 was also reviewed to help with organizing the tests.

3.3 Materials

Pultruded and hand lay-up GFRP are the two types of glass fiber reinforced polymers (GFRP) evaluated in this study. A brief description of a glulam beam is also given since these GFRP materials were designed to be used as tension reinforcement in glulam beams.

3.3.1 Pultruded Phenolic GRFP

The pultruded GFRP was designed and formulated by a team of University of Maine, Orono Maine and Winona State University, Winona Minnesota engineers. It was manufactured at Strongwell, Chatfield Minnesota. This GFRP consists of approximately 54% unidirectional glass fiber, 22% phenolic resin, and 24% voids by volume. It is approximately 3.3mm (0.13in) thick and 120mm (4.725in) wide

(Figure 3.1). The reinforcement used is made of E-glass fibers (10-20 microns), which have high tensile strength (1.7 GPa, 250 ksi) and low density (2.54 g/cm^3)

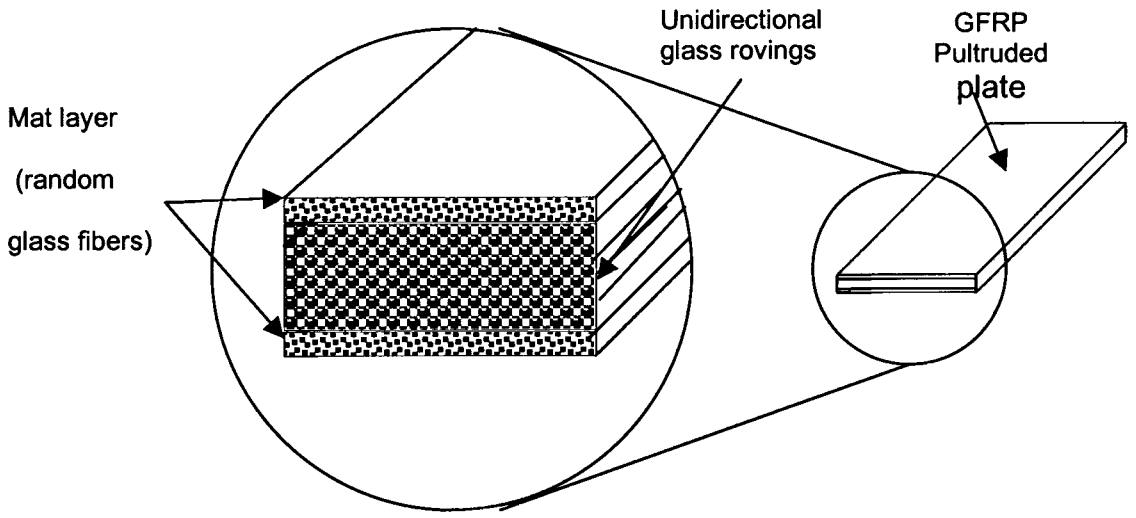

Figure 3.1 Cross Section of GFRP Showing the Different Layers

compared to mild steel; 0.640 GPa (92 Ksi) and 7.8 g/cm^3 respectively (Agarwal, 1990). These fibers are also the least expensive ($0.6/lb) compared to other common fibers (carbon- $8.0/lb) and most readily available. The fibers have also been coated with a suitable sizing to enhance bonding with the phenolic resin. The matrix used is a one-part phenolic resin supplied by Georgia Pacific. It is a thermosetting resin and cures at high temperature. It is formulated to produce maximum wetting of fibers. Good wetting ensures good bonding and better protection of the fibers. Phenolic resin is used as the matrix because of its low cost compared to epoxies as well as its fire resistance characteristics and good bonding with wood.

The GFRP is encased on both faces by a thin mat layer. The surface mat layers consist of randomly oriented short glass fibers, which constitute high porosity. The porosity facilitates bonding of the GFRP with wood or other material

through mechanical interlocking. When bonded to wood laminations, the unidirectional glass fibers are aligned parallel to the wood grain (longitudinal).

The GFRP was manufactured using the pultrusion method, which can only produce constant cross-section composites. A schematic view of a pultrusion process used to manufacture the pultruded GFRP is shown in Figure 3.2. The process consists of pulling continuous rovings of glass fibers/mats through a resin bath, and then through a preforming die where it is shaped and excess resin is removed.

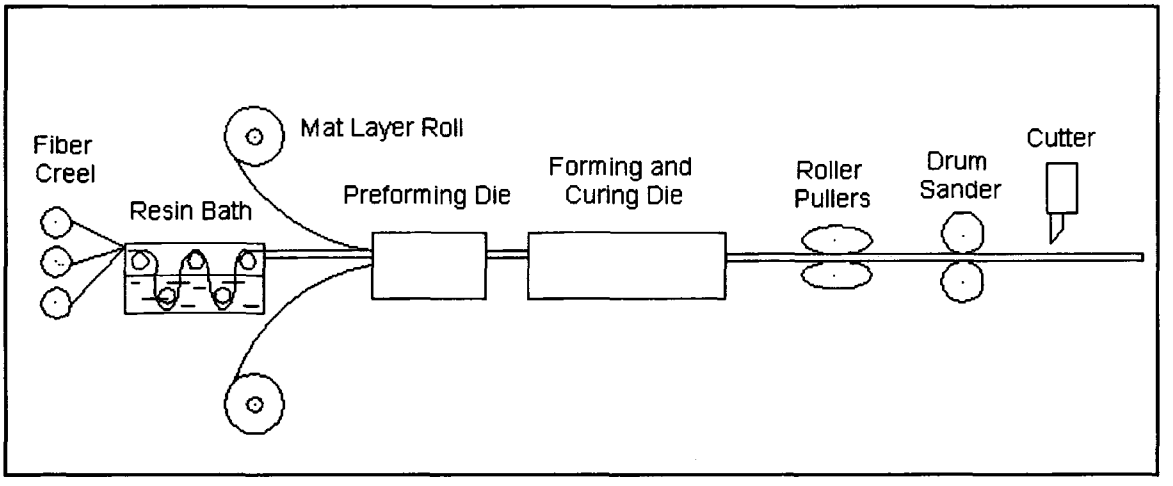

Figure 3.2 Schematic of the Pultrusion Method for Resin Starved Mat Layers

The unidirectional core is then surfaced with the mat layer, on top and bottom faces. It then goes through a heated die where the section is cured continuously. Special pullers are used at the front end of the pultrusion process to pull the section continuously. Cut-off saws are used at the end of the production line to section the composite as desired. The GFRP is passed through a drum sander to remove the gloss from both faces, and then rolled for shipment.

Different types of GFRP were pultruded by varying the resin quality and quantity. A letter and a number designated the different types of GFRP. The ultimate GFRP manufactured was designated K-1 after several cyclic-delamination tests were done on its predecessors, I-2 and I-3 to evaluate bond compatibility with wood. The manufacturing parameters for this GFRP cannot be disclosed due to pending patents. In this study only K-1 pultruded GFRP was used.

3.3.2 Hand Lay-up GFRP

The hand Lay-up GFRP consists of unidirectional woven E-glass fibers in a Phenol Resorcinol Formaldehyde (PRF) adhesive matrix. The glass fiber fabrics were provided by Brunswick Technologies, Inc (BTI) of Brunswick, Maine. The unidirectional glass fabrics weighed 26 oz/yd^2. They were shipped in rolled mats of varying widths. The resin (GP 4242) and hardener (GP 4554) were both obtained from Georgia Pacific Resins, Inc.

The matrix is a three-part adhesive that was prepared by mixing water, hardener and resin in an 18:12:70 ratio respectively. This ratio allowed a workable time of only 45 minutes. The powdered hardener was first mixed with water to form liquid slurry followed by the addition of resin. The mixture was stirred for at least five minutes to ensure uniform consistency. A resin impregnator was used to infuse the resin into the woven fiber mats. The gap between the rollers was adjusted to obtain pre-cure 50:50 ratio of fiber to resin.

Mats were cut to 280cm long and then after being impregnated with adhesive they were folded to form five-layered 50cm long plates. Each plate was then pressed between two steel plates and clamped at 550kPa (80 psi) for 24 hours at room temperature. They were allowed to dry for two weeks at room temperature after unclamping. Tensile coupons were then cut from these plates using a wet diamond saw. The typical properties of the adhesive mix are given in Table 3.1.

Table 3.1 Typical Properties of PRF Uncured Adhesive Mix [GP PUB 151]

Appearance	Red/brown-slurry
Mix Ratio; parts by weight	70 resin : 30 hardener (water added)
Wet Density , lbs./gal (kg/l). @ 25 C	9.5(1.13) – 9.7(1.16)
Viscosity, cps @ 25 C	3000- 6000
pH	8.7-9.0
Free Formaldehyde, %	< 1.0
Gelation Time at 25 C	1.58 – 2.25 hours

3.3.3 Glue-Laminated Beam (Glulam)

The cross-sectional dimensions and length of sawn lumber are limited by the size of the tress available to produce this type of lumber. Thus when span becomes long, sawn lumber is impractical and glulam beams are used. Glulam beams (Figure 3.3) are fabricated from thin laminations of solid wood, which can be end-jointed and glued together to produce wood members of practically any size that can be shipped.

The structural properties of glulam members in most cases exceed those of sawn lumber (Breyer, 1993). A reason for this is that laminating wood optimizes material by dispersing the strength reducing defects in the laminating material throughout the member. Glulam beams also make efficient use of available structural material by incorporating high-quality laminations in the portions of the cross-section that are more highly stressed. Phenol Resorcinol Formaldehyde (PRF) is the common adhesive used in glue-laminating plants.

Glulams also have a number of advantages. Large glulam have good fire resistance because they are charred in a fire and not readily consumed.

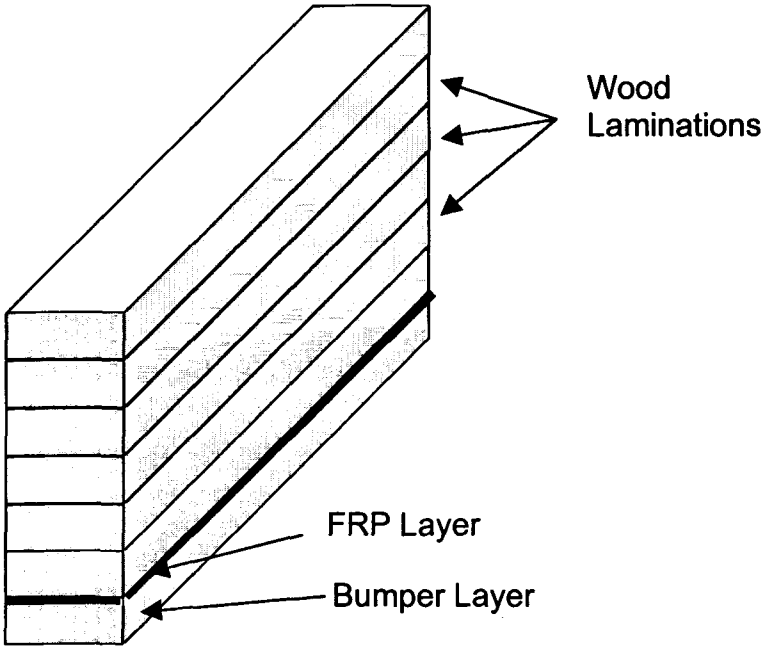

Figure 3.3 An FRP Glulam Showing Location of FRP Reinforcement

The outer charred layer acts as a thermal shield to the core. Glulam beams exhibit good fatigue strength and are aesthetically pleasing. Another advantage is that they do not rust or corrode and therefore are used in industrial storage buildings for alumina, salt and potash, which corrode steel. Glulam beams can be strengthened with fiber-reinforced plastics (FRP) just as concrete is reinforced with steel. The FRP is usually laminated into the beam in the tension zone. They are typically called FRP-Glulam (Figure 3.3). The GFRP used in this study is intended as a tension lamination for glulam beams.

3.4 Summary of Test Program

To evaluate environmental durability, the pultruded GFRP was exposed to different artificial environments. At the end of the exposure period, the specimens were tested for both static and fatigue strength retentions. The wet-preg GFRP was tested for static and fatigue control properties. The following section (section 3.4) describes how the exposure environments were prepared. Section 3.5 describes the testing methods followed to determine strength retention. The entire test matrix is given in Table 3.2.

Table 3.2 Summary of Entire Test Plan

Test Type and Method		Number of Specimens						
		Total No. Of Specimens	Pultruded GFRP					Hand Lay-up GFRP
			Dry Control	Hot Water	Freeze-Thaw ICBO AC 125	Simulated seawater ASTM D 1141 ICBO AC 125	UV Weathering ASTM G 53 ICBO AC 125	Dry Control
Density ASTM D 792		10	5					5
V_f, Voids ASTM D 2584		10	5					5
T_g, DMTA ASTM D 5418 and ASTM E 1640		25	5	5	5	5	5	
Longitudinal Tensile properties ASTM D 3039		42	7	7	7	7	7	7
Interlaminar Shear Strength ASTM D 2344		50	10	10	10	10	10	
Fatigue Strength ASTM D 3479	70%	9	5					4
	60%	9	5					4
	50%	25	5	4	4	4	4	4
	40%	25	5	4	4	4	4	4
	30%	25	5	4	4	4	4	4
	20%	25	5	4	4	4	4	4
Residual Strength ASTM D 3479	10%	18	18					
Microscopy	SEM	7	1	1	1	1	1	2
	STEREO	13	1	1	2	2	2	5

3.5 Exposure Methods

Pultruded FRP was exposed to five different environments as shown in Table 3.2 in addition to room temperature and humidity. Hand lay-up FRP was not exposed to any of the environments but conditioned to room temperature and humidity only. These five exposure environments are known to degrade FRP material properties. Pultruded specimens were exposed to the different environments as per ASTM or ICBO AC 125 specifications.

To simulate actual conditions in glulam beams, all pultruded specimens were primed with PRF and allowed to dry for two weeks before exposure. Instead of exposing test coupons, 25.4cm (10in) long plates were exposed with the as received width (12cm, 4.725in) to reduce edge effect and ensure uniform diffusion. The exposed edges were sealed off with a durable epoxy adhesive. The epoxy was cured at room temperature and not cured in an oven to avoid any pre-exposure effects. Seven 12.7mm (0.5in) wide tensile coupons could be cut from each plate. High-density Polyethylene (HDPE) tanks, which are known to be inert to most solvents, were used to expose the specimens to different solutions. Wherever applicable only TYPE I distilled water was used in preparing the solutions. Each tank had a capacity of 20 liters (6 gal) and a separate tank was used for each exposure setting. The tanks were also covered with a spill-proof lid to minimize evaporation and spilling during handling. The exposure test matrix is given in Table 3.3.

Table 3.3 Exposure Parameters for Pultruded GFRP

Exposure		No. Of plates*	Exposure Parameters	Duration	Conditioning Method	Retention as per ICBO AC 125
A	Control	8	50% RH, 23°C	3000 hrs	Relevant ASTM	-
B	Freeze-thaw cycling	8	-18°C –12 hrs 38°C –12 hrs	3 weeks at 38°C followed by 20 cycles	ICBO AC 125	90%
C	Hot Water	16	45°C (100% RH)	3000 hrs	ASTM D 570	-
D	UV weathering	8	63°C, 102 min UV + 18 min of UV+water spray	2000 hrs	ASTM G 53, ICBO AC 125	90%
E	Simulated seawater	8	8.2 pH (100% RH)	3000 hrs	ASTM D 1141	85%

*Plate size: 11cm x 25cm. Seven tensile coupons (12.7mm wide) were cut from each plate.

3.5.1 Priming Method

Prior to exposure to the different environments, all pultruded specimens were primed with PRF, which is commonly used to bond wood in glue-laminated beams. The hand lay-up GFRP did not need to be primed as it was not exposed to the different environments and did not have surface porosity like the pultruded GFRP. The priming method consisted of simply painting the surface with PRF and using a roller to ensure consistent penetration. The adhesive was rolled over twice on each face and excess adhesive was immediately wiped off with a squeegee.

The specimens were kept upright in a rack and dried at room temperature for three weeks. The rationale behind priming is that the GFRP will always be primed with the adhesive just as any wood lamination in a glue-laminated beam and this will simulate real-life conditions.

3.5.2 Room Temperature Conditioning (Control specimens)

Room temperature specimens, designated as control specimens were kept in a humidity and temperature-controlled laboratory. The humidity and temperature were maintained at 50 ± 10% RH and 23.0 ± 3° C (73° F) respectively. The specimens were conditioned at the aforementioned humidity and temperature for at least three weeks before testing. This period includes PRF primer cure time.

3.5.3 Freeze-thaw Cycling

ICBO AC-125 specified this exposure method. It is intended to measure the damage caused by thermal shock due to sudden change in temperature and humidity. Ten plates of pultruded FRP were exposed to this environment. A 300-watt heater with a thermostat was used to maintain the temperature. A water pump with a 4-liters/min capacity was used to circulate the water. The water was TYPE I distilled. The first step of this method consisted of conditioning the specimens in a heated bath (Figure 3.4) at 38°C (100°F) for three weeks.

The second part consisted of cycling the specimens between -18° C (0° F) in a freezer for twelve hours and then in the heated bath at 38° C (100° F) for another twelve hours. This cycling was done for twenty days.

Thus the complete conditioning period was about six weeks. The specimens were then removed from the bath and stored in a sealed plastic bag at room temperature until tested for static and fatigue properties.

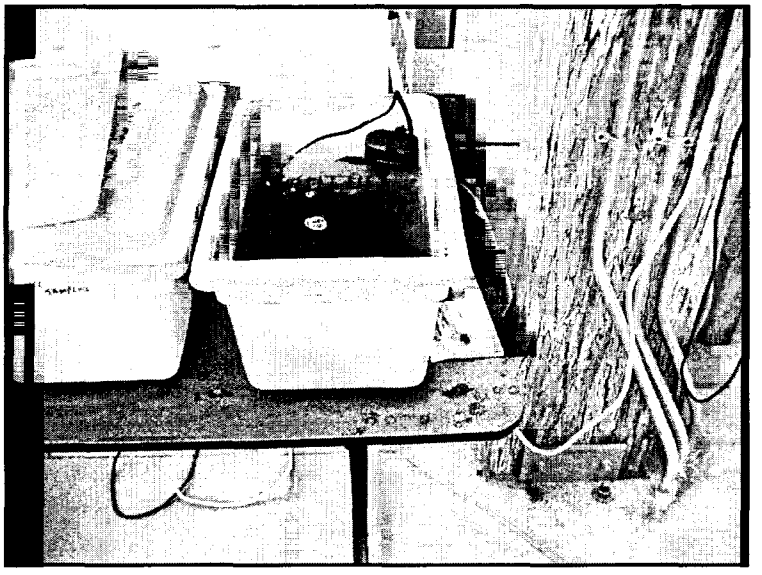

Figure 3.4 Freeze-Thaw Conditioning Tank

3.5.4 Hot Water Exposure at 45° C (115° F)

This test was done to measure moisture adsorption according to ASTM D 570 and effect of moisture at high temperature. Since the GFRP will be bonded to wood in a glue-laminated beam, it is expected to absorb a certain amount of moisture from both faces. To accelerate the adsorption process specimens were conditioned by submerging them in 45°C (115° F) distilled water. An HDPE tank equipped with a 1000-watt water heater and a circulating pump was used to maintain the desired environment (Figure 3.5). The plates were exposed to this environment for 3000 hours (125 days) to allow uniform concentration of moisture throughout the specimen.

Fresh distilled water was used to replace water lost due to evaporation. An external digital thermometer with an alarm was used to monitor isothermal conditions.

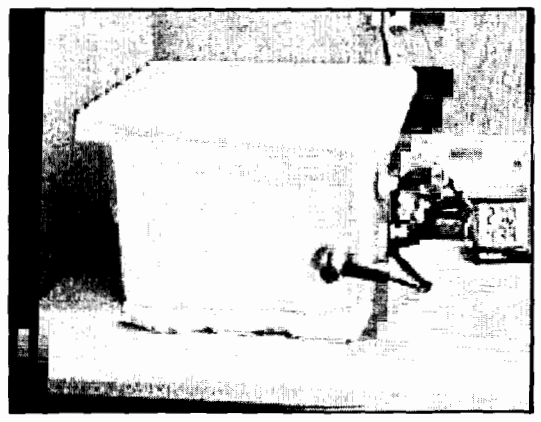

Figure 3.5 Hot Water Conditioning Tank

3.5.5 UV+Spray (Simulated Exterior Weathering)

ICBO AC 125 recommends this test and ASTM G 53 describes the testing method. It is an accelerated simulation of exterior exposure. Eight plates were exposed to a combination of UV light, high temperature, and water spray at cyclic intervals. The UV light with an irradiance of 0.55 $W/m^2/nm$ using UVA 340nm (peak radiation) fluorescent bulbs and 63° C chamber temperature was used to simulates sunlight during a hot day. Although sunlight radiation consists of wavelengths greater than 315nm and beyond the infrared (>700nm), shorter wavelength radiation (<300) penetrates FRP more and as a result causes more damage than longer wavelengths (ASTM G53).

The normally distributed radiation wavelengths of UV-A bulbs range between 315 and 400nm which is a better simulation of sunlight compared to UV-B lamps which emit radiation of shorter wavelengths. Water spray represents rain. All these factors are known to cause degradation in FRP materials. The specimens were directly exposed in a weatherometer (QUV) for 2000 hours. All eight plates were exposed on only one side for 102 minutes of UV followed by 18 minutes of UV and distilled water spray. The water was supplied and recycled from a 190-liter (50-gal) reservoir, which was connected to the weatherometer and replenished every 500 hours (Figure 3.6).

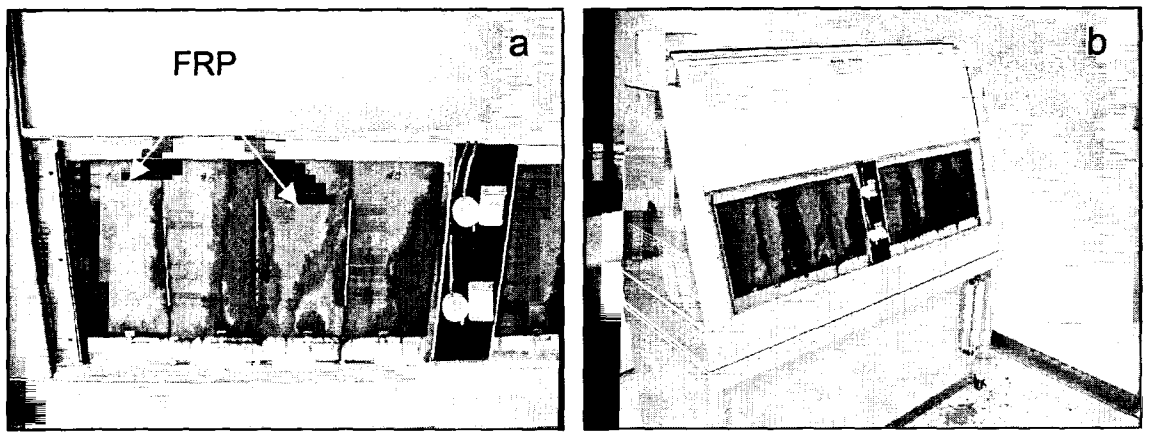

Figure 3.6 UV Weathering Chamber (b) Showing FRP Exposure Set-up (a)

3.5.6 Simulated Seawater (Salt Water Resistance)

Salt water was prepared in accordance with ASTM D 1141 (Substitute Ocean Water) method. Only reagent grade chemicals were used. Three types of stock solutions were prepared as shown in Table 3.4.

Table 3.4 Composition of Stock Solutions Used in Preparing Seawater.

Stock Solution 1		Stock Solution 2		Stock Solution 3 (in 10 Liters)	
$MgCl_2 \cdot 6H_2O$	555.6 g/L	KCl	69.5 g/L	$Ba(NO_3)_2$	0.994 g
$CaCl_2$ (anhydrous)	57.9 g/L	$NaHCO_3$	20.1 g/L	$Mn(NO_3)_2 \cdot 6H_2O$	0.546 g
$SrCl_2 \cdot 6H_2O$	2.1 g/L	KBr	10.0 g/L	$Cu(NO_3)_2 \cdot 3H_2O$	0.396 g
		H_3BO_3	2.7 g/L	$Zn(NO_3)_2 \cdot 6H_2O$	0.151 g
		NaF	0.3 g/L	$Pb(NO_3)_2$	0.066 g
				$AgNO_3$	

The simulated seawater was then prepared by combining common salt, anhydrous sodium sulfate ($NaSO_4$), and the stock solutions 1,2 and 3 in 20 liters (6 gal) of TYPE I water such that the resultant solution was composed of chemicals in the concentration shown in Table 3.4.

Table 3.5 Chemical Constituents of Simulated Seawater as Per ASTM D 1141

Compound	Concentration, g/L
NaCL	24.53
$MgCl_2$	5.2
$NaSO_4$	4.09
$CaCl_2$	1.16
KCl	0.695
$NaHCO_3$	0.201
KBr	0.101
H_3BO_3	0.027
$SrCl_2$	0.025
NaF	0.003
$Ba(NO_3)_2$	0.0000994
$Mn(NO_3)_2$	0.0000340
$Cu(NO_3)_2$	0.0000308
$Zn(NO_3)_2$	0.0000096
$Pb(NO_3)_2$	0.0000066
$AgNO_3$	0.00000049

Ten plates were stacked vertically on a HDPE rack and immersed in the seawater for 3000 hours. The pH was maintained and adjusted to 8.2 with drops of 0.1N sodium hydroxide (NaOH) solution. The tank was stirred every week to maintain uniform concentration throughout the tank.

3.6 Test Methods

Physical, mechanical and fatigue properties were determined according to ASTM specified methods. The laboratories in which the testing were conducted were temperature and humidity controlled at 23.0 ± 3° C (73°F) and 50% ± 5% RH. This section describes the methods used to determine physical, mechanical and thermal properties of both exposed and unexposed pultruded, and hand lay-up FRP. The testing matrix is shown in Table 3.2 (section 3.4).

3.6.1 Physical Properties

Physical properties evaluated in this study include density, volume fraction of resin, reinforcement, and voids content. The glass transition temperature (Tg) was also evaluated for both control and exposed specimens.

3.6.1.1 Density by Volume Displacement Method

Density was determined by the liquid displacement method using a laboratory density determination kit and an analytical balance. ASTM D 792 was followed while conducting this test. Five specimens with 2cm sides were cut from a plate using a wet diamond saw. The specimens were then washed with tap water and conditioned at room temperature (23°C, 73°F) and humidity (50 ± 5 % RH) for 4 days. The specimens were weighed in air and then weighed again by completely submerging them in distilled water (Specific gravity = 1g/cc).

3.6.1.2 Fiber, Resin, and Void Volume Fractions by Ignition Loss Test

This test method involves burning the specimens in a furnace such that only glass fibers remain. The test method specified in ASTM D 2584 was followed. A rule of thumb for a well-fabricated composite material is that the void content should be less than 1% (Agarwal 1990). Higher void content can adversely affect the mechanical, and durability properties of FRP. Higher void content results in poor fatigue strength (higher crack density), greater susceptibility to moisture penetration and weathering, and increased variation in strength properties (Agarwal, 1990).

Only the control pultruded and hand lay-up FRP were tested for void content and fiber volume fraction. Five control specimens were prepared and cut as described in section 3.6.1.1. The specimens were weighed and placed on aluminum crucibles and then heated at 565°C in a muffled furnace for two hours. At the said temperature all polymeric and volatile materials burned off and only glass fibers remained. The remains were cooled to room temperature in desiccators (to prevent moisture condensation) and weighed again. The difference in weight constitutes the weight of resin in the composite sample. The weight of the remains constitutes the weight of fibers. The volume fraction (V_f) of fiber is determined by using the following equation (Agarwal, 1990):

$$V_f = (\rho_{Ce}/\rho_f)\, W_f \qquad \text{Eqn 3.1}$$

In the above equation, ρ_{Ce} is the experimental density of the composite material obtained by the method described in the preceding section, ρ_f is the density of the glass fiber, taken as 2.54 g/cc. W_f is the weight fraction of the glass fibers

(residue weight). The void content was calculated according to ASTM D2734. The equation for void content is given by:

$$V = 100 - M_d\left(\frac{r}{d_r} + \frac{g}{d_g}\right) \qquad \text{Eqn 3-2}$$

where :

M_d = measured composite density

r = resin, weight %

g = glass, weight %

d_r = density of resin, and

d_g = density of glass.

3.6.1.3 Glass Transition Temperature (T_g)

Tg is the characteristic temperature at which glassy amorphous polymers become flexible (soften) due of the onset of concurrent motion of large segments of the polymer molecule. Tg is typically used to determine extent of cure and evaluate effect of plasticization in the exposed specimens. A Dynamic Mechanical Thermal Analyzer (DMTA) was used to determine the Tg of the two GFRP used in this study. The tests were done according to ASTM E1640 and D 5418 specifications. An increase in the Tg implies further curing (the resin has become stiffer) whereas a decrease in the Tg implies softening of the resin (plasticization). Five specimens from each exposure environment were tested using a DMTA. A DTMA machine measures mechanical and viscoelastic properties with change in temperature. It applies a dynamic load to measure the

difference in the viscous and elastic properties. A DMTA applies a temperature ramp beyond the Tg temperature and measures the change in elastic modulus (storage modulus) and viscous modulus (loss modulus). The force was applied in a dual cantilever (Figure 3.7) fashion.

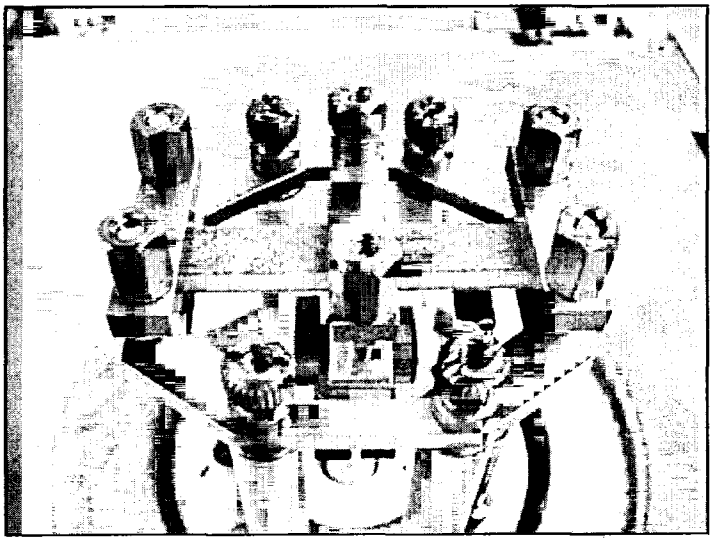

Figure 3.7 Dual Cantilever Set-up for Pultruded GFRP on a DMTA

Five specimens of the pultruded FRP from each conditioning were cut to dimensions with a diamond saw and conditioned at room temperature and humidity for 4 days prior to testing. The specimens were cut to 44.5mm long and 6.4mm wide from the pultruded plates. The DMTA test parameters were set in accordance with ASTM D 5418 method. A Rheometric Scientific DMTA IV with Nitrogen cooling capability was used to determine the Tg and flexural modulus changes in the specimens. The testing parameters are given in Table 3.6. The frequency and load application were adjusted to obtain clear and accurate DMTA graphs.

Table 3.6 DMTA Test Parameters.

DMTA Parameters	Value
Geometry Type	Dual Cantilever
Test type	Dynamic Temperature Ramp
Frame size	Large (34mm)
Center Clamp	Small (2mm)
Sample size (LxWxD)	32.0 mm x 6.3mm x 3.3mm
Frequency	1 Hz
Temperature ramp	23° C to 300° C
Temperature ramp rate	2° C / min
Strain	0.002 %
Initial static force	0.1 N

3.6.2 Mechanical Properties

The mechanical properties measured include longitudinal tensile strength, Young's modulus, strain to failure, and interlaminar shear strength. The pultruded specimens were cut from plates as shown in Figure 3.8. The hand lay-up specimens were cut to 23cm long and 1.9cm wide. Straight edge coupons of unidirectional FRP have been found to perform better in static tests than others with varying widths (ex. Dog-bone) (Curtis, 1989).

3.6.2.1 Tensile Strength and Young's Modulus

The FRP coupons were tested for tensile strength using the method specified in ASTM D 3039. The FRP cutting configuration is shown in Figure 3.8.

Static tensile testing was conducted before and after exposure to various

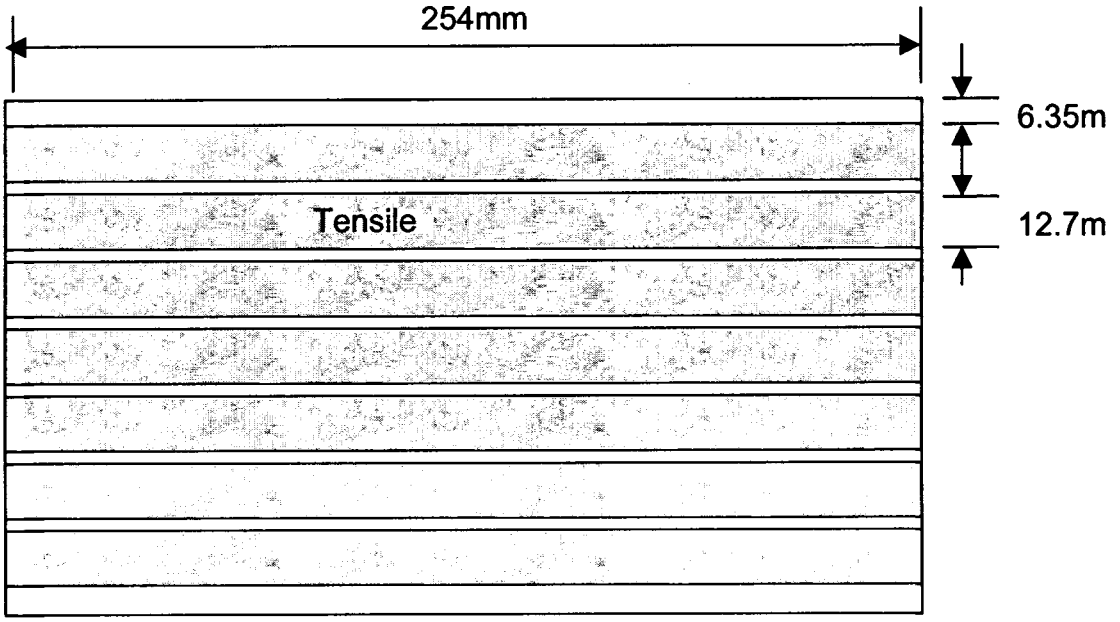

Figure 3.8 Specimen Cutting Configurations for Pultruded GFRP

environments to determine the ultimate tensile strength (UTS), strain to failure, and the Young's modulus of elasticity. Seven coupons from each exposure environment were tested using the Instron 8801, 100 KN (22 kip) mechanical testing machine. An extensometer was used to measure strain in the specimen. The specimens were tested at a strain rate of 1.27mm/min (0.05in/min).

3.6.2.2 Apparent Interlaminar Shear Strength

This test was done to determine change in bond properties of the interface between the fiber and the resin as well as resin properties. Rectangular specimens measuring 22.86mm x 6.55mm x 3.3mm (L x W x D) were cut from a plate using a water-cooled diamond saw.

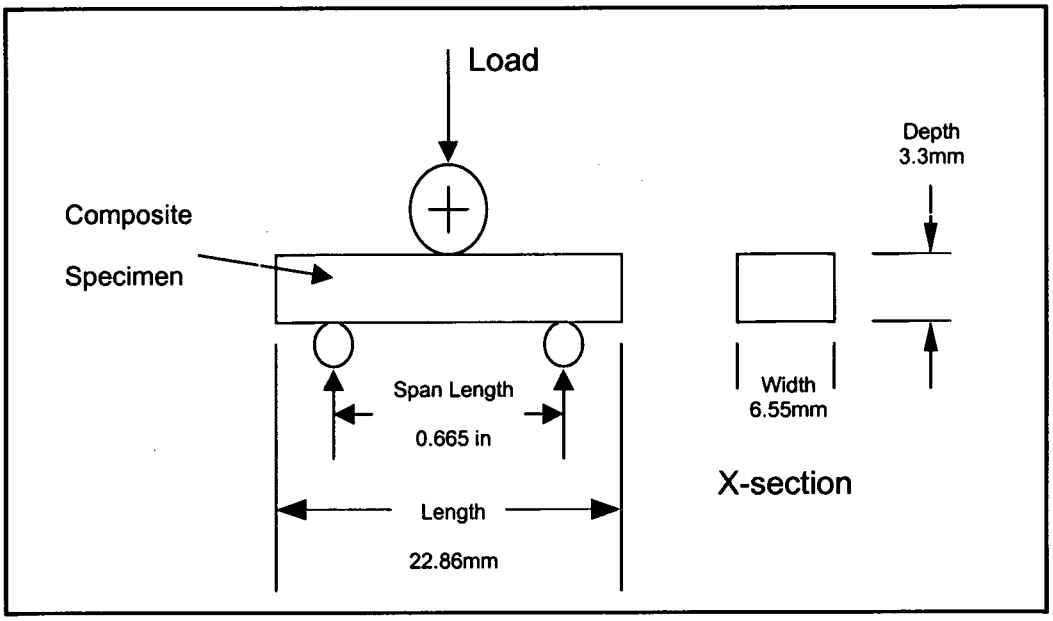

Figure 3.9 Schematic of Interlaminar-Shear Testing Fixture and Sample

The dimensions were cut according to the length/thickness ratio (L/d) of seven and span/thickness ratio of five as specified by ASTM D2344. This test is a simple three-point bend test. A schematic of the fixture is shown in Figure 3.9. Seven specimens from each exposure environment were tested for interlaminar shear strength.

3.6.3 Fatigue Properties

The fatigue properties evaluated are the fatigue life at different stress levels and the residual strength at 10%UTS after 3 million cycles of fatigue. The fatigue life is the number of cycles a specimen endured before failure, at a particular stress level. The residual strength of only the pultruded GFRP was evaluated. The procedure used to evaluate both fatigue life and residual strength is given below.

3.6.3.1 Fatigue Life

The fatigue life was determined in accordance with ASTM D 3479. Specimens were cut from plates as shown in Figure 3.8. In addition to the control specimens, the fatigue life of all the exposed specimens were also determined. The parameters used for the fatigue test are given in Table 3.7. The applied stress is reported as the percentage of ultimate tensile strength (UTS) of unexposed (dry control) specimens, which is 703.26 MPa (102 ksi). The specimens were tested for fatigue only in the longitudinal direction, as they will be used in practice.

Table 3.7 Fatigue Test Parameters for Pultruded and Hand Lay-up GFRP

Fatigue Parameters	Calculation/comment	Parameters
Attack time	Initial time to gradually increase amplitude	20 seconds
Stress Ratio (R)	(min stress/max stress)	0.1
Frequency	# of cycles per second	20 Hz
Mean stress	(max stress + min stress)/2	See Table 3.8
Amplitude	(Max stress - mean stress)	

A bridge girder such as an FRP-Glulam beam will always carry a constant dead load. The fatigue test was designed in a similar manner where the specimen is cycled between a minimum and a maximum load or stress, both being in tension. The ratio of minimum to maximum stress applied is called the stress ratio (R). In this study an R ratio of 0.1 was used. This test is also commonly called a Tension-Tension fatigue test because both the minimum and maximum stresses cause the specimen to be always in tension. The cyclic stress applied to the specimens was a sinusoidal waveform with a frequency of 20Hz (Figure 3.10). Specimens were tested at different stress levels and the S-N curve was plotted on a logarithmic scale. The fatigue waveform settings for exposed and unexposed pultruded GFRP are shown in Table 3.8. The hand lay-up specimens were also tested at proportional stress levels.

Table 3.8. Fatigue Waveform Settings for All Pultruded GFRP

Stress level (UTS Control)	Sample size		Waveform settings (12.7mm wide by 3.3mm thick specimens)		
	Control	Exposed	Max stress (MPa)	Mean stress (MPa)	Amplitude (MPa)
80 %	5		563	310	253
70 %	5		492	271	221
60 %	5		422	232	190
50 %	5	4	352	197	155
40 %	5	4	281	155	126
30 %	5	4	211	116	95
20 %	5	4	141	76	65

UTS (control)= 703.26 MPa (102 Ksi)

Five specimens were tested at each stress level for the control group and four at each stress level for the exposed groups. A servo hydraulic mechanical testing machine (INSTRON 8801 100 KN) was used to generate the waveform. The INSTRON actuator was controlled by software from a PC provided by the manufacturer. Running a fatigue test consisted of entering all the parameters shown in Table 3.7 and Table 3.8, and setting the interrupts so that the machine automatically stops when a specimen fails. Failure is said to occur when the specimen could no longer maintain the minimum load applied. The trip limit was set at 10% below the minimum load. For example if a specimen were cycled between 9000 N (max) and 900 N (min), failure would occur if the minimum load drops below 810 N. Since failures have been observed to be abrupt, these limits were set to prevent the machine from completely separating the fractured pieces and to allow visual examination of the fracture surface.

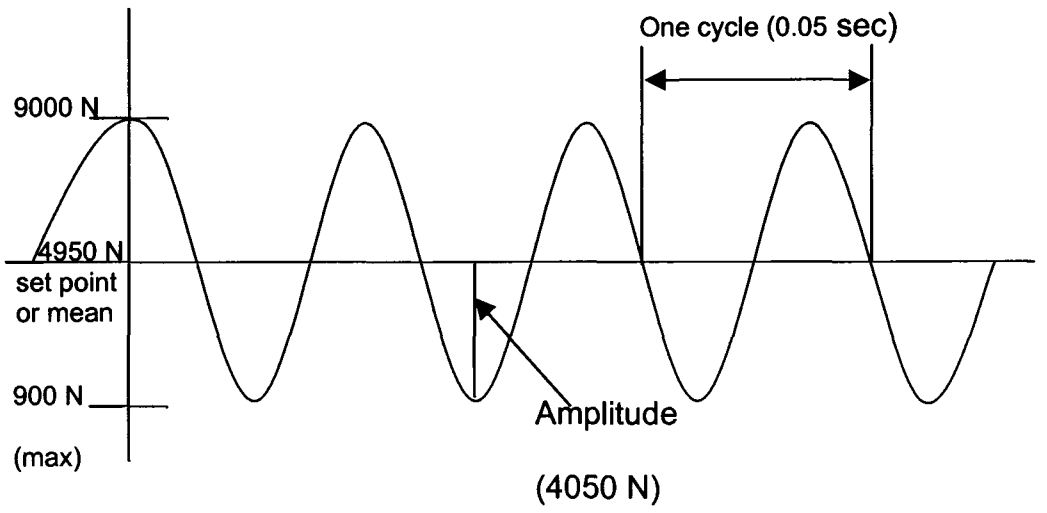

Figure 3.10 An Example of Fatigue Cycle Waveform

An attack time was used to gradually increase the amplitude to the desired load. This was done to minimize impact loading on the GFRP as well as to allow proper alignment of the specimen between the grips. The fatigue life was recorded both in the PC and in test data book.

3.6.3.2 Residual Strength

Residual strength is the term used to define the remaining static strength of a specimen after it has been subjected to a certain number of fatigue cycles. To determine residual strength fatigue cycling was interrupted and static tensile tests to failure were conducted. Only the unexposed pultruded GFRP was tested for residual strength. The residual strength degradation was obtained at only one fatigue stress level (10%). To obtain a residual strength diagram, specimens were tested as shown in Table 3.9.

Table 3.9 Residual Strength Testing Parameters for Pultruded GFRP

Maximum Stress (%UTS-Control)	Cycles after which residual strength was determined	No. of specimens for each number of elapsed cycles
10 %	0.5 million, 1 million and 3 million	6

3.6.4 Microscopy

A light microscope was used to examine failure samples for possible trends in the failure mode. A stereomicroscope as well as a transmitted light microscope with polarized light was used to observe surface features. Both microscopes were connected to a digital camera to allow pictures to be taken and stored. A Scanning Electron Microscope (SEM) was used to examine fiber interface and bond characteristics in the pultruded and hand lay-up failed specimens.

4 RESULTS OF PHYSICAL AND MECHANICAL TESTS

4.1 Introduction

The results of the physical and mechanical tests of the pultruded and hand lay-up GFRP are presented in this chapter. This chapter is organized into two main sections. The first section (section 4.2) presents the physical data and the next section (section 4.3) covers the static mechanical properties of the two GFRP. All tests were done according to ASTM specified methods. Statistical analysis was done using Analysis of Variance (ANOVA) at the 5% significance level. A summary of the findings is given at the end of the chapter. The results of fatigue tests are given in Chapter 5.

4.2 Physical Properties

The results of the ignition loss tests are given in Table 4.1 and 4.2. The results are explained in the following sections.

4.2.1 Density, Volume Fractions and Void Content

Pultruded GFRP

The density of the pultruded GFRP (unprimed) is approximately 1.75 g/cc (Table 4.1). The fiber volume fraction, which includes unidirectional and randomly oriented short fibers in the mat layer, is approximately 54%. However the fiber

volume fraction of the core alone, which consists of *unidirectional* fibers only, is approximately 70%.

Table 4.1 Density and Ignition loss Results of Pultruded and Hand Lay-up GFRP

	Sample size	Pultruded GFRP		Hand Lay-up GFRP	
		Volume fraction %	COV %	Volume fraction %	COV %
Fiber volume fraction V_f	6	54.19	1.31	65.1	0.92
Resin volume fraction V_m	6	21.07	2.89	27.02	4.29
Void volume fraction V_v	6	24.74	1.87	8.06	6.66

Table 4.2 Density of Pultruded and Hand Lay-up GFRP

	Composite g/cc	Glass g/cc	Resin g/cc
Pultruded GFRP	1.75	2.54	1.08
Hand Lay-up	2.01	2.54	1.33

The SEM images (Figure 4.1), taken on smooth cross section of the GFRP support the results of the ignition loss tests. The mat layer has high voids content (45%) and low fiber volume fraction compared to the core. Each mat layer is approximately 0.55mm thick and the core is approximately 2.2mm thick. The thickness of the GFRP varies along the width because it was belt sanded after pultrusion. SEM images also indicate that the wetting of fibers by the resin is poor. The resin volume fraction (lost weight) of the entire GFRP is approximately 21.7%.

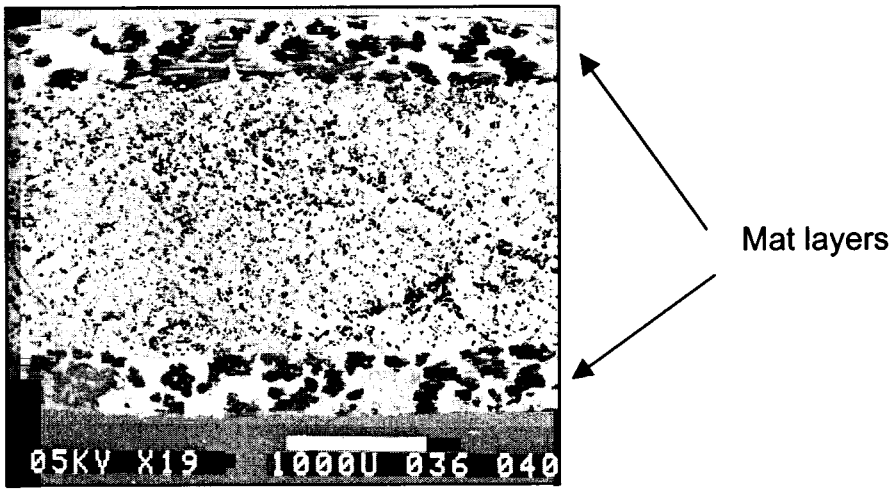

Figure 4.1 SEM Image of Pultruded GFRP Cross-Section

The void content of the pultruded GFRP was approximately 24.7%, which is considered very high compared to common FRP materials. This figure also exceeds the ICBO AC 125 requirement of 6% or less. However, this void content is primarily due to the mat layers, which are intended to allow adhesive penetration and thus improve bonding with solid wood and other wood composites. Priming the surface with PRF resin seals off most of the surface voids, but not completely (see Figure 4.2). The phenolic resin also appeared to be highly porous (see Figure 4.3). This porosity must have been formed during the manufacturing process when the resin cured in the pultruder forming-die.

The curing process of phenolic resin is known to produce significant amount of water from the condensation reaction (Tavakoli et al 1990). Branco et al (1994) also stated that they observed internal voids in the phenolic composite they were testing. They concluded that the voids were due to entrapped water bubbles produced during composite manufacture.

Previous attempts by the author, to produce pure cast resin in a conventional oven resulted in the formation of large quantities of bubbles in the cast. These bubbles are due to the formation of water produced during condensation reaction and consequently the observed porosity in the resin. An important observation made during burn out tests is that the pultruded GFRP did not produce any flames during ignition loss tests. The residue left behind after the ignition test consisted of glass fibers only, which separated easily when probed with a glass rod. This indicated that the resin had completely vaporized.

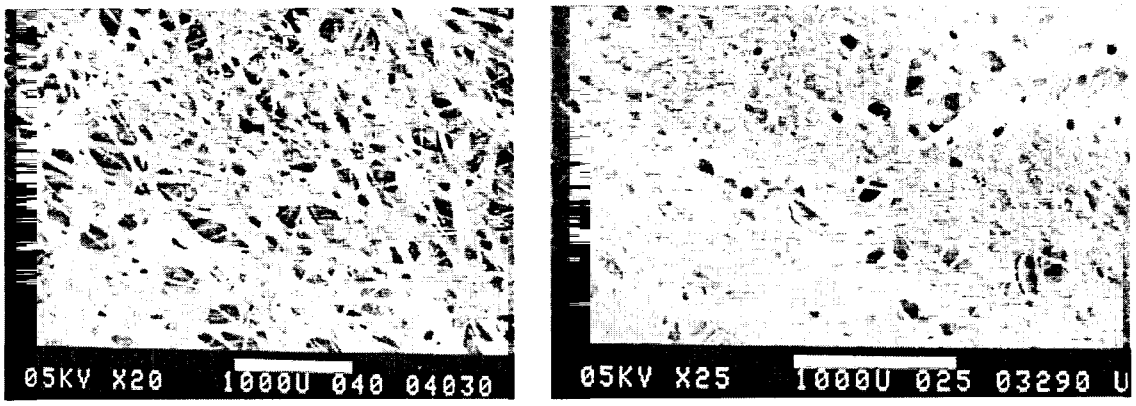

(a) (b)

Figure 4.2 SEM Image of Unprimed (a) and Primed (b) Surface of Pultruded GFRP

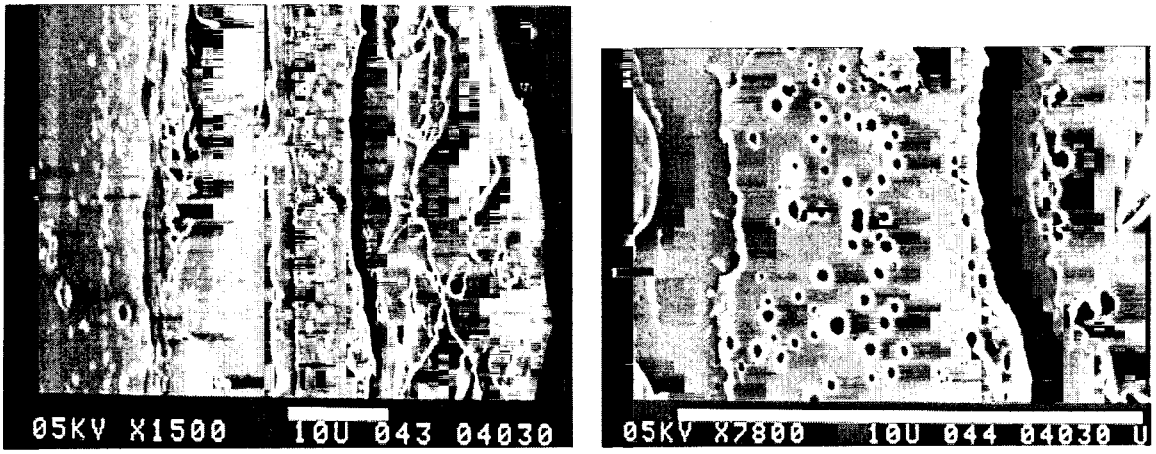

(a) (b)

Figure 4.3. (a) and (b), SEM Image of Fractured pultruded GFRP Showing Voids in the Resin

Hand Lay-up GFRP

The hand lay-up GFRP was made of five layers of woven unidirectional glass mats (Figure 4.4). The fiber, resin, and void volume fractions of this GFRP are approximately 65%, 27.02% and 8% respectively.

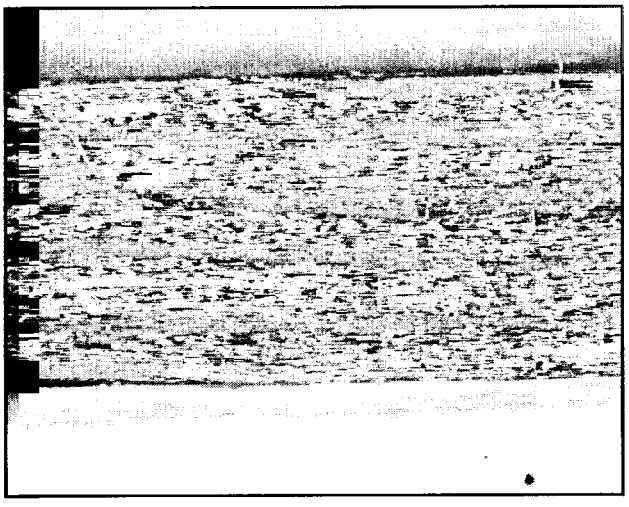

Figure 4.4 Stereomicroscope Image (16x) of Hand Lay-up GFRP Showing the 5 Glass Layers Along the Edge (thickness)

Unlike the pultruded GFRP, the hand lay-up GFRP does not have porous surface mat layers and thus we observe a comparatively higher fiber volume fraction and lower voids content. Bare fibers (Figure 4.5) observed through a SEM indicate that the fiber wetting is generally poor. Good wetting is usually indicated by fibers completely circumfused by resin without interfacial gaps.

During ignition loss tests, no flame was observed around the specimens even at 565°C. This confirms that phenolic resins do not combust at high temperature. This characteristic behavior has been advantageously used in applications where fire resistance is an important consideration; for example handles for cutlery items.

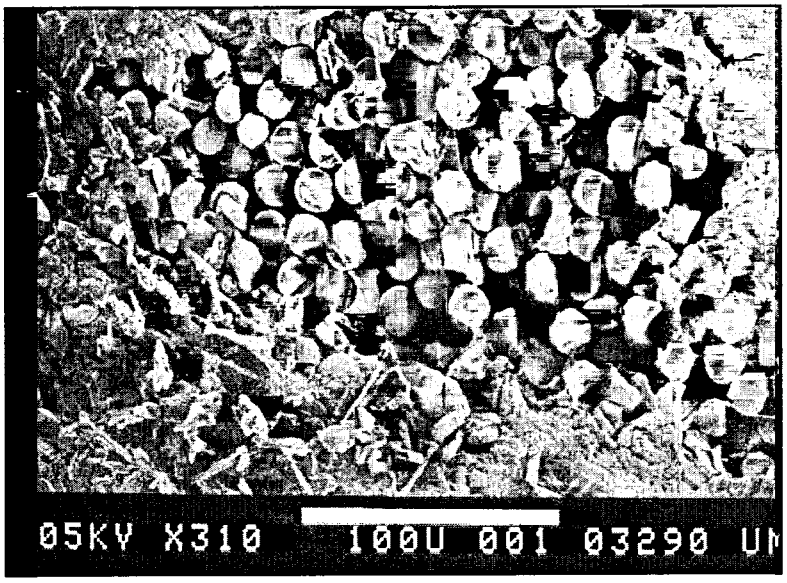

(a)

(b)

Figure 4.5 SEM Image (a) and (b) of Hand Lay-up GFRP Cross-Section Showing Poor Wetting of Fibers

4.2.2 Glass Transition Temperature (Tg)

Dynamic mechanical thermal analysis (DMTA) tests were done on the exposed and control pultruded specimens only. The results are given in Table 4.3. In summary, the Tg following the various exposures ranged from 194°C to 207°C, with simulated seawater specimens and UV weathered specimens exhibiting the lowest and highest Tg respectively (see Appendix D). Analysis of Variance (ANOVA) was used to verify the differences in the results. The Tg of control specimens is 201°C, which is high compared to common types of thermosetting resins such as epoxies (60-175°C), polyesters (110°C), and vinyl esters (75-105°C) (Bauccio, 1994). Statistical analysis (ANOVA) of the Tg using a significance level of 0.05 (95% confidence) shows that, except for freeze-thaw specimens, all other exposures had a significant change in the Tg. The DMTA diagram of freeze-thaw specimens exhibited two loss modulus peaks. The first peak, which was lower in magnitude, was observed at approximately 120°C and the second occurred at the actual Tg. Since water boils at 100°C, it is possible that the first peak represents water loss.

The possibility that this first peak is associated with the PRF primer has been ruled out since preliminary tests with unprimed pultruded GFRP also exhibited such peaks between 90 and 150°C. The water present is due to the water immersion in freeze-thaw cycling. The second peak clearly represents the glass transition temperature, Tg. Following the second peak, the viscous property decreases without any recovery. The elastic modulus (storage modulus) continuously decreases with increase in temperature and levels off after the Tg.

The maximum temperature was set to 300°C because it was known from previous tests that the Tg of this particular phenolic GFRP would not exceed this value.

The Tg of hot water specimens decreased by approximately 5.4°C. This decrease may be due to plasticizing effects of water. Water tends to swell and increase the free volume of the polymer thus decreasing Tg. Moisture is known to significantly alter the viscoelastic property of polymeric thermosetting resins (Dillard et al, 1991). The effect of matrix plasticization of thermosetting polymer such as vinyl ester due to water ingression has been reported by Liao et al (1998). Sridharan et al (1998) also claimed that moisture (water) acts as a plasticizer to vinyl ester matrix systems, causing a fall in tensile properties. The loss modulus curve of the hot water pultruded GFRP exhibited two peaks similar to the freeze-thaw specimens (Figure 4.6).

UV weathered specimens exhibited the highest increase in Tg. The Tg increased by approximately 5.2°C. An increase in Tg usually implies post curing. This may have been the case with UV weathered specimens. The temperature within the UV chamber was kept constant at 63°C with relatively short period of water spray. High temperature along with UV radiation may have further cured the resin. Since the water spray was only active for 18 minutes every 2 hours, it is possible that this short duration coupled with the high temperature did not allow sufficient time for water to be absorbed in the GFRP. Thus the effect of moisture may have been rendered insignificant. The weathering effect inside the

UV chamber caused significant erosion of the mat layer. The dark PRF primer turned into pale purple exposing the surface fibers.

The Tg of simulated seawater specimens decreased by approximately 7.6°C. The lowering of Tg can be attributed to plasticizing effects of water. These specimens also exhibited two loss modulus peaks, but the first peak was very small in magnitude compared to the second.

Table 4.3 Glass Transition Temperature (Tg) of Pultruded GFRP

Exposure	Sample size	Tg (°C)	COV%
Control	5	201.06	1.33
Freeze-thaw	5	203.66	2.35
Hot water	5	196.44	0.79
UV weathering	5	207.01	0.70
Simulated Seawater	5	194.23	1.00

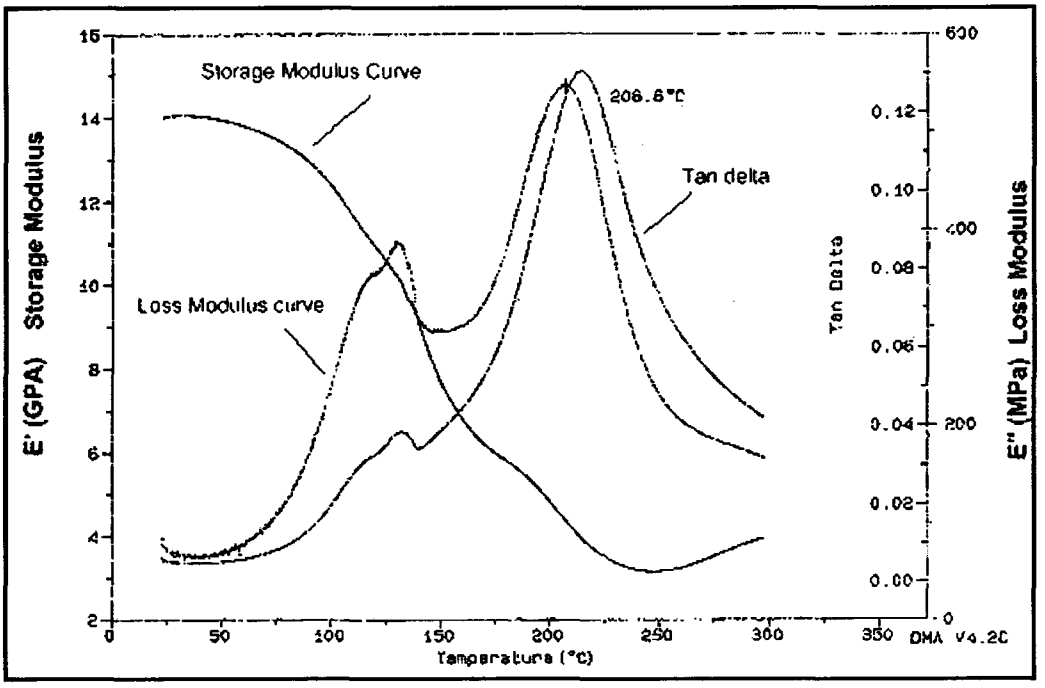

Figure 4.6 DMTA Diagram of Pultruded GFRP - Hot Water Specimen

4.3 Mechanical Properties

4.3.1 Interlaminar Shear Strength

The interlaminar shear strength (ILSS), also called short beam shear helps to determine the change in the fiber-matrix interface bond strength. The ILSS of pultruded control and exposed specimens are given in Table 4.4. Failure was observed as a single horizontal shear crack that extended longitudinally in the core of the specimens. Tension failure of mat layer or core did not occur in any specimen. As a result all failures were considered valid. The average interlaminar shear strength of the control pultruded specimens is 24.29 MPa (3523 Psi).

Table 4.4 Interlaminar Shear Strength of Pultruded GFRP Specimens

Exposure	Sample size	Interlaminar Shear Strength (MPa)	Standard Deviation (MPa)	COV %	Reduction (5% level)
Control	10	24.29	1.15	4.76	0
Freeze-thaw	10	23.53	1.39	5.9	0
UV Weathering	10	21.56	1.161	5.39	11%
Hot Water	10	22.82	1.23	4.25	6%
Simulated Seawater	10	23.55	1.237	5.25	0

UV weathered specimens had the lowest interlaminar shear strength. The ILSS of UV weathered specimens decreased by 11%. Hot water exposure also caused statistically significant decrease (6% reduction) in the ILSS. The ILSS loss in hot water specimens may be attributed to damaging effects of moisture in the interface. Several authors have reported this effect suggesting that the damage mechanism is due to moisture corrosion caused by exchange of alkali

metal ions (Na^+ and K^+) in the glass and hydrogen ions in the attacking fluid (H^+) (Liao et al, 1998). The specimens in both these exposures were not only exposed to 100% water immersion but also high temperature (45°C hot water and 63°C UV). Thus it is difficult to ascertain which of the two factors caused more damage.

4.3.2 Longitudinal Tensile Properties.

Pultruded GFRP

The average longitudinal tensile strength (see Table 4.5) of the pultruded control GFRP is 703.22 MPa (102 ksi). The Young's modulus is 40.56 GPa (5.88 msi) with a strain to failure of approximately 2.0%. The tensile failure of the control pultruded specimens was characteristic of unidirectional composites. Failure initiated with the outer mat layer fracture and a few longitudinal fiber rupture along the edges. Close to the ultimate stress progressive fiber fracture along the edges were observed. At ultimate stress, failure occurred abruptly with massive fiber fracture (explosion) and longitudinal shear splitting (Figure 4.7).

The longitudinal tensile strength of freeze-thaw specimens decreased by approximately 10%. Hot water specimens were affected the most. The tensile strength of hot water specimens reduced to 480 MPa (31.74% reduction). This result clearly indicates that the fibers have been damaged due to a combination of moisture adsorption and high temperature.

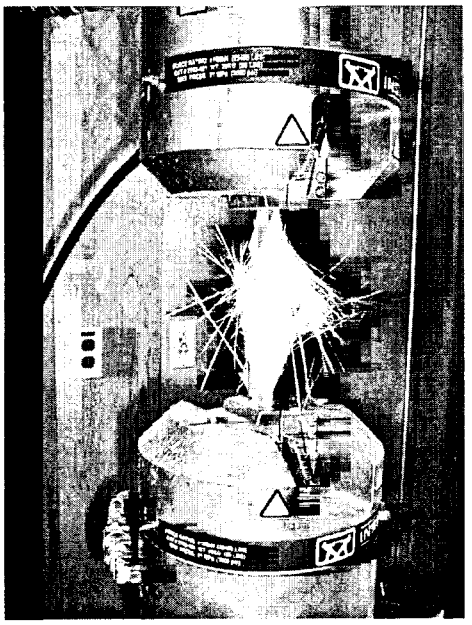

Figure 4.7. Tensile Failure of Pultruded GFRP Seen Between Instron Grips

UV weathered specimens, exhibited almost no significant change in tensile strength. The standard deviation of these specimens was low indicating uniform properties. The failure mode of these specimens was also different from the control group. The characteristic explosion of fibers was not observed and instead the coupon failed abruptly at ultimate stress with mostly longitudinal shear splitting (Figure 4.8). The ultimate tensile strength of simulated seawater specimens reduced by only 7%. However, the change is statistically insignificant due to the large standard deviation.

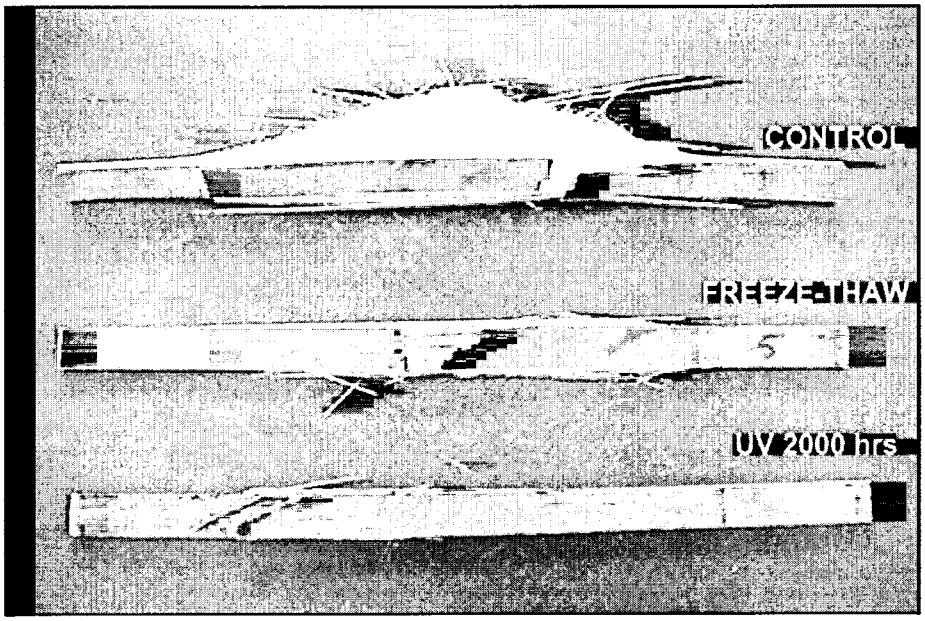

Figure 4.8. Tensile Failure Mode of Pultruded GFRP at UTS

No change was observed in the Young's modulus of any of the exposed specimens (see Table 4.6 and Figure 4.11). Any change observed was not statistically significant at the 5% level.

Hand Lay-up GFRP

The longitudinal tensile strength of hand lay-up GFRP specimens is approximately 422 MPa (61.29 ksi). The strength varies significantly as observed from the high COV (18%) (see Table 4.5). The modulus of elasticity of this GFRP is approximately 36 GPa (5.33 msi). Failure mode is characterized by transverse tensile fracture in the gage length with some fraying of fibers as shown in Figure 4.9. Transverse fracture tends to propagate along a region on the surface where a cross-weave was present.

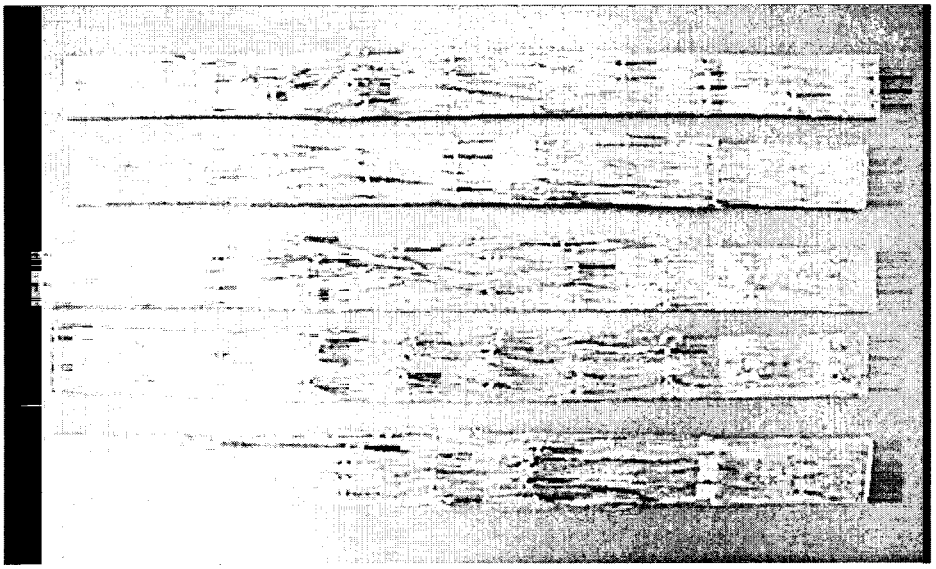

Figure 4.9 Hand Lay-up GFRP Specimens Failed in Static Tests

Table 4.5 Longitudinal Tensile Strength of Pultruded and Hand Lay-up GFRP

	Pultruded GFRP					Hand Lay-up GFRP
	Control	Freeze-thaw	Hot Water	UV 2000 hrs	Simulated Seawater	Control
Sample size	7	7	7	7	7	7
Average (MPa)	703.22	636.73	480.07	699.44	653.85	422.59
COV %	4.99	8.39	4.05	2.78	8.39	18.25
Strength reduction		9.5%	31.7%	0.5%	7%	NA

Table 4.6 Longitudinal Young's Modulus of Pultruded and Hand Lay-up GFRP

	Pultruded GFRP					Hand Lay-up GFRP
	Control	Freeze-thaw	Hot Water	UV 2000 hrs	Simulated Seawater	Control
Sample size	7	7	7	7	7	7
Average (GPa)	40.56	39.88	41.16	40.87	40.25	36.75
COV %	2.49	3.29	1.81	2.4	2.67	9.45

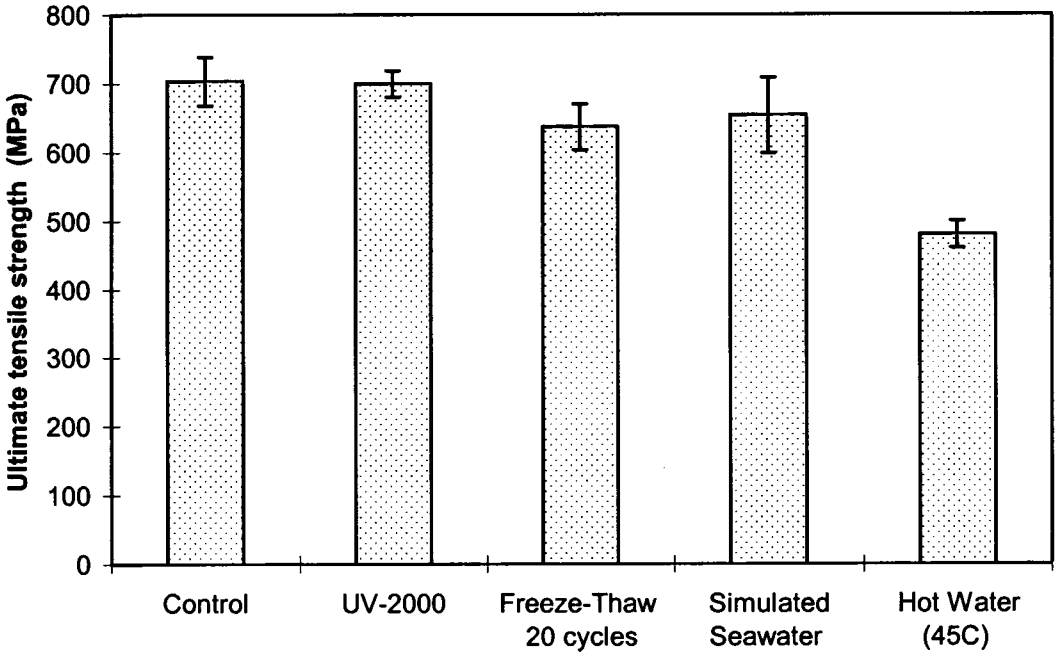

Figure 4.10 Longitudinal Tensile Strength of Pultruded GFRP vs. Exposure. Error Bars Indicate One Standard Deviation

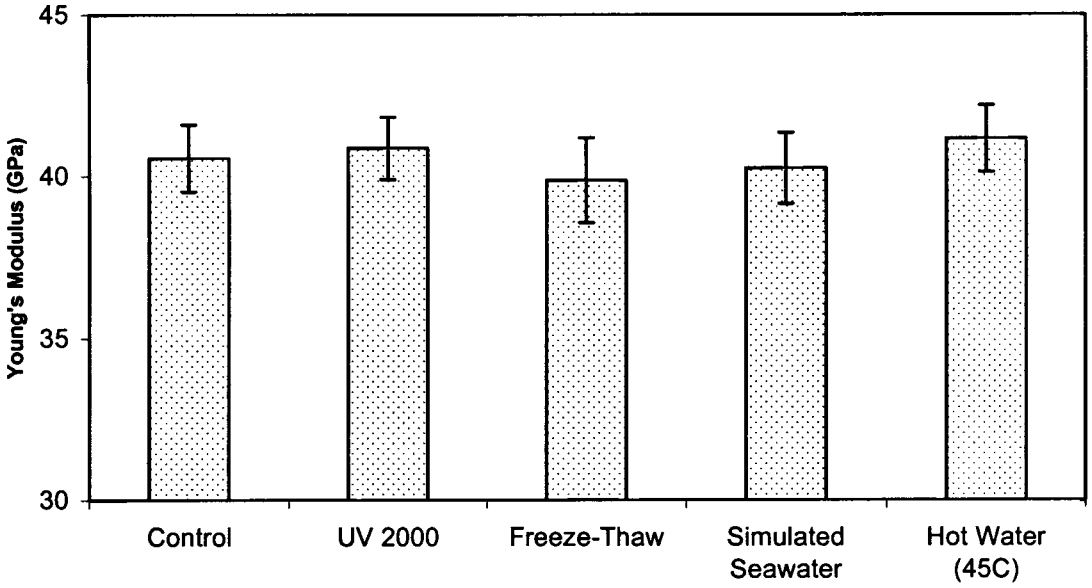

Figure 4.11 Tensile Young's Modulus of Pultruded GFRP vs. Exposure. Error Bars Indicate One Standard Deviation

4.4 Summary

Two types of E-glass reinforced phenolic composites (pultruded and hand lay-up) were tested for physical and mechanical properties. The pultruded GFRP was exposed to different accelerated environments and after the exposure period, the mechanical strength retentions were determined. The findings are summarized below.

- From ignition loss tests it was observed that the void volume fraction of pultruded and hand lay-up GFRP were 24% and 8% respectively and exceeds the recommended 6% or less by ICBO AC 125. SEM images of pultruded GFRP revealed large number of pores in the resin. These pores may have been formed due to condensation reaction during curing of phenolic resin.
- The pultruded control specimens had a Tg of 201°C. UV weathered specimens showed an increase in Tg (207°C) whereas hot water (197°C) and simulated seawater (194°C) specimens exhibited a decrease in Tg. The increase in Tg can be attributed to post curing of the resin and the decrease in the Tg is mostly due to plasticizing (softening) effects of water.
- The interlaminar shear strength of UV weathered specimens was reduced by 11%. Although slight changes were observed in other exposure environments, the changes were not statistically significant.
- Hot water exposure caused the highest reduction in tensile strength. The ultimate tensile strength of the hot water specimens was reduced

by as much as 31%. Hot water specimens also exhibited a reduction in ILSS (6%). Thus, it may be concluded that hot water exposure damaged both glass fibers and the interface. Freeze-thaw specimens exhibited a 10% reduction in tensile strength. The damage can be attributed to resin and fiber-resin interface deterioration caused by moisture ingression. Salt water did not cause any statistically significant change in the tensile strength.

- None of the exposed specimens showed any statistically significant change in Young's modulus.
- UV weathered specimens indicate that high temperature can further cure (post curing) the resin if polymerization was not complete in the manufacturing process. If the cross-linking of polymer chains were complete in the manufacturing process, no increase in the Tg would be observed. Although UV showed no degradation in tensile strength, the ILSS was reduced by 11%. This indicates that UV had some effect on the interface. The difference in the thermal expansion coefficients of the glass fiber and resin may be a possible explanation of the reduction in ILSS.
- Except for hot water exposure test, which was not specified by ICBO, all the tests that were specified by ICBO AC 125 passed the minimum strength retention.

5 RESULTS OF FATIGUE TESTS

5.1 Introduction

This chapter describes the results of all the fatigue tests conducted in this study. The first section describes the results of fatigue tests conducted on exposed and control pultruded GFRP followed by a discussion on fatigue failure mechanism. The next section describes the results of the fatigue tests conducted on the hand lay-up GFRP. The following section describes the results of residual strength tests followed by a summary of the chapter.

5.2 Fatigue Strength of Pultruded GFRP

Fatigue tests were conducted using a servo hydraulic INSTRON machine at constant amplitude with a stress ratio of R=0.1 and a frequency of 20 Hz. Specimens were tested at different stress levels until failure, and the test was stopped at 3 million cycles if no failure occurred. For the control type, five specimens were tested at each of the seven stress levels (80%, 70%, 60%, 50%, 40%, 30% and 20% UTS). For the exposed types, four specimens were tested at each stress level (50%, 40%, 30%, 20%). The control specimens were tested first to observe material variability and to estimate failure boundaries. S-N diagrams were developed for each exposure type and then compared with the control to observe any change in fatigue behavior. Fatigue testing presented

many problems, which were solved earlier during dry runs to obtain maximum number of valid results.

5.2.1 Failure at Grips

Failure at the grips was the most persistent problem in fatigue testing. Other authors have recorded this problem also (Bronco et al, 1996; Lorenzo et al, 1986). Initially, it was thought that tabs were needed at the gripping area of the pultruded GFRP to reduce failure at grip edges. Failure at the grip edge is mainly due to high stress concentration. Rectangular specimens were tested with a variety of tab types and adhesives. Glass fiber reinforced epoxy tabs with a 15° machined tapered edge were used with little success. The tabs remained intact but the mat layer sheared off at both high (>50% UTS) and low (<50% UTS) stresses. In the next attempt, thin aluminum strips were bonded to the coupons with polyurethane (PU) adhesive. This type of tab was attempted due to the success reported by few authors who tested similar FRP materials (Bronco et al, 1996). This time the mat layer was intact and well bonded to the core but the adhesive bond failed before actual fatigue failure of the specimen. The PU adhesive penetrated the mat layer very well, which was evident from the foaming action observed during adhesive application. However, the PU adhesive did not bond very well to the aluminum strips in spite of careful material cleaning and preparation.

Two other adhesives, an epoxy and a methacrylate industrial strength adhesive were used with the aluminum strips, but unfortunately failure at the

grips persisted. The grip pressure was also adjusted to find an optimum value. The grip pressure had to be adjusted to prevent crushing and slippage in the grip area. Finally coupons were tested with no tabs. The mat layer, although damaged by the gripping, was beneficial in protecting the core from the rough serrated faces of the grips. This produced very few failures at the grips for higher stress fatigue tests and almost no failure at the grips for lower stresses. Thus, all fatigue tests were conducted without tabs. Specimens that failed at the grips were discarded and not used in the data analysis.

5.2.2 S-N Curves of Pultruded Specimens: Effect of Environmental Exposure

The S-N curve of control pultruded specimens is presented in Figure 5.1. The entire data set is given in Appendix C. The S-N curves were plotted and analyzed using Microsoft Excel. The abscissa represents number of cycles to failure in the logarithmic scale (base 10), while the ordinate represents the maximum tensile strength applied on the specimens in percentage. The S-N curves were drawn using a linear fit of the data (least squares method). The fatigue lives of exposed specimens were compared to the control values at the same stresses.

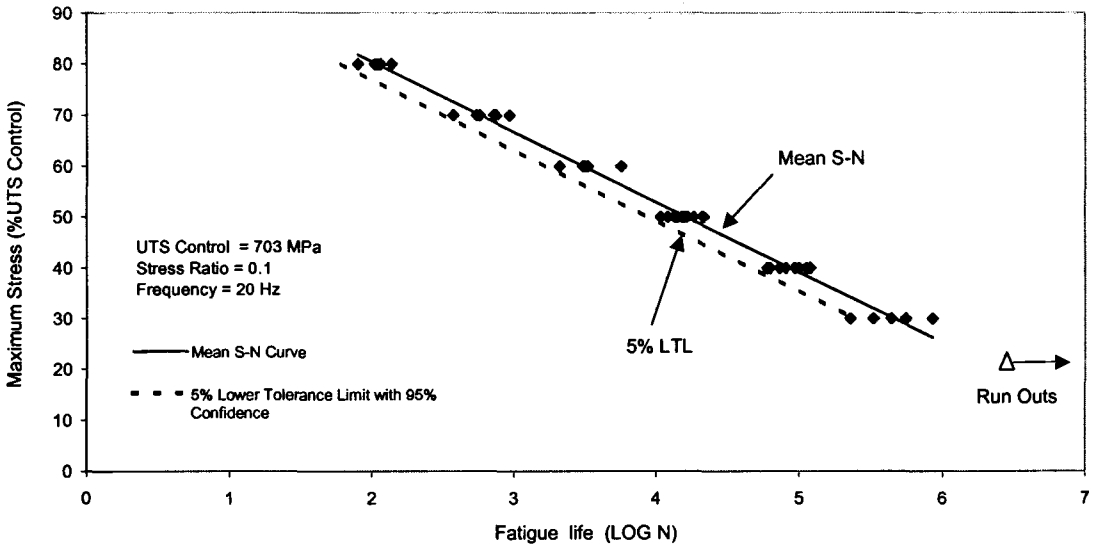

Figure 5.1 S-N Curve of Control Pultruded GFRP with 5% LTL with 95% Confidence

The S-N curve has a negative slope, which is indicative of the fact that lower applied stresses result in higher fatigue lives. The five control specimens that were tested at 20% UTS exceeded 3 million cycles of fatigue (Run outs).

S-N Curves Of Exposed Specimens

The S-N curves of exposed specimens (see Figure 5.2) also exhibited the general trend seen in control specimens. The entire data set is given in Appendix C. In qualitatively comparing the S-N curves of the exposed specimens with that of the control, three characteristic behaviors were observed. UV weathered specimens stand out from other S-N curves and show a slight decrease in the fatigue life as compared to the control at high and low stresses (the slope of the S-N curve is approximately equal to the control specimens but the curve is

shifted down). The rest of the exposure types, which include hot water, simulated seawater and freeze-thaw cause an increase in the fatigue life compared to the control S-N curve for stresses lower than 45% UTS. As for stresses higher than approximately 45% UTS, the fatigue life decreases compared to the control specimens. In other words, the slopes of the S-N curves of these exposures appear to be less steep than that of the control. Table 5.1 summarizes the fatigue strength of the pultruded GFRP at different cycles.

An analysis of variance (ANOVA) show that the fatigue life of UV weathered and hot water specimens are not statistically different from the control specimens at a significance level of 0.05. This is indicated by the F-statistic value, which is smaller than the F_{crit} in the corresponding exposures (Table 5.2).

Table 5.1 Fatigue Strength (% of Mean UTS Control) of Pultruded GFRP

Exposure		% UTS Control (UTS Control = 703 MPa)			
		100000	1 million	2 million	3 million
A	Control	39.0	25.5	21.3	18.9
B	Freeze-thaw	41.0	31.1	28.1	26.3
C	Hot water	40.9	29.1	25.6	23.5
D	UV weathering	36.3	23.1	19.2	16.8
E	Simulated seawater	41.8	30.6	27.2	25.2

Table 5.2 Statistical Analysis of Mean Life at 30%UTS Using ANOVA

Exposure		Fatigue Life at 30%UTS (Cycles)	Means compared	F	F_{crit}	Significance α=0.05
A	Control	490,600				
B	Freeze-thaw	$1.3\ 10^6$	A-B	8.33	5.59	Different
C	Hot water	805,900	A-C	1.55	5.99	Not different
D	UV Weathered	278,300	A-D	1.98	5.99	Not different
E	Salt water	$1.17\ 10^6$	A-E	10.82	5.99	Different

Freeze-thaw and salt-water exposures caused statistically significant increase in the fatigue life over the control (Table 5.2) at 30%UTS. This is detected by the F-statistic, which is higher than the F_{crit} value. At 30% UTS-control, the fatigue lives of freeze-thaw and salt water specimens increased by 166% and 139% respectively. At 40% and 50% UTS, the fatigue lives of exposed specimens are not any different from the control. Fatigue strength of exposed specimens was not tested at stress level higher than 50%UTS-control.

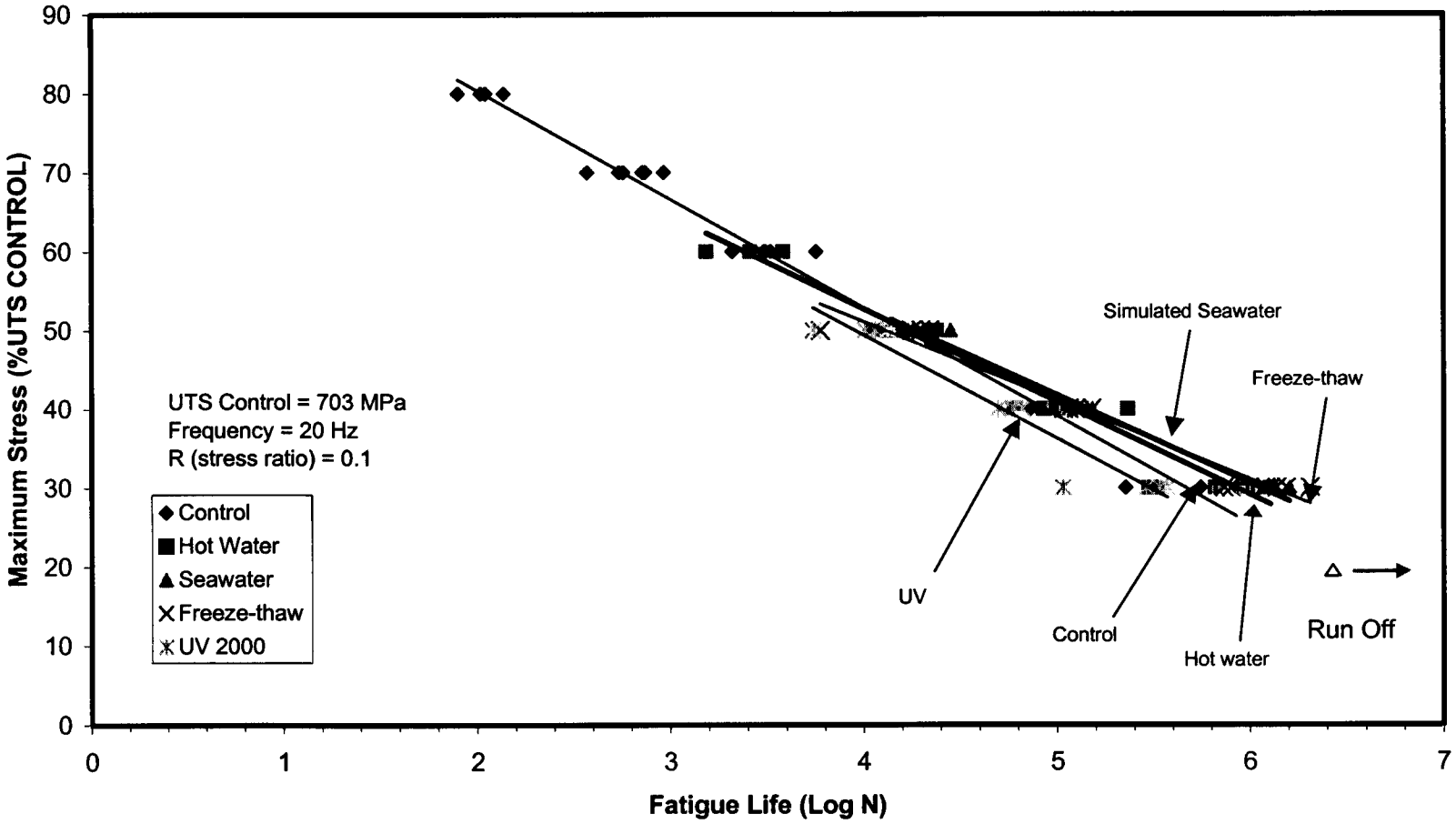

Figure 5.2 S-N Diagrams of Exposed and Control Specimens

The S-N curves were modeled using the Log-normal linear equation given below. It must be noted that the logarithm used in all the equations is the logarithm to the base ten.

$$\sigma_a = -A Log N_{mean} + B \qquad \text{Eqn 5-1}$$

For mean S-N, A = 13.942, B = 108.06

Where: σ_a is the maximum applied stress,

N is the number of cycles to failure

A and B are constants.

For example if the desired mean fatigue life were 3 million cycles (Log_{10} N = 6.477) then the mean applied maximum stress would be 18%UTS (UTS Control = 703 MPa, 18%UTS = 126 MPa). The parameters A and B for each exposure are listed in Table 5.3. The parameter A represents the slope of the curve and B, which is the intercept of the linear equation, represents the mean ultimate tensile strength.

Since fatigue cycling was limited to 3 million cycles, no apparent fatigue threshold or endurance limit were observed. However, it can be deduced from the fatigue tests that the S-N curve behaves differently below 20%UTS. This can be further substantiated by the fact that at 20% UTS, the strain is approximately 0.35%, which is below the strain to failure of the phenolic resin; 0.45%. Thus, at stresses lower than 20%, the matrix damage mechanism is different and consequently the fatigue behavior is expected to be different.

Table 5.3 S-N Curve Parameters For Exposed and Control Pultruded GFRP

Exposure		A	B	Actual UTS (%UTS Control)
A	Control	13.9	108	100
B	Freeze-thaw	10	91.2	92.4
C	Hot water	11.8	100	69.6
D	UV weathering	13.1	102	100
E	Simulated Seawater	11.1	97.7	94.8

5.3 Statistical Analysis of S-N Data

Two methods are shown for providing upper and lower bounds for the fatigue data: (1) 5% Lower Tolerance Limit (one sided) and, (2) 5^{th} Percentile. The tolerance limit method has been used for fatigue design of steel, wood and polymer composites (Wirsching, 1983; Bond et al, 1998; Roland et al, 1996). The tolerance used in this study is the one-sided lower 95% tolerance limit for 95% of the population. Since we are interested in the lower limit for safe design, this tolerance limit can also be called the 5% Lower Tolerance Limit (5%LTL) with 95% confidence. This tolerance limit describes a lower limit to the data, above which one can say that at least 95% of future observations (or sampled normal population) will have a 95% survival probability. The 5% LTL was used here because it provides a precise statistical lower boundary which is not too stringent for widely scattered fatigue data (Bond et al, 1998). The tolerance limit was calculated according to a method described by Wirsching (1983). The method is

described in Appendix C. The equation used for calculating the tolerance limit is given below:

$$\text{Log } N_{5\%LTL} = \bar{x} - ks \qquad \text{Eqn 5-2}$$

where , $N_{5\%LTL}$ = Fatigue life with 95% survival probability

$\bar{x}$ = mean life calculated from the best-fit straight line at a particular stress level,

k = tolerance coefficient (k=2.126, n=40 for control) corresponding to the total sample size and required population (p=95%),

s = standard deviation of the mean S-N curve

The tolerance limit is parallel to the mean S-N curve (see Figure 5.1). The equation of the tolerance limit in terms of stress level and fatigue life for the control pultruded GFRP is given by:

$$\sigma_a = -13.95 Log N_{5\%LTL} + 105 \qquad \text{Eqn 5-3}$$

5th Percentile

The 5th percentile line for the control pultruded GFRP is shown in Figure 5.3. It was obtained by finding the 5th percentile values at each stress level. The line was then drawn by fitting a linear regression line (least squares line) through all the stress levels. At each stress level, 5 specimens were tested. Therefore the student *t* distribution was used to obtain the 5th percentile.

$$\bar{x} \pm ks \qquad \text{Eqn 5-4}$$

where: $\bar{x}$ is the mean fatigue life at each stress level

s is the sample standard deviation at each stress level

k is 2.015 for n=5 and α =0.05 (Hogg, 1987, p 449)

The equation of the 5th percentile line of control pultruded GFRP is given by:

$$\sigma_a = -14.5 Log N_{5th} + 107 \qquad \text{Eqn 5-5}$$

where: σ_a is the applied maximum stress in percentage

N_{5th} is the 5th percentile value of the fatigue life

The 5th percentile line and the 5%LTL line would be very close to each other if potted on the same graph. This is because the equations (Eqn 5-3 and 5-5) are about the same. However, the 5%LTL is more sensitive to the number of specimens and thus more statistically sound compared to the 5th percentile line. The 5th percentile line is dependent on the standard deviation at each stress level whereas the 5%LTL pools the entire data set and uses one standard deviation which is constant at every stress level. Thus the 5%LTL is parallel to the mean S-N curve unlike the 5th percentile line.

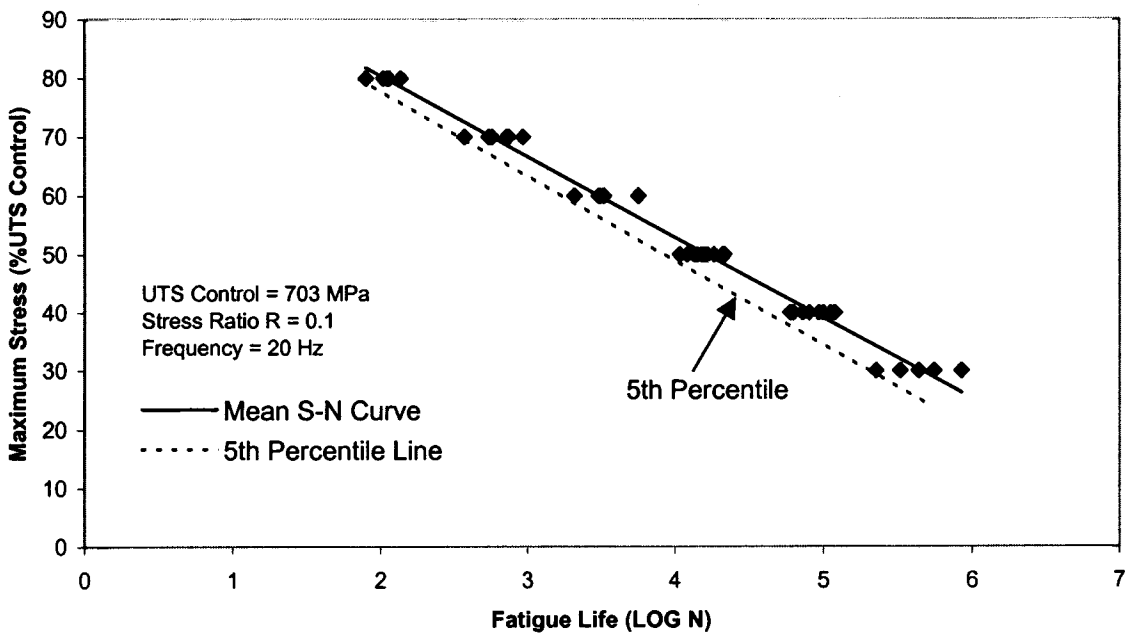

Figure 5.3 S-N Curve of Control Pultruded FRP with 5th Percentile Line

A 95% *confidence* interval on the *mean* is also sometimes used and many authors have reported S-N curves with this statistical analysis (Little, 1979; ASTM E 739). However, this interval only estimates the *mean* S-N curve with a 95% confidence and not the *entire* population. An example of this is given in Appendix C.

Although UV weathering did not cause statistically significant change in fatigue life compared to the control, it was the worst-case scenario for combination of fatigue with environmental exposures used in this study. This is merely because fatigue life of UV specimens were lower than those of all other exposures, which caused some increase in fatigue life at 30%UTS control.

The mean S-N curve of UV weathered specimens with both the 5%LTL with 95% confidence, and the 5th percentiles are given in Figure 5.4. The equation for the 5%LTL tolerance limit of UV specimens is given by:

$$\sigma_a = -14.13 Log N_{5\%LTL} + 79.12 \qquad \text{Eqn 5-6}$$

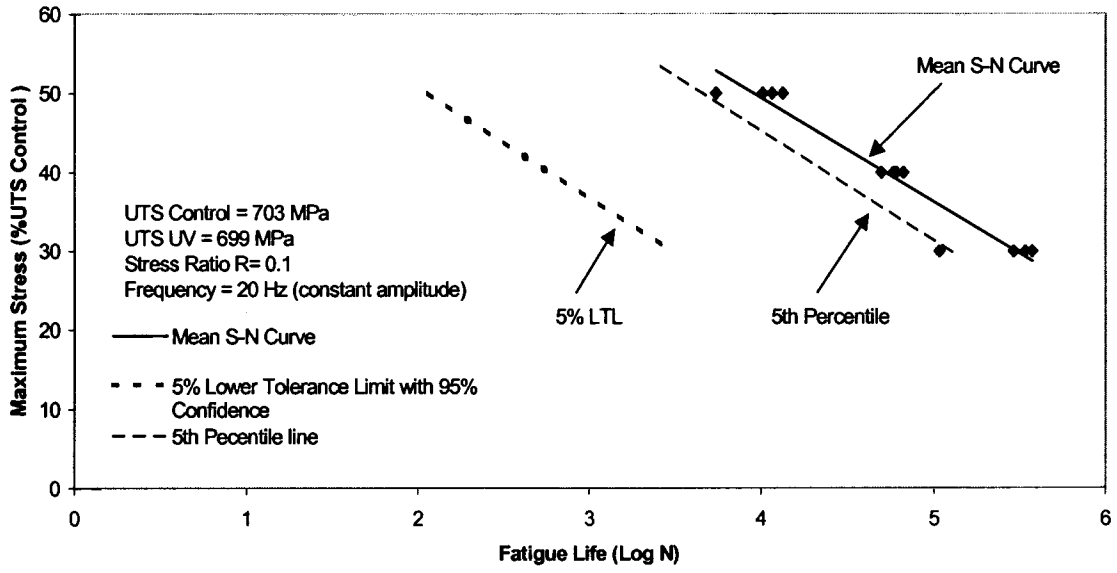

Figure 5.4 S-N Curve of UV Weathered Specimens with 5% LTL with 95% Confidence and 5th Percentile Lines

Due to the small number of UV weathered specimens available for testing fatigue life, tolerance limit coefficient k was large and hence the 5%LTL is much further away (left) from the mean. Since the 5th percentile line is based on the standard deviation at *each stress level*, this line is much closer to the mean S-N curve compared to the 5%LTL. The author recommends testing at least 30 specimens total for future work.

5.4 Fatigue Failure Mechanism in Pultruded GFRP

The fatigue failure mechanism observed was identical in all the pultruded specimens whether exposed or unexposed, but dependent on the applied stress. The failure types are described in Figure 5.5. The common failure mechanisms include edge cracks, longitudinal cracks, abrupt fiber fracture, and shear delamination.

The differences in failure mode due to decreasing stress level can be seen in Figure 5.6 (a). As the stress level decreases, the failure mode changes from explosive blooming effect at 80%UTS (Figure 5.6-a left) to a simple transverse crack at 30%UTS (Figure 5.6-a right). Specimens that were tested at relatively high stresses (>50%UTS) failed in a fashion (Type 3) similar to static failure tests (blooming explosive failure) as shown in Figure 5.5.

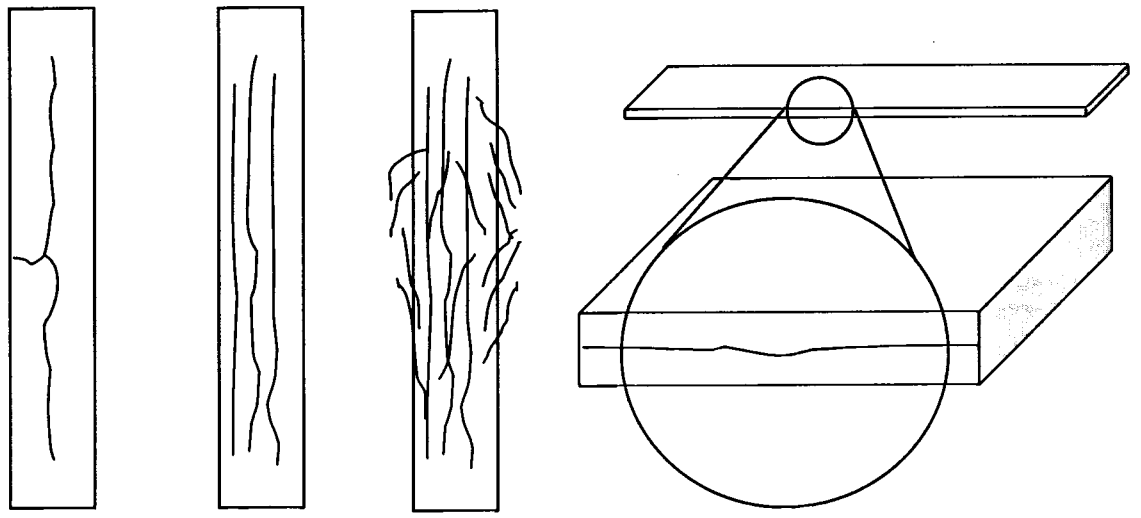

Figure 5.5 Common Fatigue Failure Modes in Pultruded GFRP

At 50% UTS, hot water and simulated seawater specimens exhibited numerous longitudinal cracks (Type 2) as shown in Figure 5.7 (a) and (b). At 40% UTS some specimens also exhibited Type 2 failures (see Figure 5.8-b). At relatively low stress levels damage appeared to accumulate progressively (Type 1,2 and 4) and no specimens exhibited explosive blooming effect.

At lower stresses failure was mostly characterized by progression of a single crack, which usually originates at one edge in the gauge length (see Figure 5.9 a and b) and propagates perpendicular to the loading direction along the width of the coupon. This type of crack is named as Type 1 in this study (see Figure 5.8 a). The crack however never seemed to propagate along the entire width but branched off parallel to the loading direction along the length of the coupon, often terminating at the opposite edge or resulting in longitudinal splitting. This type of failure has been observed by Curtis (1989) and Liao et al (1998), and is characteristic of unidirectional materials. In some cases an edge crack initiated with abrupt fiber fracture resulting in instant failure as seen in Figure 5.6 (b). Another failure type is characterized by a shear crack (or delamination), which runs along the edge through the thickness (Type 4) (see Figure 5.8 c, and 5.10 a and b) and splits the coupon into two pieces. This type of delamination often terminated at the grip edge. The specimens that were tested at 20%UTS showed no cracks or delamination.

In almost all cases, the mat layer failed prematurely before any edge crack or delamination occurred. However, a crack in the mat layer often indicated

where an edge crack initiated. Figure 5.7-b clearly shows a mat layer fracture tracking the progress of a longitudinal or transverse split.

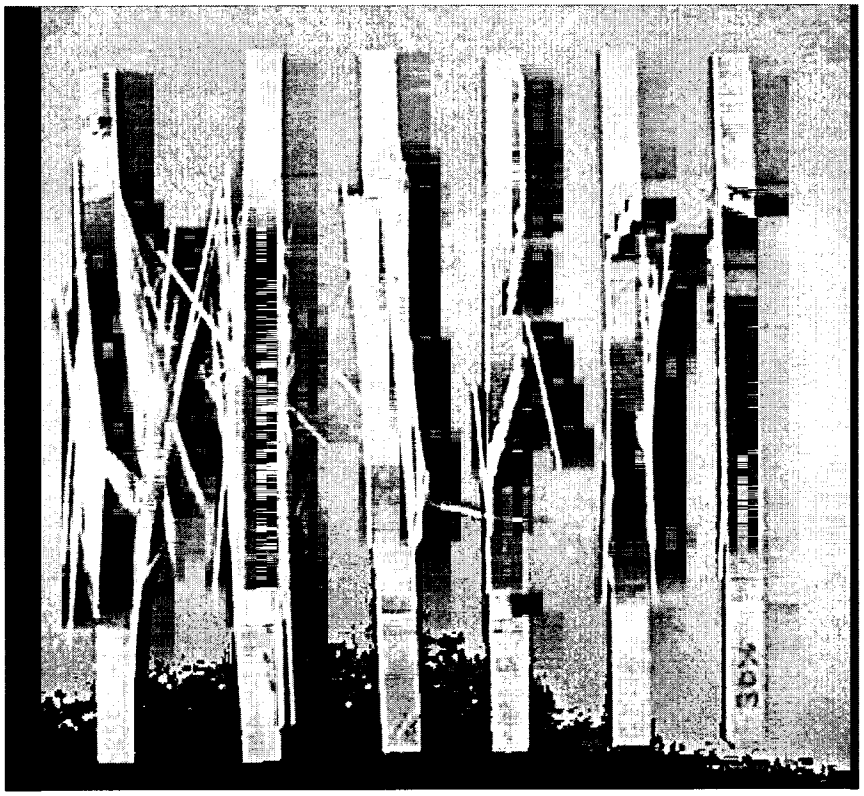

(a)

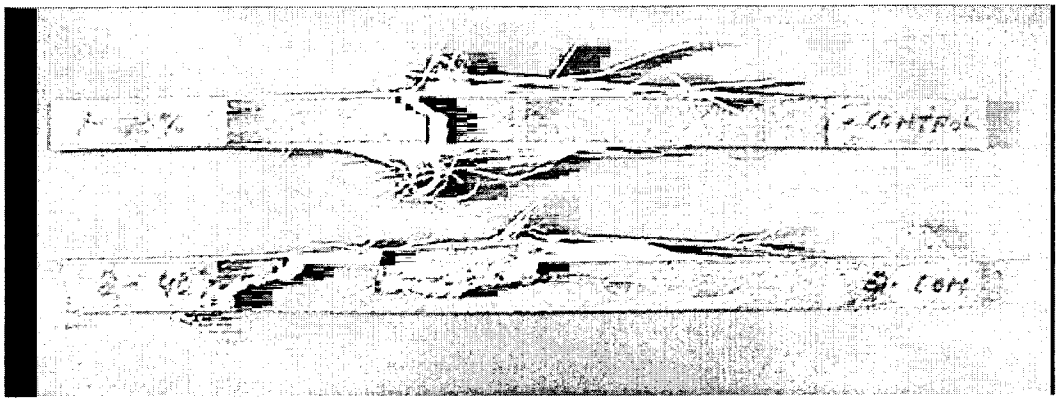

(b)

Figure 5.6 Fatigue Failure Mode in Control Pultruded GFRP, (a) Specimens Tested From 80%UTS (left end) to 30%UTS (right end), (b) Edge Crack at 40%UTS

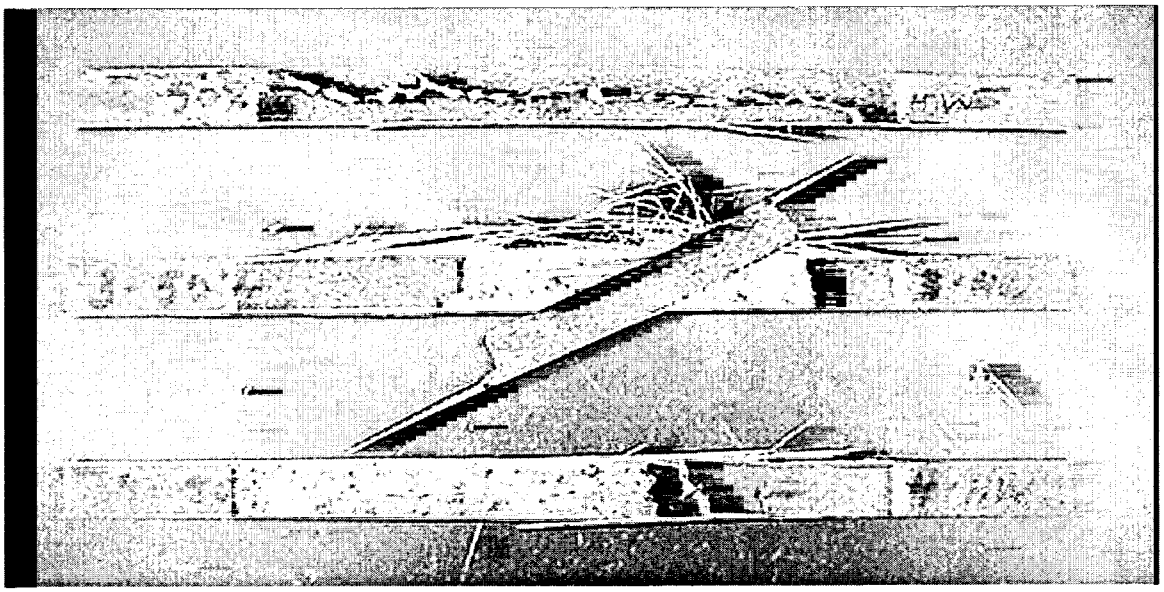

(a)

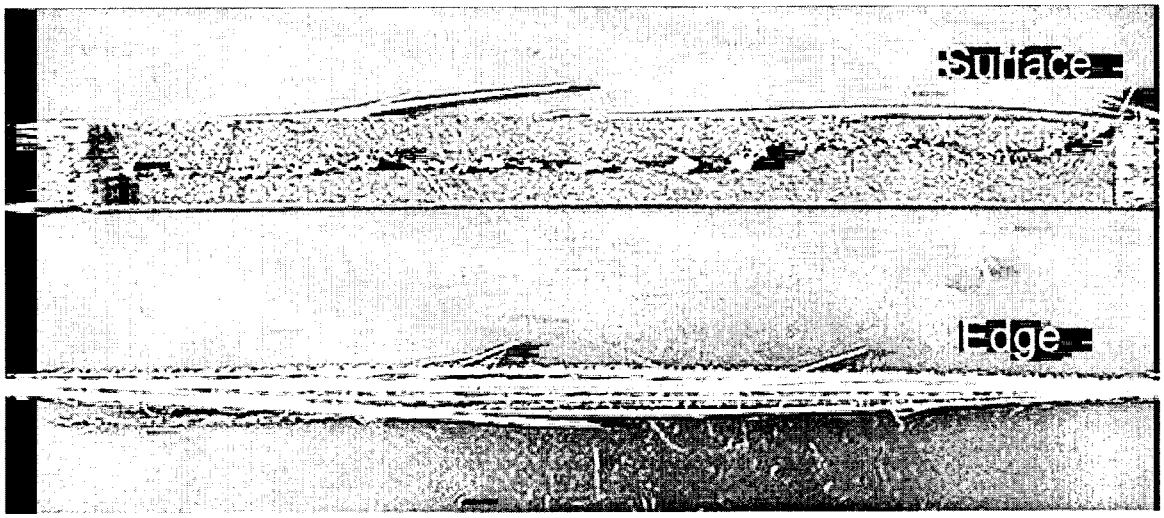

(b)

Figure 5.7 Fatigue Failure Mode of Exposed Specimens: (a) Hot Water at 50%UTS, (b) Simulated Seawater at 50%UTS

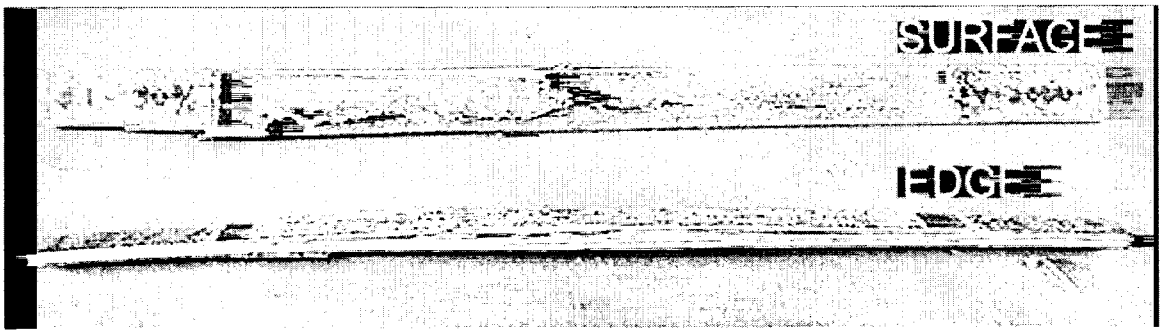

(a)

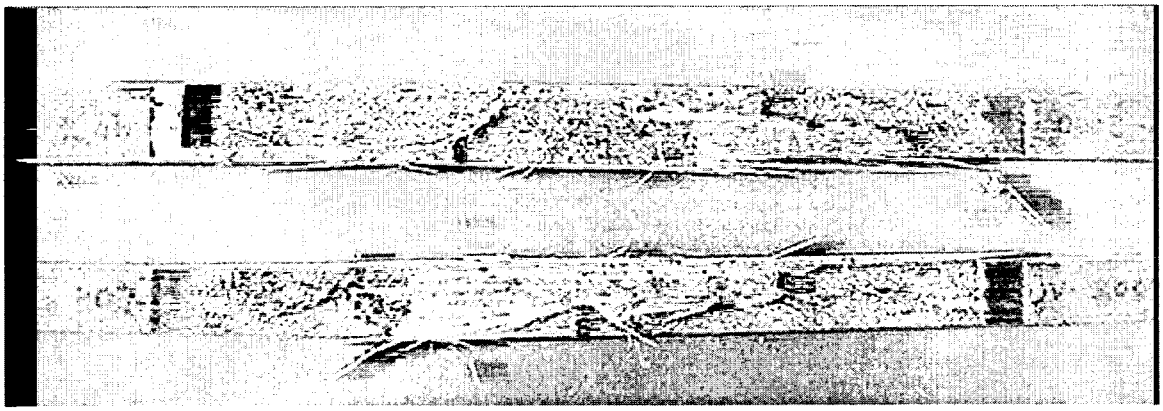

(b)

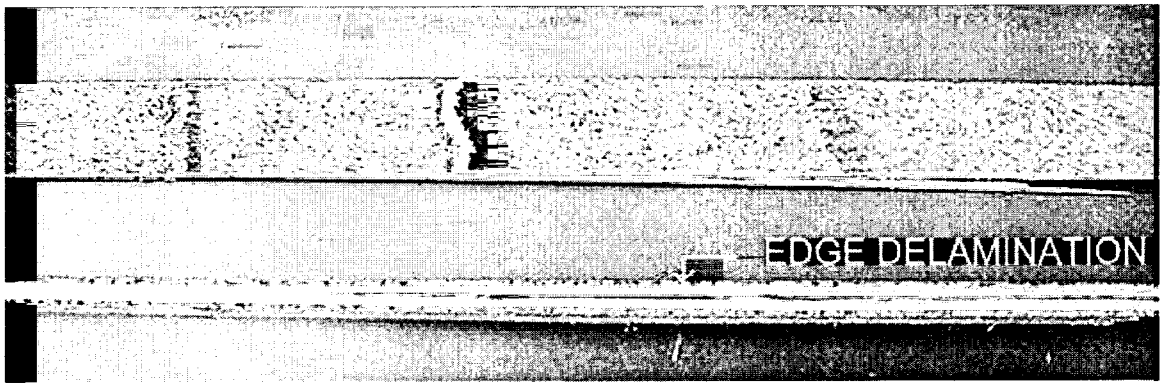

(C)

Figure 5.8 Fatigue Failure of Exposed Specimens: (a) UV Weathered at 30%UTS Showing Edge Crack, (b) UV Weathered at 40%UTS Showing Longitudinal Splitting, (c) Freeze-Thaw at 40%UTS Showing Shear Delamination

(a)

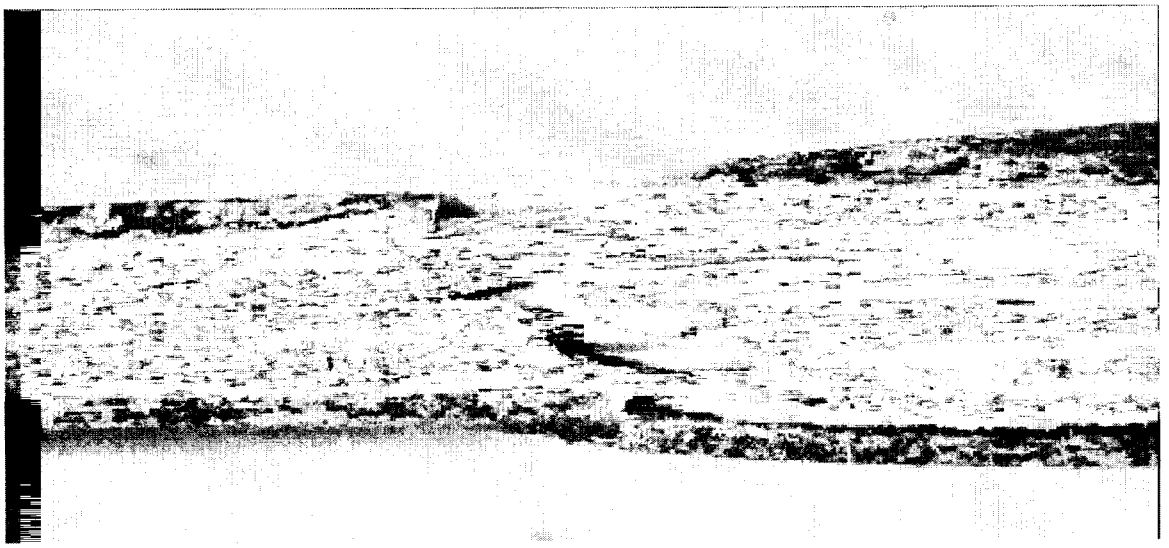

(b)

Figure 5.9 Stereoscope Images (16X) of UV Weathered Specimens (30%UTS) Showing Edge Cracks

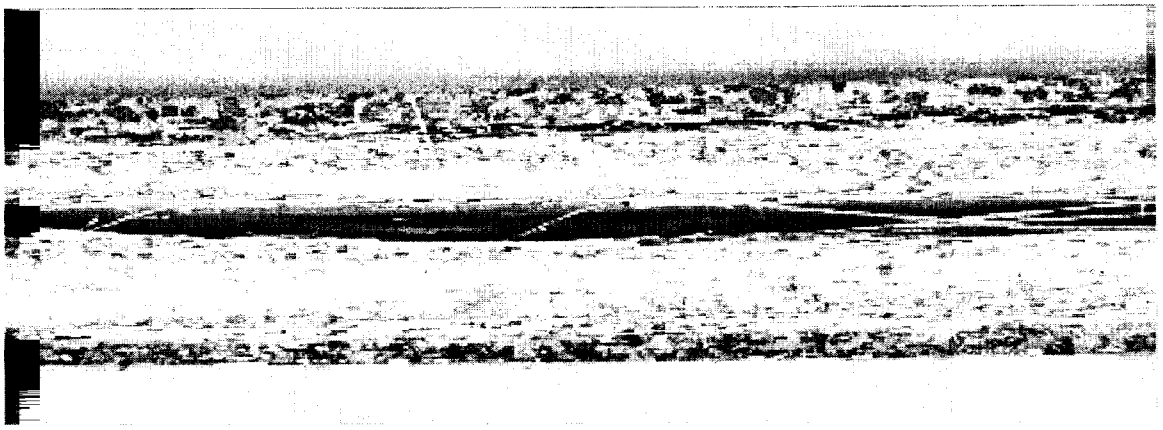

(a)

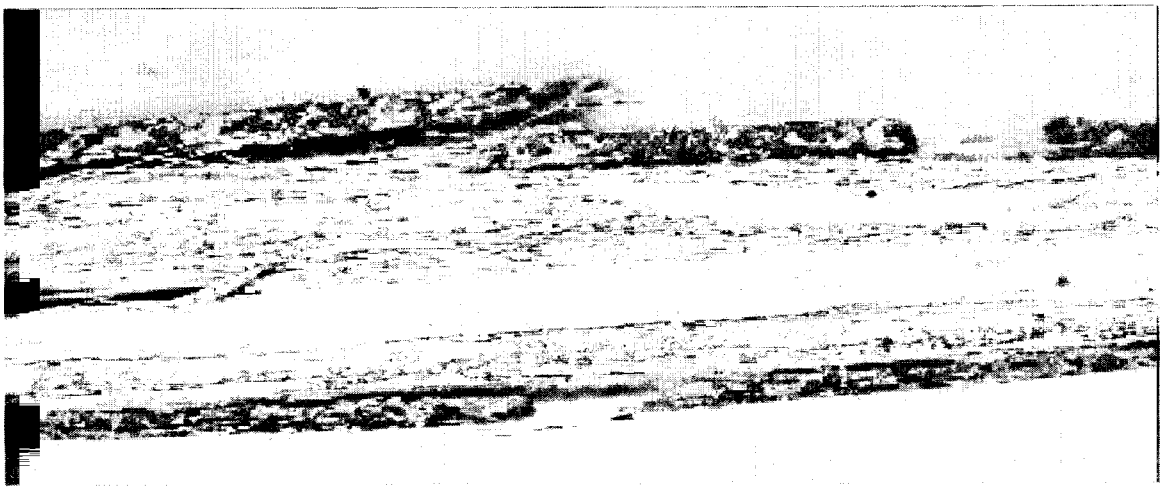

(b)

Figure 5.10 Stereoscope Images (16X) of UV Weathered Specimens (40% UTS) Showing Edge Delamination

5.5 Fatigue Strength of Hand Lay-up GFRP

The S-N curve of hand lay-up GFRP was plotted using the same method described in section 5.2. Figure 5.11 shows the mean S-N diagram of the hand lay-up GFRP with the 5% LTL line. The fatigue life at 26%UTS is approximately 1 million cycles. All specimens tested at 20% UTS exceeded the 3 million cycles limit set on the testing machine. The equations for the mean S-N curve, the 5% LTL line, and the 5th percentile line are given below:

Mean S-N curve	$\sigma_a = -10.42 LogN + 90.7$	Eqn 5-7
5% LTL	$\sigma_a = -10.8 LogN_{5\%LTL} + 85.6$	Eqn 5-8
5th Percentile	$\sigma_a = -10.52 LogN_{5th} + 87.5$	Eqn 5-9

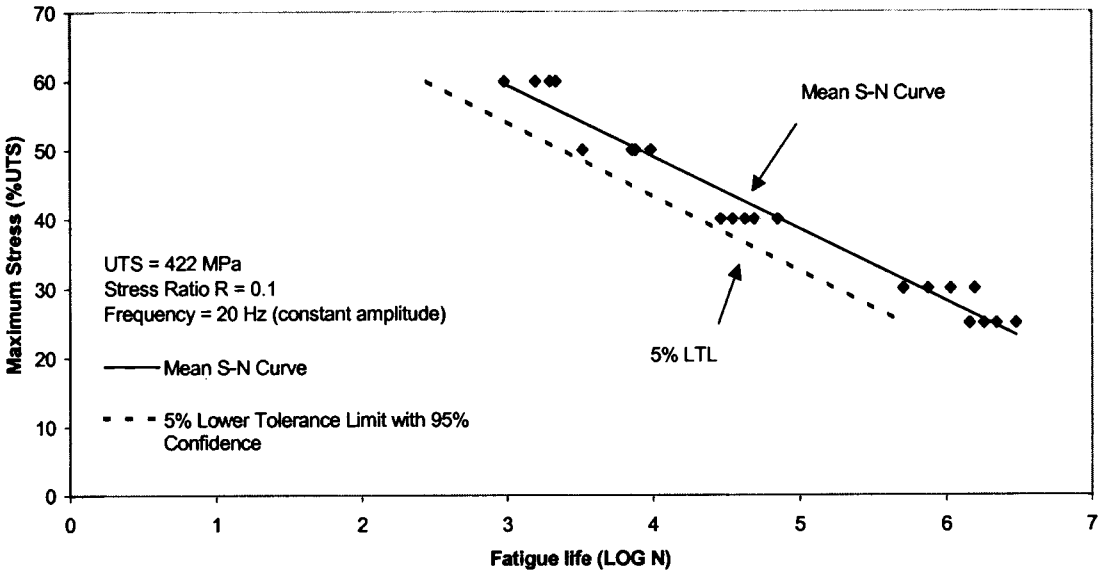

Figure 5.11 S-N Diagram of Hand Lay-up GFRP with 5% LTL with 95% Confidence

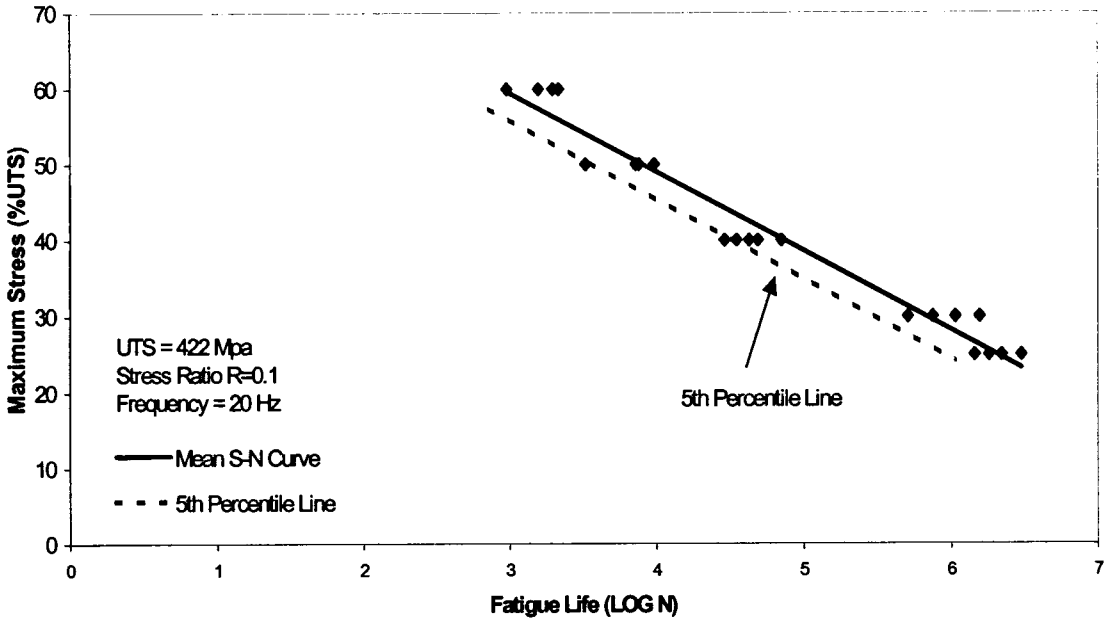

Figure 5.12 S-N Diagram of Hand Lay-up GFRP with the 5th Percentile Line

Failure Mechanism in Hand Lay-up GFRP

At higher stresses, most specimens failed with a combination of longitudinal splitting and tensile failure at the grip edge. Failure was observed as matrix cracking followed by fiber rapture and longitudinal splitting, which extended along the length of the specimen and usually terminated at the grip edge as shown in Figure 5.13. Grip failures although unavoidable, were not the primary source of failure, and thus were considered as valid results. It must be noted that grip failures seem to occur only after the coupons had developed a longitudinal or edge crack. As for lower stresses, most failures initiated with a crack in the narrow edge of the coupons like Type 1 mode. Most often these cracks propagate along the entire width leading to complete failure as shown in Figure

5.13 and 5.15. Specimens that were tested at 20% UTS showed no cracks or delamination.

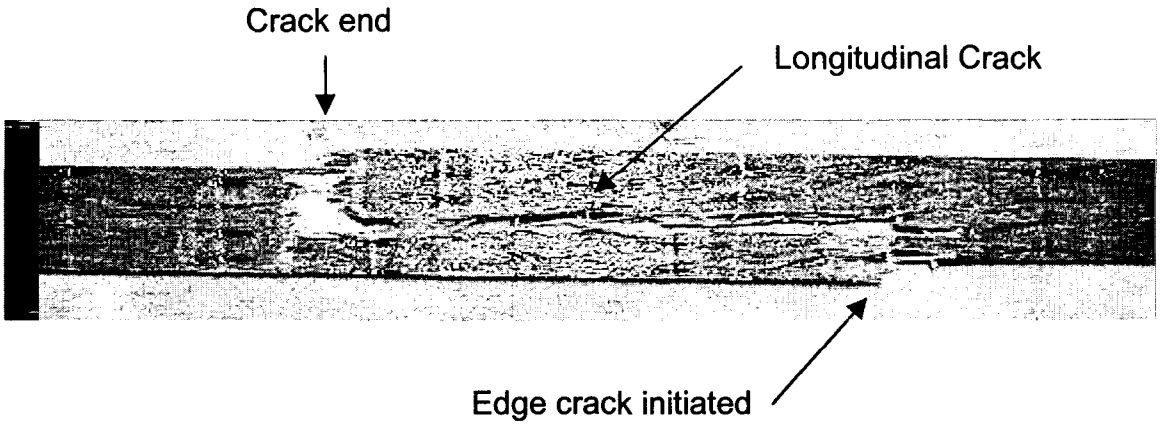

Figure 5.13 Typical Fatigue Failure of Hand Lay-up GFRP at High Stress (60%UTS)

It is quite evident from the S-N diagram (Figure 5.11) that the fatigue strength of the hand lay-up GFRP exhibits high variability compared to the pultruded type. This is mainly due to the hand lay-up process, which introduces many variables such as temperature and humidity at impregnation, speed and thickness of the impregnator, clamp pressure, and curing period.

In Figure 5.14, the S-N curve of hand lay-up and pultruded GFRP are given in the same plot on a normalized scale for comparison purposes. The S-N curve of pultruded GFRP is steeper than that of the hand lay-up type. This indicates that at lower stresses, the hand lay-up GFRP would have relatively higher fatigue lives compared to the pultruded GFRP on a %UTS basis.

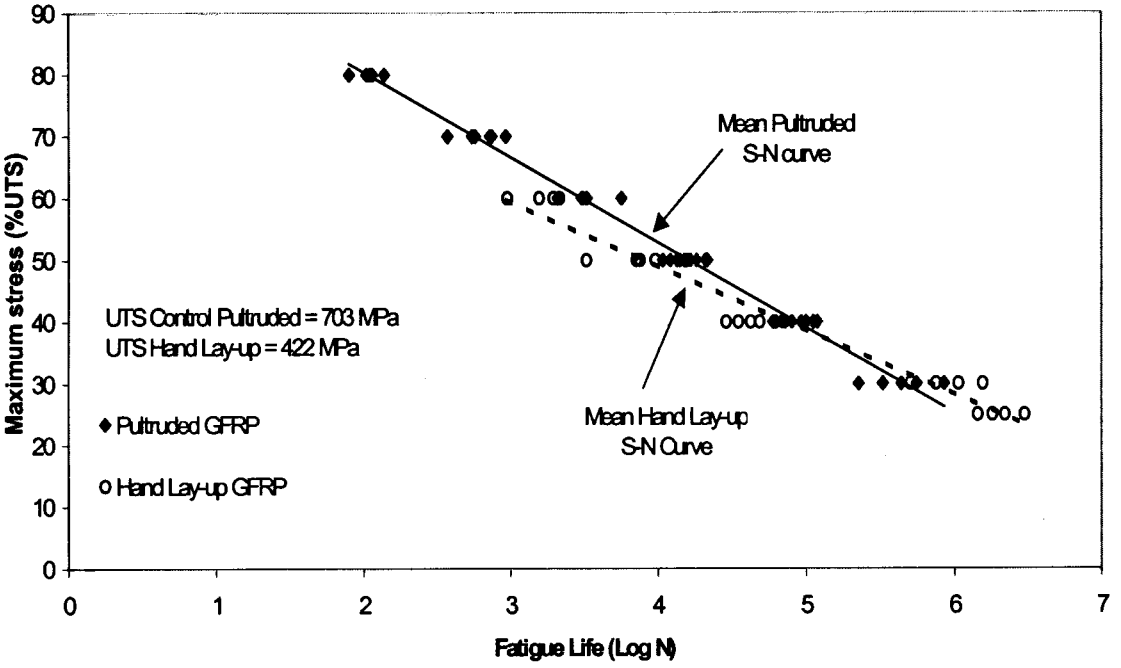

Figure 5.14 S-N Diagram of Pultruded and Hand Lay-up GFRP

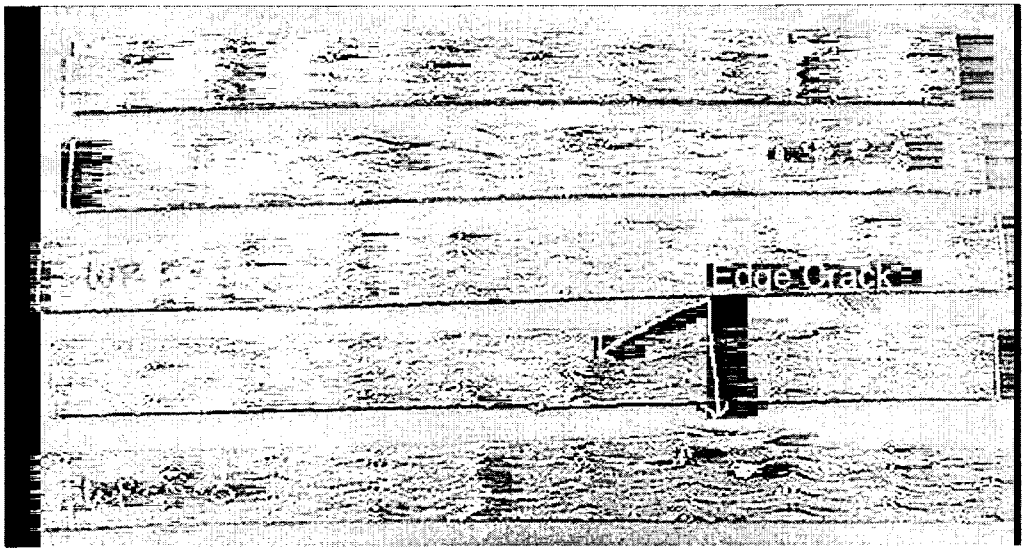

(a)

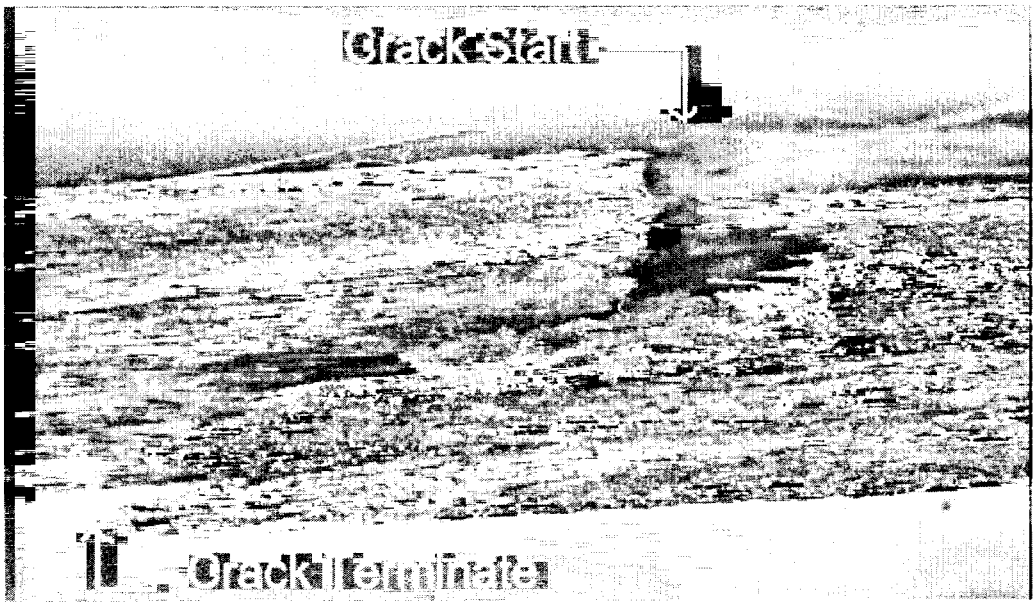

(b)

Figure 5.15 Hand Lay-up Fatigue Specimen Edge (thickness) (a) Edge Crack at 30%UTS, (b) Stereoscope Image (16X) of Edge Crack Starting and Ending Points.

5.6 Residual Strength of Pultruded GFRP

Residual strength was determined by fatiguing specimens at 10% UTS for 0.5, 1, and 3 million cycles, and statically testing to obtain residual tensile strength and Young's modulus (Table 5.4). Analysis of the results using ANOVA shows that the mean strengths and moduli at half, one, and three million cycles of fatigue are not statistically different from the control specimens at a significance level of 0.05.

Table 5.4 Results of Residual Strength Tests of Control Pultruded GFRP

	Sample size	Ultimate Tensile Strength		Young's modulus	
		UTS (MPa)	COV %	UTS (GPa)	COV %
Control	7	703.2	4.99	40.6	2.49
0.5 million	6	703.4	6.26	40.57	1.80
1 million	6	694.7	8.68	41.41	2.14
3 million	6	694.2	8.33	41.04	2.82

The composite strain due to 10%UTS load on the control pultruded GFRP is approximately 0.17%, which is smaller than the strain to failure of the phenolic resin, 0.45%. Thus the matrix may not have cracked as rapidly as high stress fatigue.

5.7 SEM Imaging of Fatigue Specimens

Pultruded GFRP

SEM images were taken on both pultruded and hand lay-up GFRP near fracture surfaces. Figure 5.16 shows fiber fracture and a large number of resin particles on a freeze-thaw pultruded specimen tested at 30% UTS control. This type of feature was also seen on other exposed pultruded specimens including control type (see Figure 5.17).

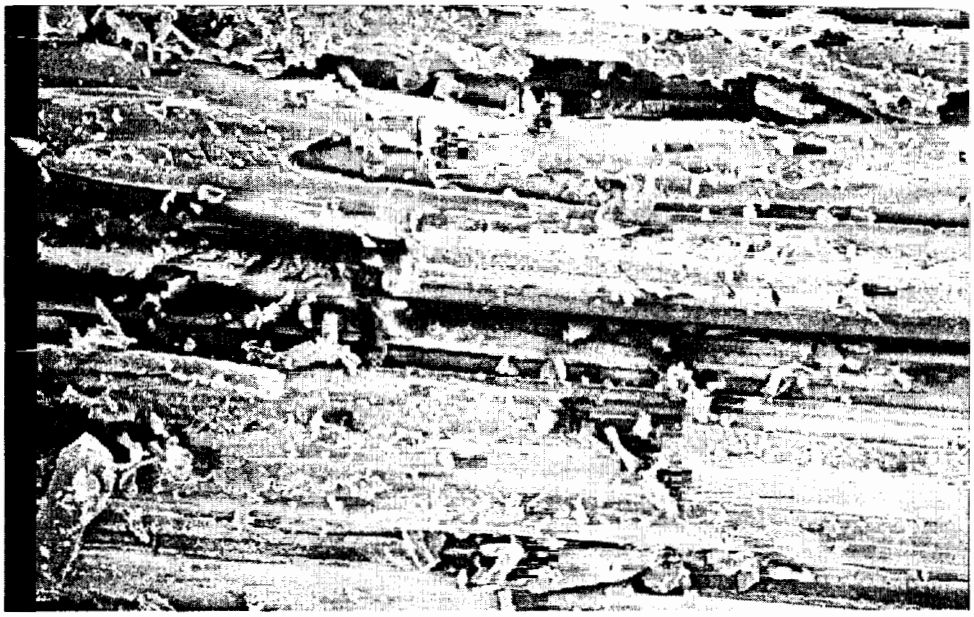

Figure 5.16 SEM Image of Freeze-Thaw Specimen at 240X Tested at 30%UTS Control

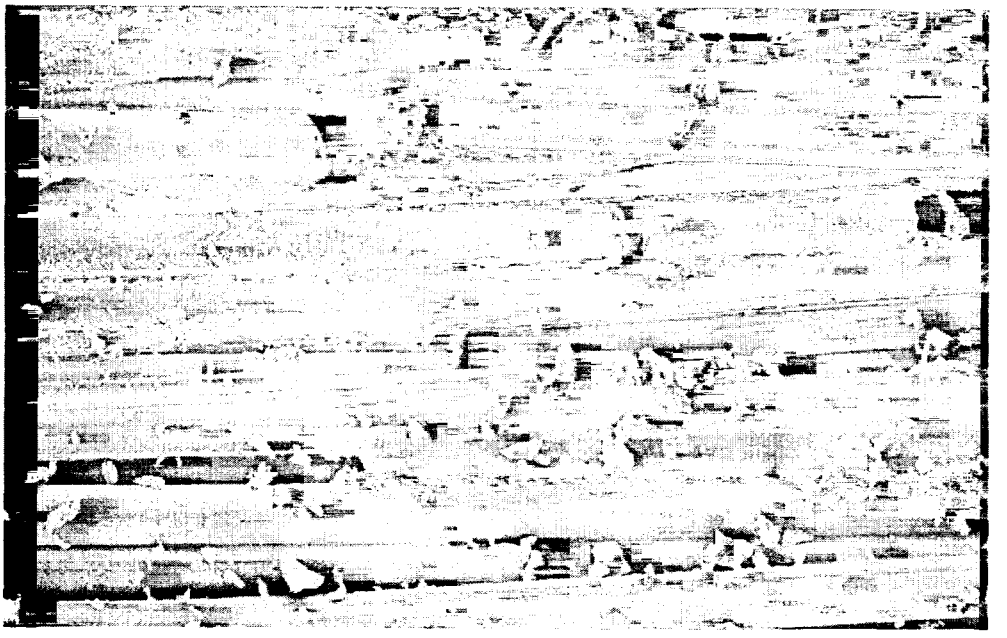

Figure 5.17 SEM Image (260X) of Control Pultruded GFRP Tested at 40% UTS

Hand lay-up GFRP

Hand Lay-up GFRP tested in fatigue show de-bonding between fiber and resin. Figure 5.18 shows a large number of resin debris. Near the fracture surface much fiber pullout is seen (see Figure 5.19). The bare fibers with little resin on them indicates poor wetting.

It can be concluded from the SEM images that failure initiated with matrix cracking followed by fiber-resin de-bonding. This resulted in fracture of those fibers that carried larger stresses, leading to ultimate composite failure.

Figure 5.18 SEM Image (240X) of Hand Lay-up GFRP Tested at 40%UTS

Showing Resin Debris and Fiber Fracture

Figure 5.19 SEM Image (120X) of Hand Lay-up GFRP Tested at 40%UTS

Showing Fiber Debonding and Fracture

5.8 Summary

Pultruded and hand lay-up GFRP were cyclically loaded at different stresses at a frequency of 20 Hz and stress ratio of R=0.1. S-N curves (Figure 5.1, 5.2 and 5.11) were developed from the fatigue tests. Additionally, pultruded specimens that were treated in different accelerated environments were also tested for change in fatigue behavior.

Pultruded control specimens were also cyclically loaded at 10% UTS and static tests were conducted at 0.5, 1 and 3 million cycles to evaluate residual strength and modulus. The results are summarized below.

- The mean fatigue life of control pultruded GFRP is approximately 1 million at 26.4%UTS (185 MPa, 26.93 ksi).
- UV weathering and hot water (45°C) exposures had no statistically significant effect on the fatigue strength at a significance level of 0.05. However, freeze-thaw and simulated seawater exposures show a statistically significant increase in fatigue lives at 30%UTS at a significance level of 0.05.
- The fatigue lives (cycles to failure) of freeze-thaw and simulated seawater specimens at 30%UTS control, increased by 166% and 139% respectively.

- UV weathering is considered that worst-case scenario for a combination of environmental exposure and fatigue. However, the difference between the fatigue lives of UV weathered specimens and control is statistically insignificant.
- The fatigue lives of all specimens (exposed and control) tested at 20%UTS exceeded the 3 million cycles limit set on the fatigue-testing machine.
- Fatigue failure mechanism was quite identical in all the specimens whether exposed or unexposed but dependent on the stress level. Failure at high stresses was mostly due to longitudinal splitting. Failure at low stresses was mostly due to the propagation of an edge crack, and shear delamination.
- Hand lay-up GFRP specimens had a fatigue life of 1 million cycles at 26%UTS (109 MPa, 15.83 ksi). Specimens tested at 20%UTS exceeded the 3 million cycles limit. Failure was mostly due to crack that initiate at the edge. The crack often propagates to the grip edge causing tensile failure.
- The residual strength tests show that when the pultruded GFRP was subjected to cyclic loading at 10%UTS, neither ultimate tensile strength nor Young's modulus changed significantly (significance level of 0.05). However, this conclusion can only be made for fatigue lives less than 3 million cycles at a stress level of 10%.

- SEM images of both pultruded and hand lay-up GFRP show a large amount of resin debris and fiber fracture near the cracks. The resin particles indicate the brittle nature of phenolic resins. The bare fibers indicate poor fiber-resin bonding. It seems failure initiated with matrix cracking followed by fiber de-bonding, and eventually fiber fracture.

6 CONCLUSIONS AND RECOMMENDATIONS

6.1 Introduction

A composite material is defined as a material consisting of two or more distinct components combined on a macroscopic scale (Jones, 1999). An FRP composite primarily consist of continuous fibers, which provide strength and stiffness, embedded in a resin system, which hold the fibers together and protect them from degradation. If the reinforcement used is glass fibers, the composite is referred to as "GFRP".

In this study two types (pultruded and hand lay-up) of phenolic GFRP materials were tested for physical, mechanical and fatigue properties. These GFRP materials were designed to be used as tension reinforcement for glulam beams. The GFRP materials were also designed to be compatible with the hygrothermal properties of wood.

To evaluate long-term durability, mechanical and fatigue properties were determined after exposing the pultruded GFRP to different accelerated environments. Some of the accelerated environments were designed according to recommendations given in International Conference of Building Officials (ICBO) Acceptance Criteria 125. American Society for Testing and materials (ASTM) testing standards were followed in all cases where applicable. The entire test matrix is given in Table 3.2.

The pultruded type was exposed to UV weathering, freeze-thaw, simulated seawater, and hot water (45°C). Table 3.3 provides details on the environmental exposures used. The hand lay-up GFRP was only tested under control conditions (no weathering).

Fatigue life was evaluated at different stress levels using a servo hydraulic testing machine. The fatigue cycle was a constant amplitude sinusoidal waveform with a frequency of 20Hz. The stress ratio (R) used was 0.1. Residual strength of the pultruded FRP was obtained at 3 million cycles for stress level of 10%UTS.

The results of both mechanical and fatigue properties were analyzed using single factor one-way ANOVA at a significance level of 0.05. For design purposes, the S-N curves were analyzed to obtain (1) the 5% one-sided Lower Tolerance limit with 95% confidence and, (2) the 5^{th} Percentile line. These lines give reasonable safe design values for fatigue design of the two GFRP examined in this study.

This chapter summarizes the results of physical, mechanical and fatigue tests. The results are discussed, and important findings are noted. This is followed by recommendations for design purposes, and for future work.

6.2 Literature Review

The literature review pertaining to this study was drawn from 6 articles on fatigue of phenolic composites, 31 articles on fatigue mechanisms and environmental effects and durability, 15 articles on modeling and 9 articles on statistical analysis of fatigue data. In summary, the following results were relevant to this work:

- Fatigue in general can be defined as the progressive permanent damage due to fluctuating load.
- Fatigue has been a design consideration ever since engineers realized that metals such as steel and aluminum might fail at stresses much below their static ultimate tensile strength when subjected to cyclic loading.
- In the past twenty years, much of the research on fatigue of FRP composites was conducted by the aerospace industry.
- Phenolic materials are becoming viable replacements of metals due to their high strength and creep resistance and dimensional stability at relatively high temperatures. They also posses good chemical and corrosion resistance (Branco et al, 1994).
- It is possible to produce large scale phenolic GFRP components with much superior fire and toxic fume emission characteristics compared to polyester and epoxy matrices (Tavakoli et al, 1990).
- Study on the fatigue of phenolic composites by Branco et al (1996) show that the fatigue life is approximately 1 million cycles at

30%UTS. The authors concluded that main failure mechanism is shear delamination between the resin and fibers.

- Moisture is known to act as a plasticizer and reduces the Tg of a GFRP.
- The damage caused due to moisture is fiber dominated and irreversible (Hayes et al 1998).
- The fatigue performance of phenolic GFRP is lower than those of epoxy and vinyl ester GFRP. This may be due to the brittles of the phenolic resin.
- The basic method for fatigue design is to limit the allowable stress such that it is below the fatigue threshold, if the threshold value is known. Another common method is to use the 5% one-sided Lower Tolerance Limit (5%LTL) as the safe design S-N curve. Safety factors may be used depending on the application.

6.3 Effects of Environmental Exposure on Physical and Mechanical Properties

Physical properties tested include density, volume fraction of fiber, resin, and voids. These properties were tested for unexposed (control) pultruded and hand lay-up GFRP. Glass transition temperature (Tg) of pultruded specimens was measured before and after each accelerated environmental exposure to determine if moisture caused any plasticization in the resin matrix.

The hand lay-up GFRP was not tested for Tg in this study. The reader is referred to reports written by Eoin Battles to obtain more information on the environmental durability of hand lay-up GFRP. The work by E. Battles include testing of Tg and Interlaminar shear strength of the hand lay-up GFRP.

Mechanical properties tested include interlaminar shear strength, ultimate tensile strength and Young's modulus. These properties were measured before and after exposure. All results were analyzed using ANOVA to check if the differences were statistically significant. The results summarized below are illustrated in Figure 6.1.

Physical Properties

- The pultruded E-glass/phenolic FRP is made of a 2.2mm core of unidirectional glass fiber rovings, encased between chopped strand mat layers, which are 0.55mm thick (see Figure 3.1). The hand lay-up GFRP is made of five layers of PRF impregnated unidirectional glass weave, which cured to a thickness of 3.5mm.
- The fiber volume fraction of the pultruded FRP is approximately 54%, with 22% resin volume fraction and 24% voids. The hand lay-up FRP consists of 65% fiber, 27% resin and 8% voids. The densities of pultruded and hand lay-up FRP are approximately 1.75g/cc and 2.01g/cc respectively (see Appendix B).

- SEM images of pultruded GFRP (Figure 4.1 and 4.2) show that the chopped glass fibers in the mat layers are randomly oriented and consist of large void spaces. The core of the pultruded GFRP also exhibited large number of voids as shown in Figure 4.3. This feature of phenolic composites was also reported by Branco et al (1992).

Glass Transition Temperature: Tg

- The glass transition temperature (Tg) of pultruded control GFRP is 201 ± 2.7°C.
- The Tg of exposed pultruded specimens ranged from 194°C to 207°C with simulated seawater specimens showing the lowest Tg and UV weathered specimens showing the highest Tg respectively (see Table 4.3). The Tg of hot water and simulated seawater specimens, which were exposed to 3000 hours, reduced by 5.4°C and 7.6°C respectively. Freeze-thaw specimens showed no statistically significant change in the Tg.
- The lowering of Tg may be due to plasticization of the matrix caused by moisture intake. Other authors who tested vinyl ester and epoxy GFRP laminates have reported this phenomenon (Sridharan et al, 1998; Liao et al, 1998). The Tg of UV weathered specimens in this study, which were exposed to 2000 hours of UVA at 63°C with periodic water spray, exhibited a 5.2°C increase. This may be due to post-curing of the phenolic matrix material. Gentry et al (1998) also reported that the increase in Tg indicates an increase in molecular weight due to post curing.

- The surface color of the mat layer of the UV weathered specimens turned from dark brown to pale purple exposing some of the surface chopped glass fibers.
- Hand lay-up specimens were not tested for Tg in this study.

Interlaminar Shear Strength

- The mean interlaminar shear strength of control specimens is 24.3 MPa with a COV of 4.76%. Statistical analysis show that the interlaminar shear strength of hot water and UV weathered pultruded specimens reduced by 6% and 11% respectively. It is possible that the reduction in ILSS was caused by degradation of the fiber-resin interface due to moisture. The ILSS of simulated seawater and freeze-thaw specimens were not statistically different from the control at a significance level of 0.05. The hand lay-up FRP was not tested for ILSS.

Ultimate Tensile Strength and Young's Modulus

- The mean ultimate tensile strength and modulus of control pultruded GFRP is 703 MPa with a COV of 5.0% and, 40.6 GPa with a COV of 2.5% respectively.
- Hot water exposure caused the highest reduction (31.7%) in ultimate tensile strength (UTS) of pultruded GFRP (see Table 4.5). This reduction in tensile strength of the hot water specimens may be due to the synergistic effect of high temperature (45°C) and 100% RH conditions.

- UTS of Freeze-thaw and simulated seawater specimens reduced significantly by 10% and 7% respectively. UV weathered specimens showed no statistically significant change in ultimate tensile strength at the 5% significance level.
- None of the exposed specimens showed any statistically significant change in the Young's modulus at the 5% significance level. Liao et al (1998a) tested pultruded vinyl ester E-glass composites in salt water and plain water and reported that the flexural modulus did not chance at the 90% confidence level in spite of conditioning for 6 months (significance level of 0.1). However, Sridharan et al (1998) also tested E-glass vinyl ester pultruded composites, at 50° C and 80° C in water for 52 days and reported an 8% decrease in the flexural modulus for both temperatures.
- The mean ultimate tensile strength and modulus of hand lay-up GFRP is 422 MPa with a COV of 18% and 36 GPa with a COV of 9.5% respectively.

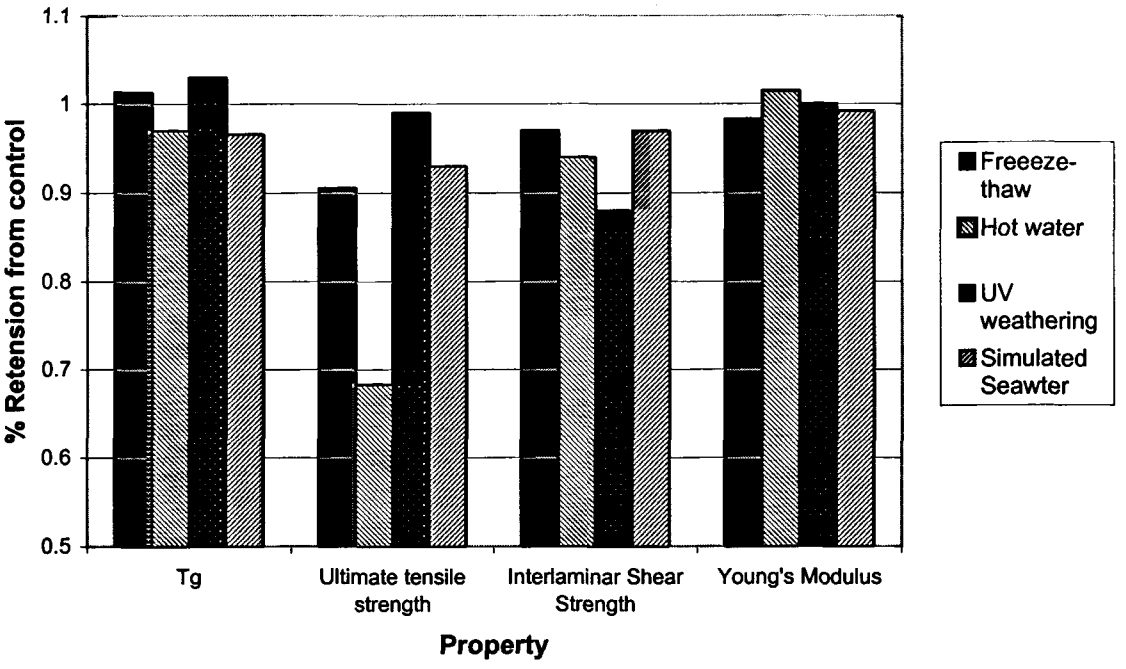

Figure 6.1 Property Retention in Pultruded GFRP

- Freeze-thaw cycling, UV weathering and simulated seawater tests were specified by ICBO AC125, which required a retention value of 85% after 3000 hours for simulated seawater, 90% retention for 2000 hours of UV weathering and 90% retention for 20 cycles of freeze-thaw. These retention values were required for tensile strength, modulus, and interlaminar shear strength. The residual mechanical properties of the pultruded specimens exposed to these environments exceeded the required retention values specified in ICBO AC 125 (see Figure 6.1). The worst condition was hot water, which was not specified by ICBO.

6.4 Fatigue Life and Residual Strength Tests

The fatigue life of control pultruded GFRP and hand lay-up GFRP was evaluated at every decade of UTS from 80% to 20%. The fatigue life of exposed pultruded specimens was tested at 50%, 40%, 30% and 20%UTS-control only. S-N curves were then developed for each exposure (see Figure 5.2). The stress ratio (R) and frequency for both were 0.1 and 20 Hz respectively. All specimens were fatigued in sinusoidal constant amplitude waveform using a servo-hydraulic testing machine. A minimum of five specimens was tested at each stress level for the control, and four for the exposed types. Equations for finding the lower 95% tolerance limit (5% LTL) and 5th Percentile line were also developed (see Figure 6.2). The results of fatigue tests are summarized below.

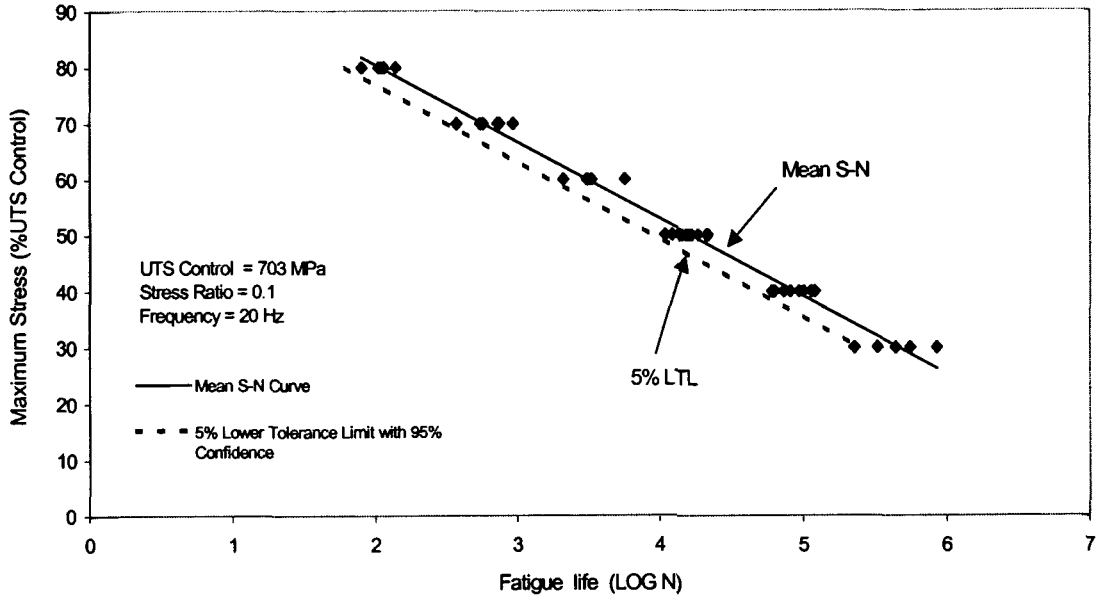

Figure 6.2 S-N Curve of Pultruded GFRP with 5%LTL with 95% Confidence

Control Specimens

- For control pultruded specimens, the mean fatigue life at 25%UTS is approximately 1 million cycles. This result is in line with other fatigue studies. Branco et al (1996) reported that at room temperature, the fatigue life of a unidirectional pultruded GFRP (700 MPa UTS) was approximately 1 million cycles at 21%UTS. They also reported that a woven pultruded E-glass phenolic FRP with 305 MPa UTS had a fatigue life of 1 million cycles at 28% UTS.
- All 5 specimens tested at 20% UTS exceeded the 3 million cycles limit.

Exposed Specimens

- At 30%UTS, freeze-thaw and simulated seawater specimens showed a statistically significant increase in fatigue lives at the 5% significance level. The mean fatigue lives of freeze-thaw and simulated seawater specimens at 30%UTS increased by 166% and 139% respectively. However, Liao et al (1998) tested glass/vinyl ester composites in four-point bend environmental fatigue (5 months) and reported that salt water (5% and 10% NaCl) has a significant detrimental effect on the fatigue life at 30%UTS. The four point bend fatigue test is much more severe than the tension-tension fatigue done in this study. Liao conducted fatigue tests simultaneous with the exposure. This is known to cause stress corrosion which induces much more damage compared to tension-tension fatigue at normal lab atmosphere as done in this study.

- The mean fatigue lives of UV weathered and hot water specimens at 30%UTS are not statistically different from the control at a significance level of 0.05. At 40% and 50%UTS none of the exposures caused any statistically significant change in the fatigue lives compared to the control specimens. Liao et al (1998) also states that above 45%UTS, water and salt water conditioning had very little effect on the fatigue life pultruded vinyl ester GFRP.
- In spite of the 31% reduction in tensile strength of hot water specimens, the fatigue performance did not change (see Figure 5.2). Figure 5.2 indicates that hot water slightly improved fatigue life of pultruded GFRP. However the change is not statistically significant at the 5% level. It is known from literature that resins with higher strain to failure perform better in fatigue. Hot water specimens exhibited a reduction in Tg, which is indicative of plasticization, i.e. reduced brittleness.
- UV weathered specimens exhibited the lowest fatigue life among all the exposures. However the mean fatigue life of UV weathered specimens was not statistically different from the control mean S-N curve at the 5% level.
- All 16 specimens (4 from each of 4 exposures) tested at 20% UTS exceeded the 3 million cycles limit.

Hand Lay-up Specimens

- Hand lay-up GFRP had fatigue life of 1 million cycles at 26%UTS. All specimens tested at 20%UTS exceeded the 3 million cycles limit. Fatigue failure mechanisms are shown in Figure 5.5. Branco et al (1996) found that a particular unidirectional hand lay-up phenolic GFRP (462 MPa UTS, $V_f = 0.42$) had a fatigue life of 1 million cycles at 44%UTS.
- The hand lay-up specimens exhibited high variability at lower stress levels (see Figure 5.11).

Fatigue Failure Mechanism

- Failure mechanism of control pultruded specimens at high stresses (>50%UTS) was similar to that of static failure, characterized by massive fiber brooming near the middle of the gauge length (Figure 4.7, 5.6- 5.9). At lower stresses, failure was characterized by cracks at the narrow edge, and longitudinal splitting with no brooming (Figure 5.8). Failure seems to initiate by matrix micro-cracks transverse to the loading direction. This results in fiber breakage or interfacial failure (fiber-resin debonding) followed by ultimate composite failure. This type of failure mechanism has been observed by others and is extensively reported in literature (Liao et al 1998a).

Residual Strength

Residual strength tests were conducted at 10%UTS. Six specimens were fatigued at each of 0.5, 1 and 3 million cycles and tested for ultimate tensile strength and modulus. The results show no statistically significant changes in tensile strength or Young's modulus at a significance level of 0.05.

6.5 Recommendations for Fatigue Design of Pultruded GFRP

The fatigue strength of a material is an important factor that most design engineers consider for structures subjected to cyclic loading. In fact 50-90% of the failure of engineering components and structures are attributed to fatigue (Gao, 1994; Beynon et al (Eds), 1999).

Advances in composite materials lead to the development of more efficient FRP structures where the allowable strength has increased significantly. This makes fatigue analysis an important part of design process because most often fatigue tends to be the controlling factor in such designs. The fatigue data of the pultruded E-glass/phenolic FRP and the hand lay-up FRP are given in S-N curves from which one may estimate the service life of a component depending on the number of cycles the structure is likely to endure during its service.

The design strength may be based on the lower 95% tolerance limit for 95% of the population. This tolerance limit has been called the 5% LTL (Lower Tolerance Limit) with 95% confidence in this study (see Figure 6.2). It assures that at least 95% of the specimens will have a 95% survival probability. It must be noted here that a designer needs to incorporate a safety factor, the magnitude of which will depend on the load uncertainty, frequency and service life.

In the following table, the mean S-N curves of control specimens are tabulated because these specimens displayed the lowest fatigue life compared to the exposed types at stresses around 30%UTS-Control. UV weathered specimens exhibited the lowest fatigue life but the difference from the control was not statistically significant at the 5% level.

The fatigue life of pultruded FRP at different stress levels is given in Table 6.1. It must be noted here that the fatigue strength at 3 million cycles is a projected value. Since fatigue strength of the pultruded and hand lay-up GFRP has not been tested at stress lower than 20%, the equations given in this study should not be used to evaluate fatigue life for stresses below 20%UTS.

Table 6.1 Fatigue Life Data of Pultruded and Hand Lay-up GFRP

Stress Level			Fatigue life (cycles)					
			Control Pultruded GFRP			Hand lay-up GFRP		
%UTS control	MPa	ksi	Mean	5th Percentile	5% LTL*	Mean	5th Percentile	5% LTL
50%	350	50	14600	8500	8700	8000	3600	1900
40%	280	40	76100	41700	45400	73300	32500	16700
30%	210	30	397100	204300	236600	669300	290800	140800
25%	175	25	906800	452000	539800	2 mill	869200	408500
20%	140	20	> 3 mill	1 mill	1.2 mill	>3 mill	2.6 mill	1.18 mill
10%	70	10	> 3 mill					

* with 95% Confidence

The data from the above table can be used to estimate the minimum fatigue life of both the pultruded and hand lay-up phenolic GFRP used in this study. Designers may include addition safety factors based on the application of the GFRP.

6.6 Recommendations for Future Work

- In this study the pultruded specimens were exposed in simulated seawater and hot water for 3000 hours only, and then tested for mechanical and fatigue properties. To get a better understanding of how the material properties change, the author recommends testing at 1000, 2000, 6000, and 10,000 hours of exposure. These tests would give a better perspective of the rate of change of properties. The author recommends similar tests for hand lay-up GFRP type
- A good continuation of this project would be the study of fatigue strength of glulam beams reinforced with GFRP. The parameters for such a test would be much different from the coupon testing. It is recommended that the fatigue loads exerted on the GFRP be 30%, 20% and 10% of UTS because this is the typical load range that the GFRP is likely to see in real life applications.
- The fatigue strength of the pultruded GFRP exposed to acidic (HCl) and highly basic solutions (NaOH) may help in better evaluating the FRP material. Freeze-thaw, hot water and simulate seawater tests may also be repeated in an environmental chamber such that the specimens are continuously exposed while subjected to cyclic loading.
- It is also recommended to test at least 10 specimens in each stress level to obtain more accurate distribution of fatigue life.
- Residual strength tests are also recommended at 30% and 20%UTS control in addition to 10%UTS.

REFERENCES

AASHTO LRFD BRIDGE DESIGN SPECIFICATION (1994), American Association of State Highway and Transportation officials, First Edition, Section 6.6, Washington, D.C.

Abdel-Magid, B., Battles, E., Dagher, H., Iqbal. M. (1999). "Durability of FRP Reinforcement for Wood," ICC'99, Session 22-C.

Aboudi, J., (1989). "Micromechanics Prediction of Fatigue Failure of Composite Materials," Journal of Reinforced Plastics and Composites, vol.8, March.

Aditya, P. K. and Sinha, P.K. (1992). "Diffusion Coefficients of Polymeric Composites Subjected to Periodic Hygrothermal Exposure," Journal of Reinforced Plastics and Composites, vol. 11, pp1035-1047.

Agarwal, B. D. (1990). Analysis and Performance of Fiber Composites, 2nd edition, New York: John Wiley & Sons.

Andersons, J. (1993). "Methods of Fatigue Prediction for Composite Laminates: A Review," Mechanics of Composite Materials, 29(6), pp545-554.

Annual Book of Standards, American Society for Testing and Materials. (1999).

ASM HANDBOOK : Fatigue and Fracture. (1999) Vol. 19, ASM International, ISBN 0871703858.

Augl, J. M. (1996). "Practical Guidelines for Moisture Diffusion Measurement in Composites," Technical Report, NSWCCARDIV-TR-96/017, Naval Surface Warfare Center-Carderock Division, July, US Navy, MD.

Ayyub, B. M., Ed. (1998). Uncertainty Modeling and analysis in civil Engineering, Florida: CRC Press LLC.

Bareishis, I. P. (1996). "The Mechanism of Fatigue Failure of Plastics," Mechanics of Composite Materials, 32(2), pp192-196.

Bathias, C. (1991). "Fracture and Fatigue of High Performance Composite Materials: Mechanism and Prediction," Engineering Fracture Mechanics, 40(4-5), pp757-783.

Bauccio, Michael, Ed. (1994). Engineering materials reference book, 2nd edition, Ohio: ASM International, Materials Park.

Beynon, J.H., Brown, M.W., Lindley, T.C., Smith, R.A., Tomkins, B. (1999). Engineering Against Fatigue, (Work of K.J Miller), Vermont: A.A. Balkema Publishers.

Bodig, Jozsef (1992). Mechanics of Wood and Wood Composites, Florida: Krieger Publishing Company.

Bradley, W. L. and Grant, T. S. (1995). "The effect of the moisture absorption on the interfacial strength of polymeric matrix composites," Journal of Materials Science, vol. 30, Nov., pp5537-5542.

Brady, Clauser, Vaccari (1997). Materials Handbook, 14th Edition, New York: McGraw Hill.

Branco, C. M., Eichler, K., and Ferreira, J. M. (1994). "Fatigue behavior of E-glass fiber reinforced phenolic composites: Effect of temperature, mean stress and fiber surface treatment," Theoretical and Applied Fracture Mechanics, vol. 20, pp75-84.

Branco, C. M., Ferreira, J. M., Fael, P., and Richardson, M. O. W. (1996). " A Comparative study of the fatigue behavior of GRP hand lay-up and pultruded phenolic composites," International Journal of fatigue, 18(4) May, pp255-263.

Branco, C. M., Ferreira, J. M., Fael, P., and Richardson, M. O. W. (1992). "Fatigue behavior of a phenolic matrix composite," International Journal of Fatigue, 14(6) Nov., pp367-375.

Breyer, D.E. (1993). Design of wood structures, 3rd edition, MacGraw Hill Inc.

Brondsted, P., Andersen, S.I. (1996). "Fatigue performance of Glass/Polyester Laminates and the Monitoring of Material Degradation," Mechanics of Composite Materials, 32(1), pp21-29.

Buck, S. E. (1997). "The combined effects of load, temperature, and moisture on the durability of E-glass/Vinyl ester composite material," 42nd International SAMPE Symposium, pp444-453.

Caprino, C., D'Amore, A., and Facciolo, F. (1998). " Fatigue Sensitivity of Random Glass Fiber Reinforced Plastics," Journal of Composite Materials, 32(12).

Case, S. W., Lesko, J. J., Cousins, T. E. (1998). " Development of Life Prediction Scheme for the Assessment of Fatigue Performance of Composite Structures," Proceedings of the CDCC Durability of Fiber Reinforced Polymer (FRP) Composites for Construction, Quebec, Canada, p69-79.

Cetim, P. C. and Ifremer, L. L. (1995). "Effects of Water Absorption and Osmotic Degradation on Long-Term Behavior of Glass Fiber Reinforced Polyester," Polymer Composites, 16(5), pp349-355.

Chatterjee, S. N., Yen, C. F., and Oplinger, D. W. (1997). "On the Determination of Tensile and Compressive Strengths of Unidirectional Fiber Composites," Composite Materials: Fatigue and Fracture, 6th Vol., ASTM STP 1285, E.A. Armanois, Ed., American Society for Testing and Materials, pp.203-224.

Chawla, K. K. (1987), Composite Materials, New York: Springer-Verlag.

Chin, J. W., Aouadi, K., and Nguyen, T. (1997). "Effects of Environmental Exposure on Fiber-Reinforced Plastic (FRP) Materials Used in Construction, " Journal of Composites Technology & Research, JCTRER, 19(4) Oct., pp 205-213.

Chin, J., J., Nguyen, T., and Aouadi, K. (1999). "Sorption and Diffusion of Water, Salt Water, and Concrete Pore Solution in Composite Matrices," Journal of Applied Polymer Science, vol. 71, pp483-492.

Coquill, Scott L. (1989). " Mechanical properties of several neat polymer matrix materials and unidirectional carbon-fiber reinforced composites," NASA contractor report, NASA CR-181805.

Curtis, P. T. (1991). "Tensile fatigue mechanism in unidirectional polymer matrix composite materials," International Journal of Fatigue, 13(5), pp377-383.

Curtis, P.T. (1989). "The Fatigue Behavior of Fibrous Composite Materials," Journal of Strain Analysis, 24(4), pp235-244.

Dekker, M., (1997). The Engineer's Cost handbook: Tools for managing project costs, New York.

Demers, C. E. (1998). "Axial Fatigue Strength Degradation of Carbon FRp Composites and E-glass FRP Composites," Second International Conference on Composites In Infrastructure, Saadatmanesh, H., Ehsani, M. R., Eds., Tucson, AZ, pp86-91.

Demers, C. E. (1998). " Tension-tension axial fatigue of E-glass fiber-reinforced polymeric composites: Tension fatigue modulus," Construction and Building Materials, 12(1) Feb, pp51-58.

Diao, X., Ye, Lin, (1995). "A Statistical Model of Residual Strength And Fatigue life of Composite Laminates", Composite Science and Technology, vol. 54, pp329-336.

Diao, X., Ye, L., Mai, Y. W. (1997). "Statistical Fatigue Life Prediction of Cross-Ply Composite Laminates," Journal of Composite Materials, 31(14), pp1442-1460.

Dillard, D. A, in Reifsnider, K. L. and Pipes, R. B. (Eds). (1991). Fatigue of Composite Materials, Vol. 4, New York: Elsevier, pp339-429.

Echtermeyer, Andreas T., Engh, B. and Buene, L. (1995). " Lifetime and Young's modulus changes of glass/phenolic and glass/polyester composites under fatigue," Composites, 26(1) Jan., pp10-16.

El Kadi, H., Ellyin, F. (1994). "Effect of stress ratio on the fatigue of unidirectional glass fiber/epoxy composite laminates," Composites, 25(10), pp917-924.

Fawaz, Z. and Ellyin, F. (1994). "Fatigue Failure Model for Fiber-Reinforced Materials under General Loading Conditions," Journal of Composite Materials, 28(15), pp1432-1451.

Fisher, John W. (1997). "Evaluation of Fatigue-Resistant Steel Bridges", Transportation Research Record No.1594. Bridges, other Structures, and hydraulics and Hydrology, pp5-17.

Foley, G. E., Roylance, M. E., and Houghton, W. W. (1983). "Life prediction of glass/epoxy composites under fatigue loading," ASME International Conference on Advances in Life Prediction Methods, Albany NY, pp301-305.

Gao, Z. (1994). "A Cumulative Damage Model for Fatigue Life of Composite Laminates," Journal of Reinforced Plastics and Composites, vol. 13 Feb., pp128-141.

Gauthier, M. (1995). Engineered Materials Handbook: Desk Edition, ASM International, Materials Park, OH.

Gentry, T. R., Bank, L. C., Barkatt, A., and Prian, L. (1998). " Accelerated Test Methods to Determine the Long-Term Behavior of Composite Highway Structures Subjected to Environmental Loading," Journal of Composites Technology & Research, JCTRER, 20(1) Jan., pp. 38-50.

Halverson, H. G., Curtin, W. A. and Reifsnider, K. L. (1997). "Fatigue life of Individual composite specimens based on intrinsic fatigue behavior," International Journal of Fatigue, 19(5), pp369-377.

Hancox, N. L. (1998). "Thermal effects on polymer matrix composites: Part 1. Thermal cycling," Materials and Design, vol. 19, pp85-91.

Harper, J. F. and Naeem, M. (1989). "The Moisture Absorption of Glass Fiber Reinforced Vinyl ester and Polyester Composites," Materials & Design, 10(6), pp297-300.

Hayes, M. D., Garcia, K., Verghese, N., Lesko, J.J. (1998). "The Effect of Moisture on the Fatigue Behavior of a Glass/Vinyl Ester Composite", Second International Conference on Composites in Infrastructure, ICCI 98, USA.

Hayes, M. D., Lesko, J. J., Cousins, T. E., Ohanehi, D. Witcher, D., and Barefoot, G. (1999). Static and Fatigue performance of a Square Tube and plate Type Fiberglass Composite Bridge Deck System.

Hogg, V. R., and Ledolter, J., Eds. (1992). Applied Statistics for Engineers and Physical Scientists. 2nd Edition.

Hwang, W., Lee, C. S., Park, H. C., and Han, K. S. (1995). "Single-and Multi-Stress Level Fatigue Life Prediction of Glass/Epoxy Composites," Journal of Advanced Materials, 26(4), pp3-9.

Huston, R. J. (1994). Fatigue life prediction in composites. International Journal of Pressure Vessels and Piping, 59, pp131-140.

Jordan, A. R. (1996). Wetpreg Reinforcement of Glulam Beams, Master's Thesis, University of Maine, Maine.

Kallmeyer, A. R. and Stephens, R. I. (1995). "Constant and Variable Amplitude Fatigue Behavior and Modeling of an SRIM Polymer Matrix Composite," Journal of Composite Materials, 29(12), pp1621-1648.

Kedward, K.T. (1992). "The treatment of fatigue and damage accumulation in composite design," International Journal of Fatigue, 14(5), pp283-294.

Kenane, M. and Benzeggagh, M.L. (1997). " Mixed-mode delamination fracture toughness of unidirectional glass/epoxy composites under fatigue loading," Composites Science and Technology, 57(5), pp597-605.

Kimball, T.E. (1995). The feasibility of glulam beams reinforced with fiber-reinfoirced plastic sheets, Master's thesis, University of Maine.

Kroschnite, J. (1990). Concise Encyclopedia of Polymer Science and Engineering, New York: John Wiley and Sons.

Lee, J., Harris, B., Almond, D.P., Hammett, F. (1997). "Fiber composite fatigue-life determination," Composites, Part A, 28(4), pp5-15.

Liao, K., Schultheisz, C. R., Hunston, D. L., and Brinson, L. C. (1998a). "Environmental Fatigue of Pultruded Glass-Fiber Reinforced Composites," Composite Materials: Fatigue and Fracture, Seventh Symposium, ASTM STP 1330, R. B. Bucinell, Ed., American Society for Testing and Materials, pp. 217-234.

Liao, K., Schultheisz, C. R., Hunston, D. L., and Brinson, L. C. (1998b). " Long-Term Durability of Fiber-Reinforced Polymer-Matrix Composite Materials for Infrastructure Applications: A Review," Journal of Advanced Materials, 30(4), pp3-40.

Little, R. E. and Ekvall, J. C., Eds. (1979). Statistical Analysis of Fatigue Data. ASTM STP 744, American Society For Testing and Materials.

Lopez-Anido, R., Howdyshell, P. A., Stephenson, L. D., and Gangarao, H. V. S. (1999). "Fatigue and Failure Evaluation of Modular FRP Composite Bridge Deck," ICC 1999. Session 4-B, pp1-6.

Lorenzo, L. H., and Thomas, H. (1986). "Fatigue Failure Mechanism in Unidirectional Composites," Composite Materials: Fatigue and Fracture, ASTM STP 907, Hahn, H. T., Ed., American Society for Testing and Materials, Philadelphia, pp210-232.

Lubin, G. (1981). Handbook of Composites, New York: Van Nostrand Reinhold.

Mandell, J. E. (1985). " Tensile fatigue of glass fibers and composites with conventional and surface compressed fibers," Technical sessions of the Fortieth Annual Conference, Reinforced Plastics/Composites institute, pp1-7.

Newby, G. B., and Theberge, J. E. (1984). "Fatigue Endurance and Creep Resistance of Thermoplastic Composites," 39th Annual Conference, Reinforced Plastics/Composites Institute, The Society of the Plastics Industry, Inc.

Newby, G. B., Theberge, J. E. (1984). "Fatigue Endurance creep resistance of Thermoplastic composites," 39th Annual Conference, Reinforced Plastic/ Composites Institute, The Society of the Plastics Industry, Inc. page1 sec16-D.

Nishioka, G. M. (1990). "Adsorption/ desorption of water on glass fiber surfaces," Journal of non-Crystalline Solids, Elsevier Science Publishers, vol. 120, pp34-39.

Nyman, T. (1996). Composite fatigue design methodology: a simplified approach. Composite Structures, vol. 35. 183-194.

O'Brian, T.K., Rigamonti, M., Zanotti, C. (1989). "Tension Fatigue analysis and life Prediction for Composite Laminates," International Journal of Fatigue, v11, n6, pp379-393.

Oikawa, Y. (1980). " Fatigue Strength of Phenolic Molding Material," J Macromol Sci Phys US-Jpn Jt Semin on Crazing, Flow and Form of Polym., 19(4), pp679-693.

Ostle, B. (1996). Engineering Statistics - the industrial experience, Wadsworth Publishing Company.

Parvatareddy, H., Wang, J. Z., Dillard, D. A., Ward, T. C. (1995). "Environmental Aging of High-Performance Polymeric Composites: Effect on Durability," Composites Science and Technology, vol. 53, pp399-409.

Plumtree, A., Shen, G. (1994). " Prediction of Fatigue Damage Development in Unidirectional Long Fiber Composites," Polymers and Polymer Composites, 2(2), pp83-90.

Reinhart, Theodore J. Dostal, Cyril A., (1987). Engineered materials Handbook: Composites, ASM International, Materials Park, OH.

Roland, K.O., Echtermeyer, A.T. (1996). "Estimation of Fatigue curves for design of composite laminates," Composites, Part A, Elsevier Science Ltd, 27(6), pp485-491.

Shutte, L. C. (1994). "Environmental Durability of Glass Fiber Composites," Materials Science and Engineering, R13, pp265-324.

Skoog, D. A.; Holler, F. J.; Nieman T. A. (1992). Principles of Instrumental Analysis, 5th edition, Saunders College Publishing.

Smets, B.M.J. (1985). "On the mechanism of the corrosion of glass by water," Philips Tech. Rev.42(2), pp59-64.

Sokolkin, Y. V. et al (1992). "Probabilistic Model of the Strength, Crack Resistance, and Fatigue Life of a Unidirectional Reinforced Fibrous Composite," Mechanics of Composite Material, 28(2), pp133-139.

Sorathia, U and Dapp, T. (1997). "Structural Performance of Glass/Vinylester Composites at Elevated Temperatures," 42nd International SAMPE Symposium, May 4th.

Sridharan, S., Zureick, A. H., Muzzy, J. D. (1998). " Effects of Hot-Wet Environment on E-glass/Vinyl ester Composites," ANTEC'98, pp2255-2259.

Starr, T. (1993). Data book of Thermoset Resins for Composites, Somerset UK.

Stinchcomb, W. W., Subramanian, S. and Reifsnider, K. L. (1995). "A cumulative damage model to predict the fatigue life of composite laminates including the effect of a fiber-matrix interphase," International Journal of Fatigue, July 1, 17(5).

Stinchcomb, W.W. and Reifsnider, K.L. (1988). "The life-Limiting Process in Composite Laminates," Basic Questions in Fatigue: Volume II, ASTM STP 924, R. P. Wei and R. P. Gangloff, Ed., American Society for Testing and Materials, Philadelphia, pp. 294-303.

Subramanian, S., Elmore, J. S., Stinchcomb, W., and Reifsnider, K. L. (1996). "Influence of Fiber-matrix Interphase on the Long-Term Behavior of Graphite/Epoxy Composites," Composite Materials: Testing and Design (Twelvth Volume), ASTM STP 1274, R. B. Deo and C. R. Saff, Eds., American Society for Testing and Materials, pp69-87.

Suri, C., Perreux, D. (1995). "The Effects of Mechanical Damage in a Glass Fiber/Epoxy Composite on the Absorption Rate," Composites Engineering, 5(4), pp415-424.

Tanaka, T., Nishijima, S., and Ichikawa, M. (1987). Statistical Research on Fatigue and Fracture, The Society of Materials Science, Japan, Current Japanese Materials Research-Vol. 2, England: Elsevier Applied Science.

Tavakoli, S. M.; Avella, M.; Phillips, M. G. (1990). " Fiber/Resin Compatibility in Glass/Phenolic Laminating Systems," Composites Science and Technology vol. 39, pp127-145.

Taylor, David (1989). Fatigue Thresholds, ISBN: 0408039213, Essex, England: Butterworth & Co. Publishers.

Tyberg, C. S. (1999). "Tough, Void Free, Flame retardant Phenolic Networks," ICC'99, Session 18-D.

Ulcay, Yusuf. (1989). "The effect of surface treatment on the bonding properties of spectra fibers for use in composite structures," University of Maryland at College Park.

Whitworth, H. A. (1998). "A stiffness degradation model for composite laminates under fatigue loading," Composite Structures, 40(2), pp95-101.

Wirsching, P. H. (1983). "Statistical Summaries of Fatigue Data for Design Purposes," NASA Contract Report 3697.

Ye, Lin, (1989). "On Fatigue Damage Accumulation and Material Degradation in Composite Materials," Composite Science and Technology, vol. 36, pp339-350.

Zimmerman, R. S. (1988). " Mechanical properties of neat polymer matrix materials and their unidirectional carbon fiber-reinforced composites," NASA contractor reports NASA CR-181631.

Appendix A: US to Metric Conversions

Unit	To convert from	to	multiply by
Length	in	cm	2.54
	ft	m	3.0480 E - 1
Area	in^2	mm^2	6.4516 E + 2
	ft^2	m^2	9.2903 E - 2
Volume	in^3	m^3	1.6387 E - 5
Mass	lb	kg	4.5359 E -1
Force	lbf	N	4.4482
Torque	lbf in	N m	1.1298 E - 1
Pressure	lb/in^3	kg/m^3	2.7679 E + 4
	psi	Pa	6894.7
	ksi	MPa	6.8947
	msi	GPa	6.8947
Fluid pressure	in Hg (32°C)	Pa	3.3863 E + 3
Temperature	°F	°C	5/9 (°F - 32)
	°C	K	°C+ 273.15
Speed	mph	km/h	1.6093
Power density	W/in^2	W/m^2	1.5500 E + 3

Appendix B: Physical and Mechanical Test Data

Figure B-1 Stress vs. Strain of Control K-1 Primed GFRP

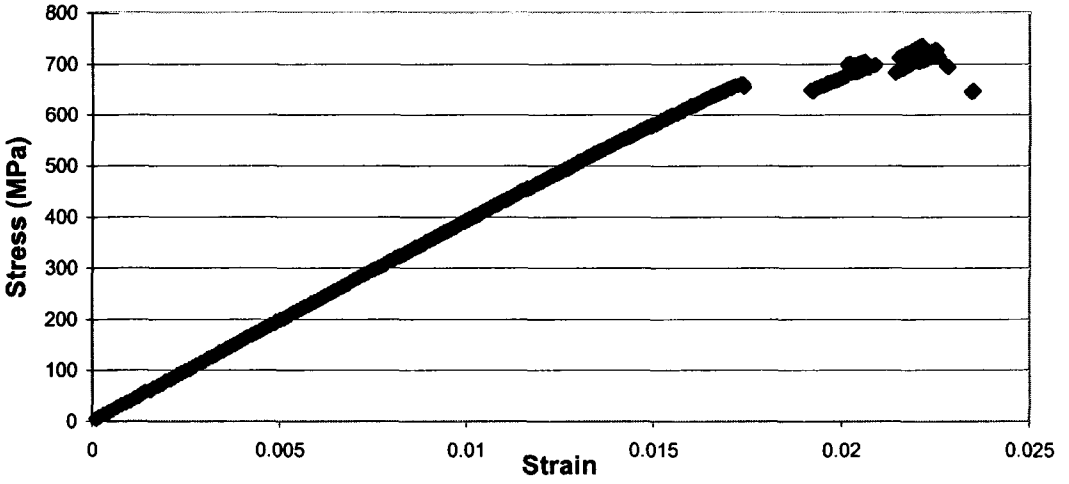

Figure B-2 Stress vs. Strain plot of Control Hand Lay-up GFRP

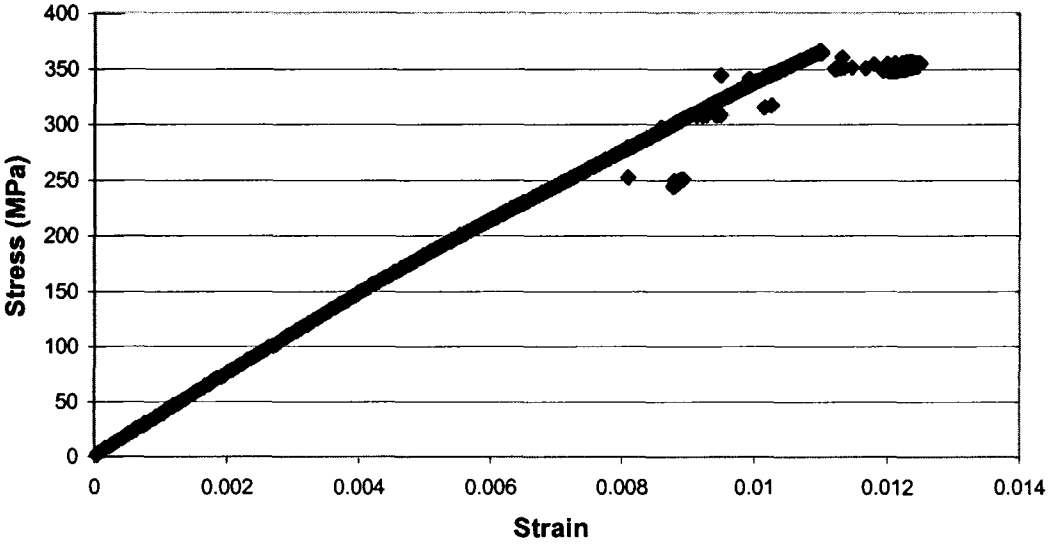

Table B-1 Tensile Strength and Modulus of Control Pultruded GFRP

Sample	Max Load kN	Tensile Strength (MPa)	Tensile modulus (GPa)	Failure mode
K-1 #1	30.749	733.255	42.430	XGM
K-1 #2	27.712	658.465	39.927	XGM
K-1 #3	27.933	664.748	40.479	XGM, minor damage at grip edge.
K-1 #4	30.923	735.921	39.548	XGM
K-1 #5	29.555	704.170	40.210	XGM
K-1 #6	29.380	697.675	40.196	XGM
K-1 #7	30.632	729.213	40.796	XGM
Average	29.555	703.350	40.512	
Std dev	1.324	32.046	0.933	
COV %	4.479	4.556	2.303	

Most GFRP failures in the above table initiated in the middle (M) of the gauge length area (G) and failed in an explosive (X) manner with much fiber fracture.

Table B-2 Tensile Strength of Control and Exposed Pultruded GFRP

Sample #	Control	Freeze-thaw	Hot water	UV Weathering	Simulated Seawater
1	733.3	617.3	483.8	725.5	618.7
2	658.5	606.5	482.3	705.5	619.1
3	664.8	649.4	460.1	699.3	675.8
4	735.9	680.2	477.2	667.9	622.1
5	704.2	677.9	512.7	702.5	681.8
6	697.7	600.1	454.2	688.7	757.2
7	729.2	625.7	490.1	706.6	602.3
Average	703.4	636.7	480.0	699.4	653.8
St Dev	32.0	32.9	19.4	17.8	54.8
COV %	4.56	5.17	4.05	2.54	8.39

Table B-3 Tensile Young's Modulus of Control and Exposed Pultruded GFRP.

Sample #	Control	Freeze-thaw	Hot water	UV Weathering	Simulated Seawater
1	42.430	39.127	40.713	39.658	38.624
2	39.927	39.514	39.810	42.051	40.313
3	40.479	38.927	40.024	40.927	40.458
4	39.548	41.844	42.740	40.355	40.306
5	40.210	40.575	41.878	42.023	40.265
6	40.196	41.037	41.575	40.844	42.196
7	40.796	38.141	41.541	40.293	39.582
Average	40.512	39.881	41.183	40.879	40.249
St Dev	0.933	1.311	1.052	0.894	1.074
COV %	2.303	3.287	2.554	2.187	2.669

Table B-4 Single Factor ANOVA - Tensile Strength of Control and Exposed Pultruded GFRP

1 Between exposures

SUMMARY

Groups	*Count*	*Sum*	*Average*	*Variance*
Control	7	4923.447	703.350	1026.954
Freeze-thaw	7	4457.128	636.733	1084.539
Hot water	7	3360.435	480.062	377.888
UV Weathering	7	4895.914	699.416	315.121
Simulated Seawater	7	4577.019	653.860	3008.159

ANOVA

Source of Variation	*SS*	*df*	*MS*	*F*	*P-value*	*F crit*
Between Groups	232295.2	4	58073.8113	49.954582	7.65E-13	2.689632
Within Groups	34875.97	30	1162.53221			
Total	267171.2	34				

2 Comparing Control and Freeze-thaw

SUMMARY

Groups	*Count*	*Sum*	*Average*	*Variance*
Control	7	4923.447	703.350	1026.954
Freeze-thaw	7	4457.128	636.733	1084.539

ANOVA

Source of Variation	*SS*	*df*	*MS*	*F*	*P-value*	*F crit*
Between Groups	15532.33	1	15532.3337	14.712185	0.002371	4.747221
Within Groups	12668.95	12	1055.74623			
Total	28201.29	13				

3 Comparing Control and Hot water

SUMMARY

Groups	*Count*	*Sum*	*Average*	*Variance*
Control	7	4923.447	703.350	1026.954
Hot water	7	3360.435	480.062	377.888

ANOVA

Source of Variation	*SS*	*df*	*MS*	*F*	*P-value*	*F crit*
Between Groups	174500.3	1	174500.298	248.42695	2.2E-09	4.747221
Within Groups	8429.052	12	702.42096			
Total	182929.3	13				

4 Comparing Control and UV weathering

SUMMARY

Groups	*Count*	*Sum*	*Average*	*Variance*
Control	7	4923.447	703.350	1026.954
UV Weathering	7	4895.914	699.416	315.121

ANOVA

Source of Variation	*SS*	*df*	*MS*	*F*	*P-value*	*F crit*
Between Groups	54.14603	1	54.1460262	0.08069	0.781206	4.747221
Within Groups	8052.45	12	671.037532			
Total	8106.596	13				

5 Comparing Control and Simulated Seawater

SUMMARY

Groups	*Count*	*Sum*	*Average*	*Variance*
Control	7	4923.447	703.350	1026.954
Simulated Seawater	7	4577.019	653.860	3008.159

ANOVA

Source of Variation	*SS*	*df*	*MS*	*F*	*P-value*	*F crit*
Between Groups	8572.294	1.000	8572.29399	4.2488503	0.061632	4.747221
Within Groups	24210.67	12.000	2017.55616			
Total	32782.97	13.000				

Table B-5 Tg of Control and Exposed Pultruded GFRP

Sample #	Control	Simulated Seawater	Hot Water	UV	Freeze-thaw
1	203.8	194.56	194.28	208.9	203.6
2	204	191.06	197.82	205.6	200.5
3	202.5	196.36	197.44	205.56	208.5
4	201.4	194.4	197.35	207.8	208.2
5	197.38	194.8	195.32	207.22	197.5
Average	201.816	194.236	196.442	207.016	203.66
St Dev	2.694	1.940	1.553	1.443	4.795
COV %	1.335	0.999	0.791	0.697	2.354

Table B-6 Single Factor ANOVA - Tg from DMTA Data of Control and Exposed Pultruded GFRP.

1 Comparing all exposures

SUMMARY

Groups	*Count*	*Sum*	*Average*	*Variance*
Control	5	1009.08	201.816	7.25628
Hot Water	5	982.21	196.442	2.41312
UV	5	1035.08	207.016	2.08268
Freeze-thaw	5	1018.3	203.66	22.993
Simulated Seawater	5	971.18	194.236	3.76208

ANOVA

Source of Variation	*SS*	*df*	*MS*	*F*	*P-value*	*F crit*
Between Groups	548.955	4	137.23874	17.819899	2.246E-06	2.866081
Within Groups	154.0286	20	7.701432			
Total	702.9836	24				

2 Comparing Control with Hot water exposure

SUMMARY

Groups	*Count*	*Sum*	*Average*	*Variance*
Control	5	1009.08	201.816	7.25628
Hot Water	5	982.21	196.442	2.41312

ANOVA

Source of Variation	*SS*	*df*	*MS*	*F*	*P-value*	*F crit*
Between Groups	72.19969	1	72.19969	14.933644	0.004779	5.317645
Within Groups	38.6776	8	4.8347			
Total	110.8773	9				

3 Comparing Control with UV weathering exposure.

SUMMARY

Groups	*Count*	*Sum*	*Average*	*Variance*
Control	5	1009.08	201.816	7.25628
UV	5	1035.08	207.016	2.08268

ANOVA

Source of Variation	*SS*	*df*	*MS*	*F*	*P-value*	*F crit*
Between Groups	67.6	1	67.6	14.476987	0.0052005	5.317645
Within Groups	37.35584	8	4.66948			
Total	104.9558	9				

4 Comparing Control with Freeze-thaw exposure

SUMMARY

Groups	*Count*	*Sum*	*Average*	*Variance*
Control	5	1009.08	201.816	7.25628
Freeze-thaw	5	1018.3	203.66	22.993

ANOVA

Source of Variation	*SS*	*df*	*MS*	*F*	*P-value*	*F crit*
Between Groups	8.50084	1	8.50084	0.5620524	0.4749012	5.317645
Within Groups	120.9971	8	15.12464			
Total	129.498	9				

5 Comparing Control with Simulated Seawater exposure

SUMMARY

Groups	*Count*	*Sum*	*Average*	*Variance*
Control	5	1009.08	201.816	7.25628
Simulated Seawater	5	971.18	194.236	3.76208

ANOVA

Source of Variation	*SS*	*df*	*MS*	*F*	*P-value*	*F crit*
Between Groups	143.641	1	143.641	26.073027	0.0009228	5.317645
Within Groups	44.07344	8	5.50918			
Total	187.7144	9				

Table B-7 Ignition Loss Results of Hand Lay-up GFRP.

Density of hand lay-up composite (experimental- liquid displacement method (LDM)) = 2.008 g/cc

Density of PRF (Phenol Resorcinol Formaldehyde) = 1.33 g/cc (manufacturer data verified by LDM)

Density of E-glass fiber = 2.54 g/cc (Manufacturer data)

Sample #	Sample wt (g)	Crucible weight (g)	Sample + crucible (g)	After Ignition loss Sample+ crucible (g)	Residue weight (glass fibers) (g)	Ignition loss (Resin) (g)	Fiber Weight fraction Wf	Fiber Volume fraction Vf (%)	Resin Weight fraction Wm (%)	Resin volume fraction Vm (%)	Theoretical density (g/cc)	Void Volume fraction Vv (%)
1	3.8207	1.2961	5.1168	4.4303	3.1342	0.69	82.03	64.85	17.97	27.13	2.56	8.02
2	3.7733	1.2839	5.0572	4.4299	3.146	0.63	83.38	65.91	16.62	25.10	2.60	8.99
3	3.7893	1.2841	5.0734	4.3944	3.1103	0.68	82.08	64.89	17.92	27.05	2.56	8.06
4	3.7544	1.2993	5.0537	4.4177	3.1184	0.64	83.06	65.66	16.94	25.58	2.59	8.76
5	3.7952	1.2982	5.0934	4.3913	3.0931	0.70	81.50	64.43	18.50	27.93	2.55	7.64
6	3.8199	1.298	5.1179	4.4179	3.1199	0.70	81.67	64.57	18.33	27.67	2.55	7.77
						Average	82.29	65.05	17.71	26.74	2.57	8.21
						St Dev	0.76	0.60	0.76	1.15	0.02	0.55
						COV %	0.92	0.92	4.29	4.29	0.86	6.66

Table B-8 Ignition Loss Results of Pultruded GFRP

Density of pultruded GFRP obtained through micrometer measurements of small specimens

Sample #	Volume (cm3)	Crucible wt (g)	Sample+ crucible (g)	sample (g)	Experimental density (g/cm3)	Burnt Sample + Crucible (g)	Residue wt (g)	Ignition loss (wt%)	Fiber weight fraction (%)	Matrix weight fraction (%)	Fiber volume fraction %	Matrix volume fraction %	Void volume (%)
1	2.134	1.411	4.800	3.389	1.588	4.320	2.909	14.175	85.825	14.175	53.664	20.845	25.491
2	2.108	1.393	4.804	3.411	1.618	4.326	2.934	13.990	86.010	13.990	54.786	20.958	24.256
3	2.103	1.394	4.797	3.403	1.618	4.338	2.944	13.497	86.503	13.497	55.108	20.223	24.669
4	2.108	1.398	4.757	3.359	1.594	4.263	2.865	14.708	85.292	14.708	53.525	21.707	24.768
5	2.105	1.393	4.766	3.373	1.602	4.275	2.881	14.570	85.430	14.570	53.879	21.611	24.510
Average	2.112	1.398	4.785	3.387	1.604	4.304	2.907	14.188	85.812	14.188	**54.192**	**21.069**	**24.739**
St Dev	0.013	0.008	0.021	0.021	0.014	0.033	0.033	0.483	0.483	0.483	0.710	0.608	0.463
% COV	0.597	0.557	0.449	0.626	0.853	0.771	1.149	3.403	0.563	3.403	1.310	2.886	1.871

Appendix C: Fatigue Data

Table C-1 Fatigue Data of Control and Exposed Pultruded GFRP

Control		UV Weathering		Freeze-Thaw		Simulated Seawater		Hot Water (45C)	
Failure Cycles	Stress Level	Failure Cycles	Stress Level	Failure Cycles	Stress Level	Failure Cycles	Stress Level	Failure Cycles	Stress Level
138	80	10222	50	22151	50	18161	50	2587	60
115	80	5469	50	17794	50	22998	50	1542	60
105	80	13369	50	5985	50	13928	50	3840	60
80	80	11580	50	19992	50	28348	50	14847	50
111	80	58406	40	125174	40	112611	40	15877	50
725	70	66552	40	107762	40	152553	40	23000	50
934	70	60680	40	115337	40	113862	40	24000	50
575	70	49742	40	152424	40	144037	40	232269	40
747	70	107648	30	1209316	30	987260	30	116490	40
374	70	373424	30	1546862	30	1611803	30	112091	40
548	70	290919	30	2058466	30	1174663	30	85093	40
5678	60	341216	30	737280	30	924413	30	298495	30
2092	60	>3 mill	20	1381440	30	>3 mill	20	1285902	30
3056	60	>3 mill	20	803552	30	>3 mill	20	661991	30
3115	60	>3 mill	20	>3 mill	20	>3 mill	20	977240	30
3304	60	>3 mill	20	>3 mill	20	>3 mill	20	>3 mill	20
21629	50			>3 mill	20			>3 mill	20
10812	50			>3 mill	20			>3 mill	20
15898	50							>3 mill	20
16640	50								
18372	50								
15152	50								
15236	50								
14140	50								
21008	50								
13520	50								
12140	50								
119601	40								
60052	40								
112282	40								
80620	40								
62871	40								
72804	40								
100000	40								
93000	40								
851227	30								
437859	30								
328886	30								
555600	30								
226718	30								

Method for calculating the 5% LTL with 95% Confidence

The method for calculating the 5%LTL with 95% confidence was according to a NASA report published by Paul H. Wirsching (1983). The method is summarized below:

- The S-N curve is plotted with Log of life vs. Stress level. The fatigue life (Log N) is called the Y axis (unlike conventional graphs). The stress level is the X axis.
- Using least squares method, the mean S-N curve is drawn with slop b and intercept a.
- The equation of the line is thus $Y_o = a + bx$
- The term b is given by:

$$b = \frac{\sum_{i=1}^{n}(xi - \overline{X})(Yi - \overline{Y})}{\sum_{i=1}^{n}(xi - X)\text{^}2}$$

- The standard deviation s is the standard deviation of the mean line. It is given by:

$$S^2 = \frac{1}{n-2}\sum_{i=1}^{n}[Yi - (a + bx)]^2$$

- The tolerance limit is then calculated by finding the k coefficient from a one-sided tolerance table for 95% of the population and 95% confidence. The equation for the tolerance line is given by:

  Log $N_{5\%LTL}$ = Y – k s. The calculation method is illustrated in Table C-2.

Table C-2 Calculation of 5% LTL for Control Pultruded GFRP

LIFE (N)	STRESS	LOG(N)	xi-Xm	Yi-Ym	(xi-Xm)*(yi-Ym)	(xi-Xm)^2	[Yi-(a+b*Xi)]^2	Yest	5% LTL
138	80	2.140	26.5	-1.817	-48.138	702.25	0.00677	2.058	1.791
115	80	2.061	26.5	-1.896	-50.236	702.25	0.00001	2.058	1.791
105	80	2.021	26.5	-1.935	-51.283	702.25	0.00132	2.058	1.791
80	80	1.903	26.5	-2.053	-54.412	702.25	0.02387	2.058	1.791
111	80	2.045	26.5	-1.911	-50.643	702.25	0.00015	2.058	1.791
725	70	2.860	16.5	-1.096	-18.085	272.25	0.00743	2.774	2.508
934	70	2.970	16.5	-0.986	-16.270	272.25	0.03851	2.774	2.508
575	70	2.760	16.5	-1.197	-19.746	272.25	0.00021	2.774	2.508
747	70	2.873	16.5	-1.083	-17.871	272.25	0.00984	2.774	2.508
374	70	2.573	16.5	-1.384	-22.828	272.25	0.04050	2.774	2.508
548	70	2.739	16.5	-1.218	-20.091	272.25	0.00125	2.774	2.508
5678	60	3.754	6.5	-0.202	-1.314	42.25	0.06946	3.491	3.224
2092	60	3.321	6.5	-0.636	-4.133	42.25	0.02893	3.491	3.224
3056	60	3.485	6.5	-0.471	-3.063	42.25	0.00003	3.491	3.224
3115	60	3.493	6.5	-0.463	-3.009	42.25	0.00001	3.491	3.224
3304	60	3.519	6.5	-0.437	-2.843	42.25	0.00081	3.491	3.224
21629	50	4.335	-3.5	0.379	-1.325	12.25	0.01635	4.207	3.941
10812	50	4.034	-3.5	0.078	-0.271	12.25	0.03002	4.207	3.941
15898	50	4.201	-3.5	0.245	-0.857	12.25	0.00003	4.207	3.941
16640	50	4.221	-3.5	0.265	-0.927	12.25	0.00020	4.207	3.941
18372	50	4.264	-3.5	0.308	-1.077	12.25	0.00325	4.207	3.941
15152	50	4.180	-3.5	0.224	-0.784	12.25	0.00071	4.207	3.941
15236	50	4.183	-3.5	0.226	-0.793	12.25	0.00059	4.207	3.941
14140	50	4.150	-3.5	0.194	-0.679	12.25	0.00322	4.207	3.941
21008	50	4.322	-3.5	0.366	-1.281	12.25	0.01327	4.207	3.941
13520	50	4.131	-3.5	0.175	-0.611	12.25	0.00581	4.207	3.941
12140	50	4.084	-3.5	0.128	-0.447	12.25	0.01512	4.207	3.941
119601	40	5.078	-13.5	1.121	-15.138	182.25	0.02372	4.924	4.657
60052	40	4.779	-13.5	0.822	-11.099	182.25	0.02108	4.924	4.657
112282	40	5.050	-13.5	1.094	-14.768	182.25	0.01603	4.924	4.657
80620	40	4.906	-13.5	0.950	-12.826	182.25	0.00030	4.924	4.657
62871	40	4.798	-13.5	0.842	-11.368	182.25	0.01569	4.924	4.657
72804	40	4.862	-13.5	0.906	-12.228	182.25	0.00379	4.924	4.657
100000	40	5.000	-13.5	1.044	-14.089	182.25	0.00582	4.924	4.657
93000	40	4.968	-13.5	1.012	-13.663	182.25	0.00200	4.924	4.657
851227	30	5.930	-23.5	1.974	-46.381	552.25	0.08399	5.640	5.374
328886	30	5.517	-23.5	1.561	-36.675	552.25	0.01518	5.640	5.374
437859	30	5.641	-23.5	1.685	-39.596	552.25	0.00000	5.640	5.374
555600	30	5.745	-23.5	1.788	-42.027	552.25	0.01092	5.640	5.374
226718	30	5.355	-23.5	1.399	-32.879	552.25	0.08109	5.640	5.374
					Sum	Sum	Sum		
					-695.753	**9710**	**0.59727**		

Xm	53.5
Ym	3.956
b	-0.07165
a	7.789842
s	0.12537
Alpha	0.95
population	0.95
k(one sided)	2.126

Best Fit line:
Y = a + bx
Where Y, a, and b are estimates
Y is Log (N)
x is stress level

5% LTL line :
Log (N) = Y - k s
where N is the fatigue life
Y is the mean fatigue life
k is the one sided lower tolerance limit
s is the standard deviation for the best fit line

Table C-3 Calculation of 5% LTL Values of Hand Lay-up GFRP

Max Stress (xi)	LOG(N) (yi)	xi-Xm	yi-Ym	(xi-Xm)*(yi-Ym)	(xi-Xm)^2	[Yi-(a+b*Xi)]^2	Y(estimate)	5% LTL
60	3.293	19.048	-1.481	-28.209	362.812	0.079	3.012	2.453
60	3.195	19.048	-1.579	-30.072	362.812	0.034	3.012	2.453
60	2.979	19.048	-1.795	-34.191	362.812	0.001	3.012	2.453
60	3.335	19.048	-1.439	-27.403	362.812	0.105	3.012	2.453
50	3.985	9.048	-0.789	-7.142	81.859	0.002	3.937	3.378
50	3.858	9.048	-0.916	-8.291	81.859	0.006	3.937	3.378
50	3.880	9.048	-0.894	-8.089	81.859	0.003	3.937	3.378
50	3.517	9.048	-1.257	-11.376	81.859	0.177	3.937	3.378
40	4.849	-0.952	0.075	-0.071	0.907	0.000	4.862	4.303
40	4.545	-0.952	-0.229	0.218	0.907	0.101	4.862	4.303
40	4.690	-0.952	-0.084	0.080	0.907	0.030	4.862	4.303
40	4.629	-0.952	-0.145	0.138	0.907	0.054	4.862	4.303
40	4.463	-0.952	-0.311	0.296	0.907	0.159	4.862	4.303
30	6.192	-10.952	1.418	-15.529	119.955	0.164	5.788	5.229
30	5.875	-10.952	1.101	-12.059	119.955	0.008	5.788	5.229
30	5.706	-10.952	0.932	-10.210	119.955	0.007	5.788	5.229
30	6.029	-10.952	1.254	-13.739	119.955	0.058	5.788	5.229
25	6.159	-15.952	1.385	-22.089	254.478	0.008	6.250	5.691
25	6.342	-15.952	1.568	-25.018	254.478	0.009	6.250	5.691
25	6.257	-15.952	1.483	-23.661	254.478	0.000	6.250	5.691
25	6.477	-15.952	1.703	-27.167	254.478	0.052	6.250	5.691
			Sum :	**-303.585**	**3280.952**	**1.056**		

Xm (mean of x)	40.95238	Best Fit line:	Y = a + bx
Ym (mean of y)	4.774		Where Y, a, and b are estimates
b	-0.09253		Y is Log (N)
a	8.56341		x is max stress level
s	0.235707		
Alpha	0.95	5% LTL line :	Log (N) = Y - k s
population	0.95		where N is the fatigue life
k(one sided)	2.371		Y is the mean fatigue life
			k is the one sided lower tolerance limit
			s is the standard deviation for the best fit line

Table C-4 Mean Fatigue Life Data of Pultruded GFRP at 30% UTS

Control	Simulated Seawater	Freeze-thaw	UV weathering	Hot water
851227	987260	1209316	107648	298495
328886	1611803	1546862	373424	1285902
555600	1174663	2058466	290919	661991
226718	924413	737280	341216	977240

Table C-5 Single Factor ANOVA – Fatigue Life at 30% UTS Control.

1 Comparing Control and Freeze-thaw

SUMMARY

Groups	*Count*	*Sum*	*Average*	*Variance*
Control	4	1962431	490607.75	76687320203
Freeze-thaw	4	5551924	1387981	3.10042E+11

ANOVA

Source of Variation	*SS*	*df*	*MS*	*F*	*P-value*	*F crit*
Between Groups	1.61E+12	1	1.61056E+12	8.329118199	0.0278378	5.987374
Within Groups	1.16E+12	6	1.93365E+11			
Total	2.77E+12	7				

2 Comparing Control and UV Weathering

SUMMARY

Groups	*Count*	*Sum*	*Average*	*Variance*
Control	4	1962431	490607.75	76687320203
UV weathering	4	1113207	278301.75	14096114228

ANOVA

Source of Variation	*SS*	*df*	*MS*	*F*	*P-value*	*F crit*
Between Groups	9.01E+10	1	90147675272	1.985993939	0.2084228	5.987374
Within Groups	2.72E+11	6	45391717216			
Total	3.62E+11	7				

3 Comparing Control and Hot Water (45°C)

SUMMARY

Groups	*Count*	*Sum*	*Average*	*Variance*
Control	4	1962431	490607.75	76687320203
Hot water	4	3223628	805907	1.7931E+11

ANOVA

Source of Variation	*SS*	*df*	*MS*	*F*	*P-value*	*F crit*
Between Groups	1.99E+11	1	1.98827E+11	1.553356151	0.2590937	5.987374
Within Groups	7.68E+11	6	1.27998E+11			
Total	9.67E+11	7				

4 Comparing Control and Simulated Seawater

SUMMARY

Groups	*Count*	*Sum*	*Average*	*Variance*
Control	4	1962431	490607.75	76687320203
Simulated Seawater	4	4698139	1174534.75	96278753572

ANOVA

Source of Variation	*SS*	*df*	*MS*	*F*	*P-value*	*F crit*
Between Groups	9.36E+11	1	9.35512E+11	10.81729223	0.0166353	5.987374
Within Groups	5.19E+11	6	86483036888			
Total	1.45E+12	7				

Table C-6 Calculation of 95% Confidence Bands for UV Weathering S-N Curve Using Equation 9 of ASTM E 739

The confidence Bands are Given by:

$$A + BX \pm \sqrt{2F_p}\,\sigma\left[\frac{1}{k} + \frac{(X-\bar{X})^2}{\sum_{i=1}^{k}(X_i - X)^2}\right]^{1/2}$$

Where Fp is obtained from F distribution table, σ is standard deviation and k is the total number of specimens.

Life	Log cycles	Stress Level				Confidence bands	
Cycles	Yi	Xi	(Xi-meanX)^2	Ycaret	(Yi-Ycaret)^2	95% Lower	95% upper
10222	4.010	50	100	4.009	0.000	3.784	4.235
5469	3.738	50	100	4.009	0.074	3.784	4.235
13369	4.126	50	100	4.009	0.014	3.784	4.235
11580	4.064	50	100	4.009	0.003	3.784	4.235
58406	4.766	40	0	4.717	0.002	4.574	4.860
66552	4.823	40	0	4.717	0.011	4.574	4.860
60680	4.783	40	0	4.717	0.004	4.574	4.860
49742	4.697	40	0	4.717	0.000	4.574	4.860
107648	5.032	30	100	5.425	0.155	5.200	5.651
373424	5.572	30	100	5.425	0.022	5.200	5.651
290919	5.464	30	100	5.425	0.001	5.200	5.651
341216	5.533	30	100	5.425	0.012	5.200	5.651
		Sum=	800	Sum=	0.297971223		

B = -0.0708
A = 7.5492
Mean X 40
Mean Y 4.717304
St dev 0.1726184 =((Sum (Yi-Ycaret)^2/(k-2))^2 = 0.2979/10
Linear equation from least squares line fit: y = -0.0708x + 7.5492
This is done by plotting stress levels in the X axis and log life in the Y axis according to ASTM E739
Total # of Specimens (k) = 12
For F distribution, n1 (numerator) =2, n2(denominator) = k-2 $\alpha = 0.05$

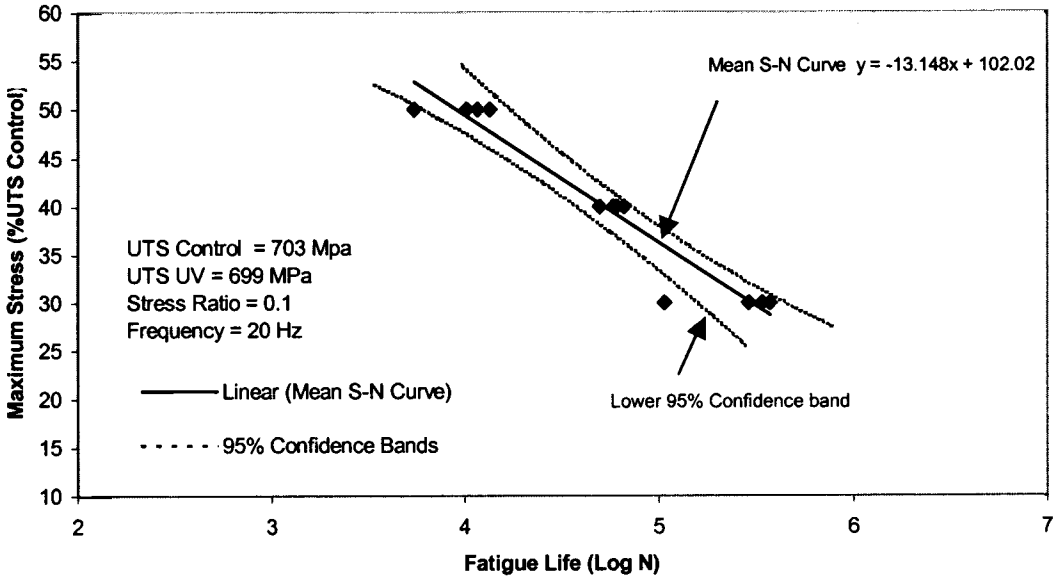

Figure C-1 S-N Curve of UV Weathered Specimens With 95% Confidence Bands

Appendix D: DMTA Plots

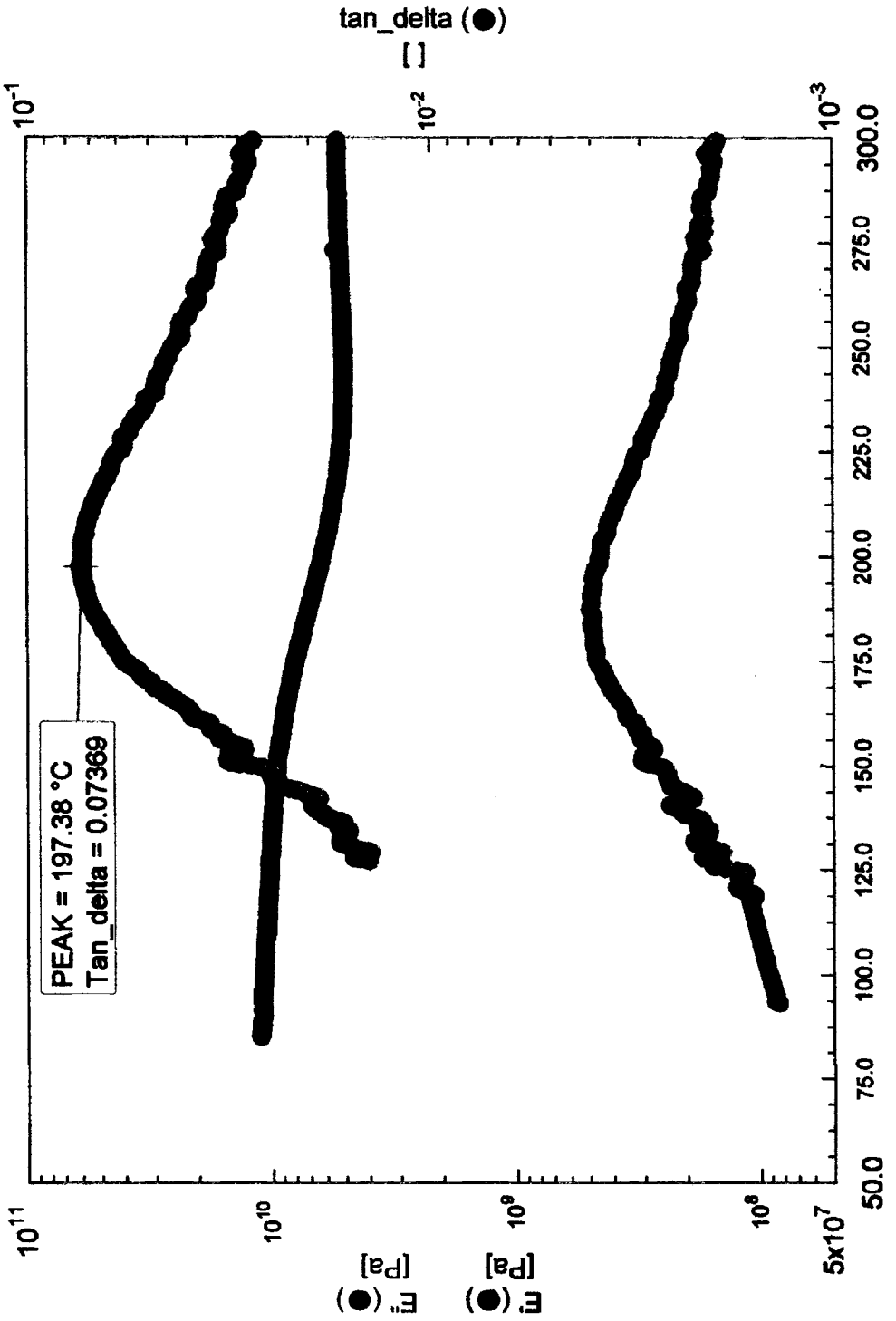

Figure D-1 DMTA Plot of Control Pultruded GFRP

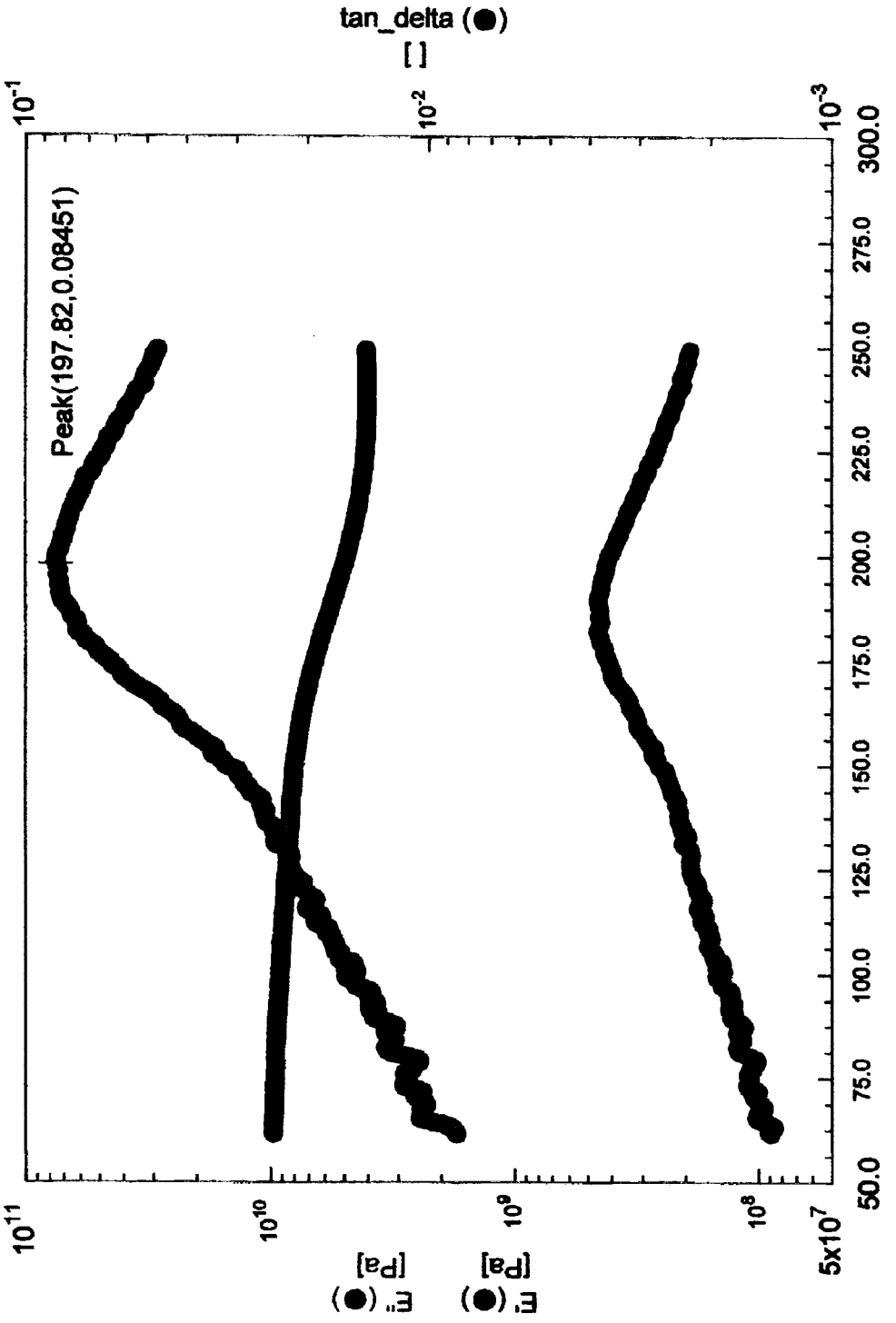

Figure D-2 DMTA Plot of Hot Water (3000 hrs) Pultruded GFRP

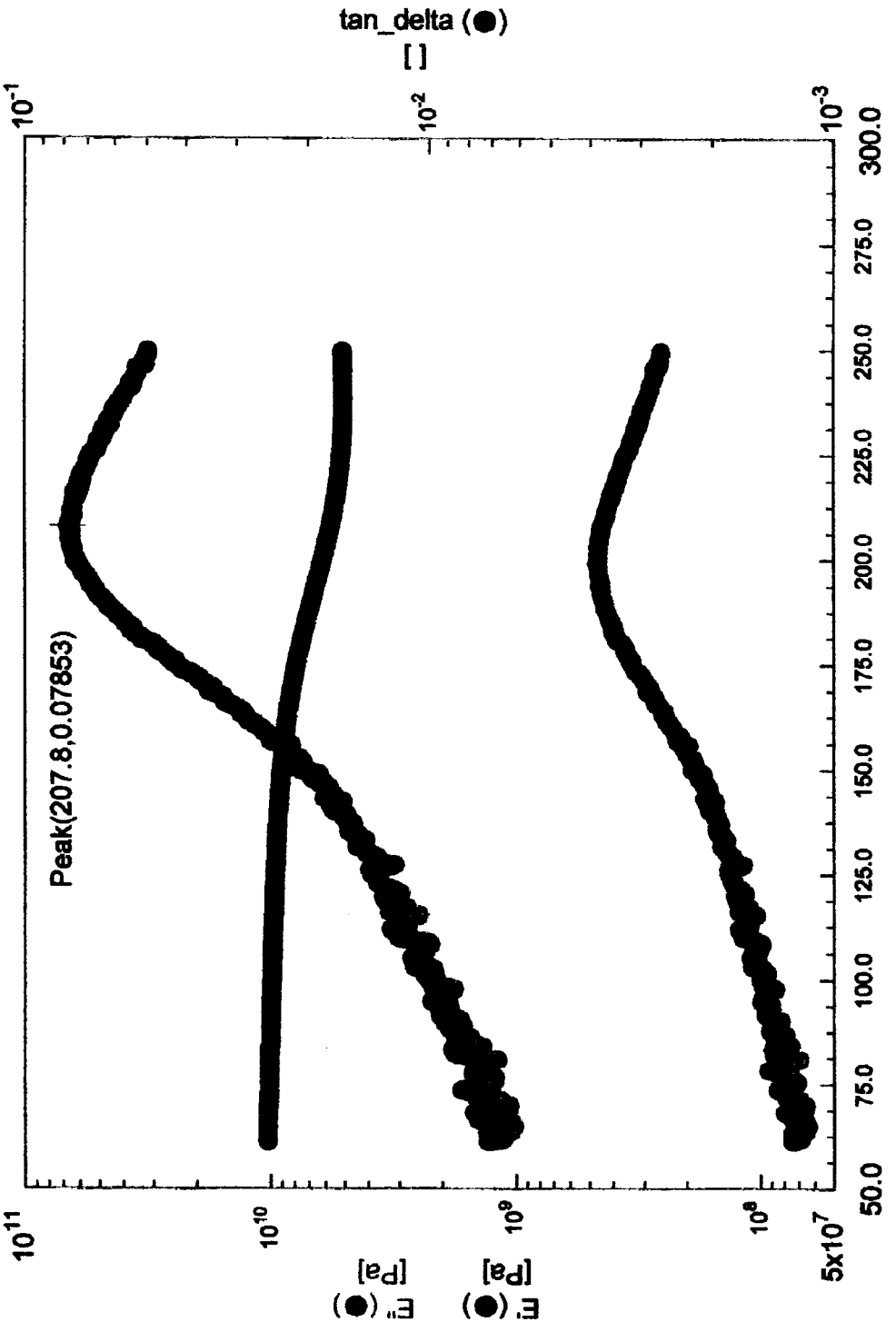

Figure D-3 DMTA Plot of UV Weathered Pultruded GFRP

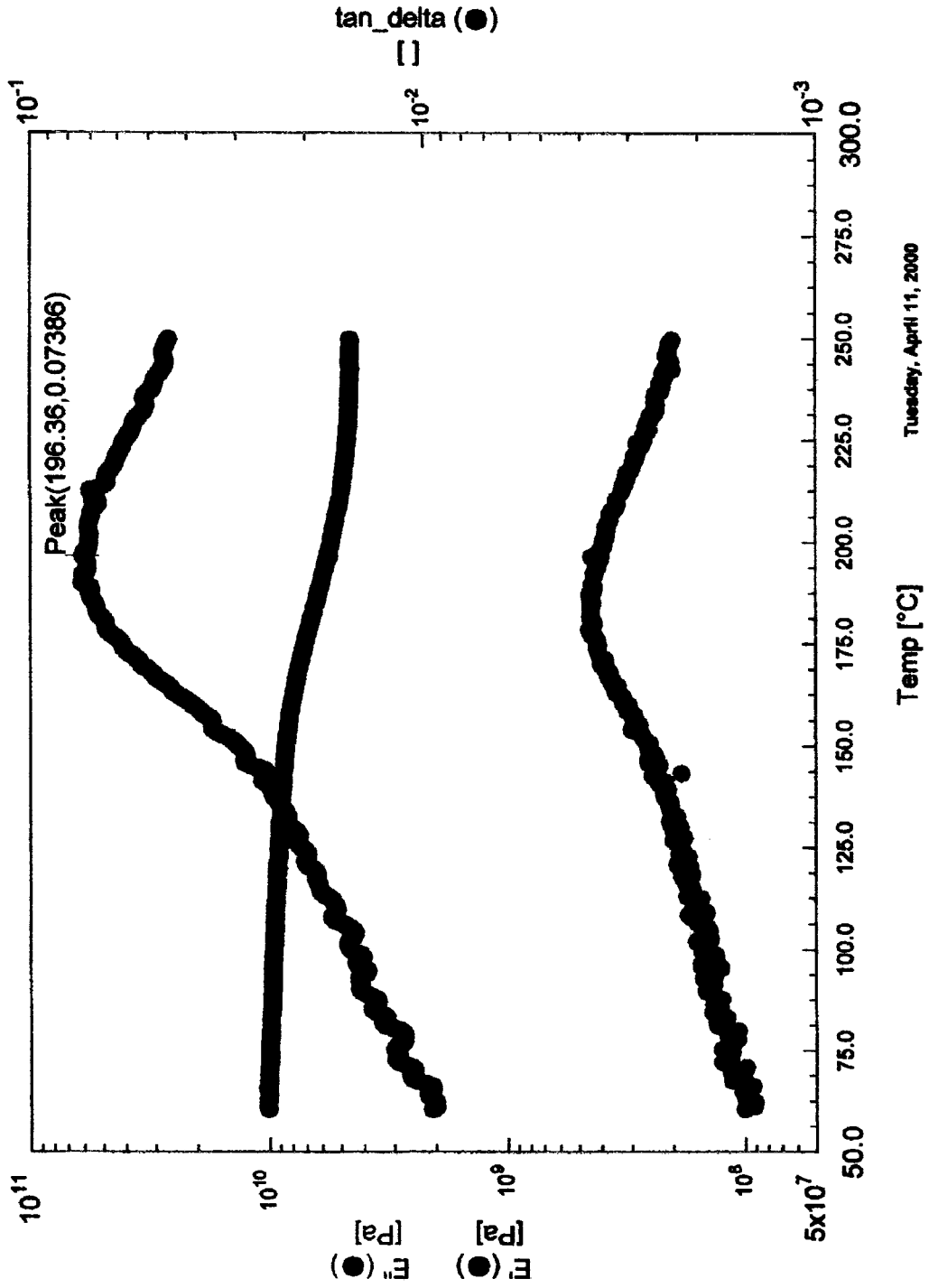

Figure D-4 DMTA Plot of Simulated Seawater Pultruded GFRP

Appendix E: List of ASTM Standards, and Specifications Used in this Study.

1. ICBO Acceptance Criteria 125- Acceptance Criteria for Concrete and Reinforced and Un-reinforced Masonry Strengthening using Fiber-Reinforced Composite Systems.
2. Pre-qualification requirements 1/24/97- CALTRANS Pre-qualification Requirements for Alternative Column Castings for Seismic Retrofit (Composites).
3. ASTM D 3039- Tensile Properties of Polymer Matrix Composite Materials.
4. ASTM D 3479- Tension-Tension Fatigue of Polymer Matrix Composite Material.
5. ASTM E 739- Practice for Statistical Analysis of Linear or Linearized Stress-Life (S-N) and Strain-Life (e-N) Fatigue Data.
6. ASTM D 2344- Apparent Interlaminar Shear Strength of Parallel Fiber Composites by Short-Beam Method.
7. ASTM D 2584- Ignition Loss of Reinforced Composites.
8. ASTM E 1049- Practice for Cycle Counting in Fatigue Analysis.
9. ASTM D 2734- Void Content of Reinforced Plastics.
10. ASTM D 1141- Standard Specification for Ocean Water.
11. ASTM D 1193- Standard Specification for Reagent Water.

12. ASTM D 2247- Standard Practice for testing Water resistance of Coatings in 100% Relative Humidity.
13. ASTM G 53- Standard practice for Operating Light-Exposure Apparatus (Carbon-Arc type) With and Without Water for Exposure of Non-Metallic Materials.
14. ASTM G 23- Standard Practice for Operating Light-and Water-Exposure Apparatus (Fluorescent UV-Condensation Type) for Exposure of Non-Metallic Materials.
15. ASTM D 570- Standard Test method for water absorption of plastics.
16. ASTM E 632 Developing Accelerated Tests to Aid Prediction of the Service Life of Building Components and Materials.
17. ASTM D 792 Density and Specific Gravity (Relative Density) of Plastics by Displacement.

BIOGRAPHY OF THE AUTHOR

Mohammed Asif Iqbal was born in Joydepur, Bangladesh on December 14th, 1972. He moved to Kuwait with his family at the age of five. He completed the metricular examination (10th Grade) from The New Indian School, Jabriyya, Kuwait. After missing almost a year of education due to the Gulf War (1990-1991), he completed the 11th and 12th grade (High School) from Indian School, Salmiya, Kuwait.

In pursuit of further education, he moved to the U.S. and completed his bachelor's degree in Composite Materials Engineering from Winona State University, Winona, Minnesota. His desire for a graduate degree and his interest in composite materials took him to University of Maine, Orono, Maine. Iqbal is a member of the Society of Plastics Engineers (SPE) and the American Society of Civil Engineers (ASCE). Iqbal is a candidate for the Master of Science degree in Civil Engineering from The University of Maine in May 2001.